GEOLOGY OF THE QUESTA MINING DISTRICT: VOLCANIC, PLUTONIC, TECTONIC AND HYDROTHERMAL HISTORY

Jeff Meyer
Department of Geological Sciences
University of California at Santa Barbara
Santa Barbara, California 93106

Robert Leonardson
Chief Geologist
Union/Molycorp
P.O. Box 469
Questa, New Mexico 87556

ABSTRACT 1
INTRODUCTION 3
PREVIOUS STUDIES AND THE HISTORY OF THIS STUDY 4
METHODS OF STUDY 8
REGIONAL SETTING AND GEOLOGIC HISTORY 9
LITHOLOGIC DESCRIPTIONS 16
Precambrian units 16
Precambrian to Paleozoic intrusions 19
Early Tertiary sediments 19
Early volcanic series (including related intrusions) 20
low-silica rhyolite tuff 21
andesite to quartz latite porphyry flows 21
hypabyssal quartz latite intrusions 23
pre-caldera basaltic andesites 24
Later volcanic series (and related intrusions) 24
Amalia Tuff 25
Questa caldera 26
Outflow tuff 28
Intracaldera tuff 29
Intracaldera megabreccia 30
Basal broken crystal zone 33
Caldera-related intrusions 35
Post-caldera intrusive units 38
Pre-mineral intrusions 39
Syn-mineral plutons 40
Post-mineral intrusions 42
Younger, mafic-suite diking 46
Evolution of the post-caldera magmatic system 47
Quaternary deposits 48
STRUCTURAL GEOLOGY 48
Precambrian structures 49
Paleozoic-Mesozoic structures 51
Early Tertiary structures 51
Mid-Oligocene to mid-Miocene structures 52
Pre-caldera extension (approximately 28 to 25.7 Ma) 52
Caldera-related structures (25.8 Ma) 53
Syn-caldera extension (25.8 Ma) 54

Post-caldera extension (25.7-24.6 Ma).....55
Post-mineralization faulting (24.2 Ma - earliest? Miocene).....60
Block-fault extension (earliest Miocene? to mid-Miocene).....63
Discussion: geometric relationships of extensional faults at Questa.....64
Mid Miocene - Recent rift-front faults.....66
Quaternary landslides.....66
Discussion: significance of caldera-related structures...67
MINERALIZATION AND ALTERATION.....69
Regional Alteration and Alteration Scars.....70
Molybdenum mineralization and related alteration.....72
Southwest ore body.....75
host rock and intrusive phases associated with mineralization.....76
structures.....80
mineralization-alteration.....82
pre-mineral biotization.....83
magmatic-hydrothermal breccia and related alteration.....83
quartz-molybdenite-pyrite veining and associated alteration.....87
molybdenite paint.....87
quartz-sericite-pyrite alteration associated with rhyolite porphyry diking.....88
quartz-fluorite-sericite-pyrite-base metal sulfide veining.....88
calcite / gypsum veining.....88
deuteric alteration.....89
Comparison to "Climax type" systems.....89
District-wide exploration model.....91
REGIONAL MODELS FOR MAGMATIC-TECTONIC INTERACTION.....92
SOUTHERN CALDERA AREA MAGMATIC-TECTONIC HISTORY.....96
COMPARISON TO OTHER EXTENDED REGIONS.....98
CONCLUSIONS.....102
ACKNOWLEDGEMENTS.....106
REFERENCES.....107
FIGURES, TABLES AND PLATES.....128

ABSTRACT

Detailed mapping of the Questa mining district reveals a complex volcanic, plutonic, tectonic and hydrothermal history. The mining district is located in the southern portion of the Oligocene Questa caldera in the Latir volcanic field. Post-caldera tilting and mid-Miocene to present uplift and erosion of the eastern flank of the Rio Grande rift allows study of stratigraphic and structural relationships over a significant vertical interval.

Latir field volcanic units overlie a Proterozoic basement that is partially covered by locally-derived Laramide sediments. The field consists of early intermediate composition extrusive and intrusive units characteristic of a composite stratovolcano field. Magmatic activity culminated in the 25.7 Ma eruption of the Amalia Tuff and formation of the Questa caldera. Activity switched to a weakly peralkaline bimodal association immediately before caldera collapse.

Exposures of the intracaldera tuff near the southern caldera margin are up to 2.5 km thick and reveal a complex megabreccia block stratigraphy that thickens toward the structural caldera margin to the south. A newly described unit, the basal broken crystal zone, locally overlies individual megabreccia blocks and block lenses, and suggests explosive initiation of migrating caldera ring-vents after short-term pauses in the caldera-fill cycle. Post-caldera intrusions along the southern caldera margin have locally developed aplitic caps that are responsible for molybdenum mineralization in the district.

Important structural features include a Precambrian shear zone, caldera-related structures, post-caldera faults related to extreme ENE extension and modern Rio Grande rift formation. The Precambrian discontinuity, evidenced by a significant N-S change in lithology and by regionally anomalous E-W to ENE striking foliation, is believed responsible for the location and linearity of the southern caldera margin, post-caldera plutons and pluton-related molybdenum mineralization. Caldera-related structures include locally-preserved fragments of caldera-margin ring faults and local caldera-floor horst and graben structures.

Extreme extension followed cooling of the thick intracaldera tuff, but preceded the one m.y. later cooling of batholith-scale intrusions below their magnetite and biotite blocking temperatures. The region of extreme extension roughly corresponds to the outline of the Questa caldera and to the geographic extent of 24.6 Ma intrusive phases. Thermal and mechanical weakening by the magmatic system are believed to have focussed regional extension into the area of the intrusions. Joints that were initially near-vertical became active as high-angle faults and subsequently became rotated to low angles as extension continued. These low-angle fault zones exerted significant controls on the location of tops of plutons, porphyry dikes and the pathways taken by hydrothermal fluids. Hydrothermal fluids, in turn are believed to have allowed the low-angle faults to remain active during rotation to extremely low angles.

Molybdenum mineralization in the district is influenced by low-angle faulting as best exemplified in the Southwest ore zone. In the Southwest ore zone, aplite that is interpreted to be the source of mineralizing fluids was intruded along a north-dipping low-angle fault zone. Fluids that were exsolved from this aplite lifted and brecciated the fault zone, forming a molybdenum-bearing magmatic-hydrothermal breccia. More distal fluids related to mineralization were channelized toward the surface along this fault zone resulting in a surface expression of the Southwest zone ore body located 700 to 1500 m south of the subsurface mineralization.

INTRODUCTION

The Questa mining district is located in the southern portion of the Questa caldera in the late-Oligocene Latir volcanic field (Fig. 1). The Latir field lies on the eastern flank of the modern Rio Grande rift near the intersection of the Jemez volcanic zone with the modern rift valley (Fig. 2). The Latir field is immediately southeast of the San Juan volcanic field and developed during the waning stages of San Juan volcanism.

Mid-Miocene to present uplift and erosion of the eastern flank of the Rio Grande rift caused deep caldera-level exposures in the southern portion of the caldera. This portion of the caldera reveals a pattern of highly tilted fault-blocks of caldera fill and caldera floor stratigraphy bounded by low-angle normal faults that are, in turn, cross-cut by high-angle normal faults (Plate 1). Present-day low-angle faults are believed to represent original high-angle normal faults that have been tilted to near horizontal during

regional extension that was concentrated over the top of post- caldera batholith-scale intrusions. High-level apexes of the post-caldera plutons intruded along an E-W trend coincident with the Precambrian structural fabric and with the south caldera margin. Fluids from these aplitic cap rocks followed the low-angle faults and deposited economically significant molybdenum mineralization.

A number of interesting geologic features are demonstrated at Questa, including: a) aspects of the intracaldera stratigraphy that indicate possible ring-vent clearing, following periods of quiescence during the caldera-filling eruption, b) a close spatial and temporal association between magmatic activity and the concentration of regional extension; c) demonstrable movements on low-angle fault planes that remained active due to pore-fluid pressures from the mineralizing hydrothermal system; and d) a structurally-controlled "Climax-type" molybdenum deposit that contains a unique high-grade core of pegmatitic minerals deposited from magma-derived fluids. The purpose of this report is to describe the geology of the Questa mining district with an emphasis on the above features. Insights gained with respect to volcanic, magmatic, tectonic and hydrothermal processes may be applied elsewhere.

PREVIOUS STUDIES AND THE HISTORY OF THIS STUDY

The region of the present study includes the southern margin of the Questa caldera and encompasses the entire Questa molybdenum mining district. The Questa molybdenum district, active since 1919, has been the focus of numerous geological investigations on both the molybdenum

deposits specifically, and on the regional volcanic and structural controls of mineral deposition. Initial studies of the mine properties included Vanderwilt (1938) and Schilling (1956). McKinley (1956, 1957) produced early quadrangle maps of the region. Ishihara (1967) conducted geological and geochemical studies and Rehrig (1969) considered the relationships of fracture patterns in the mine area to mineralization. Carpenter (1968), Clark (1968) and Clark and Read (1972) studied the greater mining district and regions to the east, and are responsible for early regional compilations. Significant studies from 1972 to 1977 were Molycorp company reports including mapping by John Landreth and Lewis Pugh, and extensive geological, geochemical and geophysical studies by the Kennecott Corporation. Work conducted by the Kennecott Corporation included a 1:2,400 scale map of the immediate mine area and 1:6,000 scale mapping of the mining district.

Beginning in 1978, Peter Lipman and others of the USGS began a regional treatment of the volcanic and igneous units that has led to "orders of magnitude" improvements in understanding the geology of the region. Among the major accomplishments of their work were the recognition of the Questa caldera and approximately cogenetic extensional deformation. Efforts by Lipman and associates include general geologic mapping (Reed et. al., 1983; Lipman and Reed, 1989), geochronologic work (Lipman et. al., 1986) and extensive geochemical analyses (e.g., Lipman, et. al., 1982) in an attempt to elucidate the overall Questa magmatic system (Lipman, 1983a; Lipman, 1984; Lipman et. al., 1986; Lipman, 1988). In conjunction with the

work of Lipman, dissertation projects were completed by Hagstrum on paleomagnetic tilting and hydrothermal resetting (Hagstrum et. al., 1982; Hagstrum and Lipman, 1986; Hagstrum and Johnson, 1986) and by Johnson on the overall petrogenesis of the Latir magmatic system (Johnson, 1986; Johnson and Lipman, 1988; Johnson et. al., 1989a, 1989b, 1990). Additionally, independent thesis and dissertation projects have been completed by Smith (1983) on the fluid inclusions and isotope geochemistry of the molybdenum mineralization, Snyder (1984) on the paleomagnetism of the mine area units, Jones (1988) on the geochemical modelling of an early complex dike swarm, and Molling (1989) on the fluid flux and chemical interactions of the hydrothermal system responsible for molybdenum deposition.

The regional work of Lipman and others led to a model of extensional deformation at Questa that closely linked caldera resurgence and regional extension. This model envisioned a "cheveron apex" geometry with listric extensional faults in the interior of the caldera down dropping blocks toward a N-S trending axis of resurgence (Lipman, 1983a,1988). The eastern and western structural margins of the caldera were envisioned as breakaway zones, the southern and northern structural margins were believed to be tear faults, and interior fault blocks were interpreted to be tilted to the east or west, away from the axis of resurgence. No listric faults were found, however in the Lipman and others mapping. Due to the complexity of the faulting and stratigraphy in relation to the regional scale

of their mapping, none of the faults responsible for tilting in the area were recognized.

Work by Questa mine personnel was strongly influenced by the model of Lipman and others (Leonardson et. al., 1983) until low-angle faults were discovered in the immediate mine area. These faults became recognized as responsible for tilting in the region and as important controls for localizing molybdenum mineralization. Recognition of low-angle faults in the immediate mine area prompted investigation by Meyer, as part of his dissertation project, to understand the style of and timing of extensional deformation in the district.

This report discusses our current understanding of the volcanic, plutonic, hydrothermal and structural history of the district. Many of the interpretations of this report are based on a recently completed 1:24,000 scale map of the Questa mining district (Plate 1) and 1:6,000 scale map of the immediate mining area (Plate 2). Significant contributions to Plates 1 and 2 were made by Jay Evans, Dave Jones, Gail Kirchner, John Landreth, Joel Metcalf, Less Osborne, Mike Schulz, Jim Shannon, and Ralph Stagan as well as the authors. This report builds on the regional research of the USGS and is based on the work of the authors as well as that of numerous past mining personnel including Steve Atkins, Gail Kirchner, Mike Schulz, Jim Shannon, Dave Jones, Less Osborne, Phil Molling, Ralph Stegan, Garry Dunlop and Virginia Starquist. Additionally, recent $^{40}Ar/^{39}Ar$ age dating by Foland and Czamanski (Czamanske et. al., 1990; Meyer and Foland, 1991) has been incorporated.

METHODS OF STUDY

Methods incorporated in this study include geologic mapping (encompassing stratigraphic, structural and petrographic studies), core logging, geochemical analysis and paleomagnetic orientation investigation. This work has been integrated with that of other researchers. Notable among the others is the mapping, geochemical and isotopic age dating work of Lipman (Lipman, 1983a, 1984, 1988; Lipman and Reed 1989; Lipman et. al., 1986), geochemical studies by Johnson (Johnson, 1986; Johnson and Lipman, 1988; Johnson et. al., 1989a 1989b, 1990), paleomagnetic work by Hagstrum (Hagstrum et. al., 1982; Hagstrum and Lipman, 1986) and $^{40}Ar/^{39}Ar$ dating by Czamanske and Foland (Czamanske et. al., 1990; Meyer and Foland, 1991).

Geologic mapping was carried out at three scales. The immediate mine area was mapped at 1:2,400, the south caldera area was mapped at 1:6,000 and the region to the east of the Red River town site was mapped at 1:24,000. The two larger scale maps were completed on high resolution (10 and/or 50 foot contour interval) base maps supplied by Molycorp Inc. Mapping in the far eastern portion of Plate 1, as well as spot mapping in regions outside of the mapping area, incorporated USGS 7.5 minute quadrangle topographic base maps. Areal photographs of varying scales also were incorporated locally as base maps. Greater than 800 m of topographic relief in the map area allows surface inspection of a significant 3-dimensional spectrum. In addition, diamond drill hole logs

and underground mine workings maps were included wherever possible for geologic control of cross-sections.

Although hydrothermal alteration of Tertiary igneous rocks is extensive in the south caldera region, several analytical studies were undertaken on the least altered rocks. Geochemical analysis of a relatively unaltered suite of the intrusive and volcanic stratigraphy was performed by Bondar-Clegg of Vancouver, British Columbia using the methods described in Table 1.

$^{40}Ar/^{39}Ar$ age dates were obtained on a number of samples from the south caldera region by Ken Foland of Ohio State University. Methods of $^{40}Ar/^{39}Ar$ analyses are described in Foland and others (1984, 1989), Czamanske and others (1990) and Meyer and Foland (1991). Paleomagnetic orientation analyses were performed on a number of samples, including many of the intrusive samples that were Ar-Ar dated, in an attempt to better define the timing of tilting and intrusive events. Alternating field demagnetizations were performed on a Molespin magnetometer at UC Santa Barbara.

REGIONAL SETTING AND GEOLOGIC HISTORY

The Questa caldera of the Latir volcanic field is located on the eastern flank of the Rio Grande rift in the Sangre de Cristo Mountains of northern New Mexico (Fig. 2). The Latir volcanic field is mid-Oligocene to earliest Miocene in age; slightly younger than the majority of volcanism in the nearby San Juan volcanic field of southern Colorado. The Latir volcanic field lies near the intersection of the modern Rio Grande rift with the

Jemez lineament, a structural zone of Precambrian ancestry that is best expressed by a line of volcanos that extends from southeastern Arizona to northeastern New Mexico (Fig. 3).

The Sangre de Cristo Range is underlain by amphibolite-grade Precambrian units that are part of an arc-related igneous and sedimentary package accreted onto the Wyoming craton between 1790 and 1650 Ma (Reed et. al., 1987). Regional units include an arc-related metaigneous suite (1765-1720 Ma), rift and/or shelf related metasediments (1720-1690 Ma), and finally arc-related metavolcanic and metasedimentary units (1660-1650 Ma)(Williams, 1990). Units in the Questa area include: a) parts of the older metaigneous suite, located south of the Precambrian shear zone (Grambling et. al., 1988; Plate 1); b) younger (1720-1690 Ma) metasediments, located north of the Precambrian shear zone (Grambling et. al., 1988; Plate 1); and c) a 1699 Ma pluton.

From late-Paleozoic to Mesozoic, the Questa region was located at or near the eastern margin of the Uncompahgre-San Luis highland (Fig. 3). Although no Paleozoic sediments were deposited or preserved in the immediate mining district area, thick pre-Tertiary sections have been preserved 6-10 km to the southeast of the Red River townsite. Sediments in the Questa area previously believed to be Paleozoic age are now interpreted to represent a hydrothermally altered Eocene unit (Lipman, 1983a). The re-interpretation of this unit implies a more extensive Uncompghre-San Luis highland along its southeastern boundary than was previously believed (Fig. 3).

Although no evidence of Laramide-age structures was found in the map area of Plate 1, the region is situated in a general zone of east-vergent, block fault-style, Laramide compressional structures that are located throughout much of the Sangre de Cristo Mountains. Thick sections of Cretaceous and Tertiary foreland basin sediments (e.g. the Raton and Poison Canyon Formations) exist to the east. These basins are probably related to Laramide thrust faults in the Moreno Valley area, east of the Questa district (Fig. 3; Plate 1 of Clark and Read, 1972). Paleocene to Eocene erosion of Laramide highlands resulted in deposition of locally-derived conglomerates and sandstones of Precambrian provenance in the south caldera area (Tcg/Ts of Plate 1)(Lipman, 1983a).

Recent awareness of the importance of Tertiary extensional tectonics has led to a reinterpretation of some structures previously mapped as Laramide. Unequivocal thrust faults of Laramide age exist in the Blue Lake area, 8 km south of the town of Red River, and along the east side of the Moreno Valley, approximately 7 km east of Red River (Clark and Read, 1972). Previously mapped thrust faults between these two areas have recently been reinterpreted as representing complex depositional and extensional fault-related contacts rather than thrust faults (Lipman and Reed, 1989; Meyer and Frost, unpublished mapping) . These reinterpreted faults are the "Lost Lake thrust fault" (Clark and Read terminology) near Lost Lake (Lipman and Read, 1989) and the "Blue Lake thrust fault" (Clark and Read terminology) in Commanche Creek (Meyer and Frost, unpublished

mapping). A regional re-examination of all Laramide structures with an appreciation for the significance of extensional overprinting is warranted.

An Eocene peneplain developed across all of the central and southern Rocky Mountain region immediately after the Laramide orogeny (Epis and Chapin, 1975). The climate during this episode was wet and temperate, and fossil floras in the region indicate that elevations were from 1500 to 3000 m lower than the present day (Axelrod and Raven, 1985). Onto this peneplain were erupted the great Oligocene volcanic fields of southern Colorado (Epis and Chapin, 1968; Steven, 1975; Steven and Lipman, 1976), fields of lesser volume in northern New Mexico including the Latir and Ortiz volcanic fields, and the extensive Mogollon-Datil volcanic field in southwestern New Mexico (Elston, et. al., 1976). Magmatic activity in the Latir volcanic field corresponds in time to the beginning of significant crustal extension in the region (Chapin and Seager, 1975; Tweto, 1979; Price and Henry, 1984; Chamberlin, 1978, 1983).

Extension along the Rio Grande rift is divided into two periods; *early* and *modern* Rio Grande rift extension. *Early* Rio Grande rift extension refers to a period of extension beginning between 32-28 Ma and ending 17-10 Ma (Chapin and Seager, 1975; Tweto, 1979; Price and Henry, 1984; Chamberlin, 1978, 1983). During this time a broad region extending from the southern Rocky Mountains to Mexico experienced approximately 30 percent extensional strain about a NE-SW to ENE-WSW extensional axis (Morgan et. al., 1986). This extension affected a region much wider in an east-west direction than the modern Rio Grande rift depression. The style

of this extension is characterized by NNW-striking block faults and half grabens (NNW-striking faults of Fig. 2).

The timing of early Rio Grande rift extension roughly corresponds to the initiation of extension throughout much of the southwestern United States. The existence of this zone of extension in a province located to the east of the "stable" Colorado plateau has been hypothesized to be the result of thermal weakening of the region due to a N-S trending belt of Oligocene volcanism (Lipman, 1981). A further implication of this model is the suggestion that local magmatic centers, such as the Latir volcanic field, have thermally weakened the crust, resulting in concentration of extension into local regions of greater than 100 percent extensional strain (Morgan et. al., 1986). Details of the degree and style of extensional block faulting, and the relationship between this faulting and higher-strain extensional areas is poorly known for the Southern Rocky Mountains. This is due to a combination of poor outcrop exposure in vegetated terrain in comparison to most of the Basin and Range province, and to a sparsity of mapping in the southern Rockies since the recognition of the style and significance of regional extension throughout the southwestern United States.

On a plate tectonic scale, it has been suggested that the Oligocene magmatic activity of the Rocky Mountain region is the result of the flat subduction of the Farallon slab about 1200 km (without taking into account later Basin and Range extension) to the west (Lipman et. al., 1972; Christiansen and Lipman, 1972). Accordingly, the Oligocene change from calc-alkaline magmatism to Basin and Range style extension may be part of

a westward sweep in magmatic activity due to the foundering of the flat subducting slab as the East Pacific Rise approached the North American continent (Coney and Reynolds, 1977). Further refinements of this model place the high-silica alkali-rich magmas associated with high-grade Rocky Mountain molybdenum deposits into a specialized petro-tectonic space, which is situated in the transition from subduction-related to extension-related magmatism (Bookstrom, 1981).

Following this period of Oligocene magmatic and tectonic activity is a period from 20-13 Ma that has been considered a magmatic "lull" over the Rio Grande rift region (Chapin, 1979). Recent isotopic age dating by Lipman and others (1986) demonstrates, however, that there were at least moderate amounts of mafic volcanic activity during this time span in the rift north of Questa.

The *modern* Rio Grande rift began forming between 10 and 17 Ma ago as indicated by the accumulation of voluminous sediments derived from Precambrian rift-flanking highlands (Izett, 1975). The major feature of the Rio Grande rift is not the rift valley itself, but the broad uplifts that flank the rift valley (Eaton, 1986). Eaton (1986) named the Rio Grande rift and its flanking uplifts the Alvarado rise and noted the similarity in profile of this uplift to profiles of the mid-Atlantic ridge. Eaton suggested that the Alvarado rise is due to a late-Miocene upwelling of mantle asthenosphere (e.g. Parker et. al., 1984) resulting in the present-day elevation of the southern and central Rocky Mountains . This hypothesis is in stark contrast to a previous hypothesis that states that the high

elevation of the Rockies results from a thick crustal root that was formed by Laramide compression (still cited widely in modern textbooks).

The axial valley of the Rio Grande rift runs from central Colorado into Mexico and, in the vicinity of Questa, is comprised of a series of oppositely-directed half-graben basins (Chapin, 1979). At Questa, the San Luis Valley - Taos Plateau segment of the rift is hinged on the west and a west-dipping normal fault with an estimated 7-8 km of throw delimits the eastern rift boundary (Lipman and Mehnart, 1979). Additionally, near Questa, a N-S striking, mid-rift horst block exposes pre-rift volcanic units of the Latir volcanic field (Thompson et. al., 1986).

Regional variation in mid-Miocene to Holocene uplift of the rift-flanking Sangre de Cristo Mountains has resulted in exposure of a north to south crustal profile in the Sangre de Cristo Mountains (figure 3 of Lipman, 1988). In the north, where there has been relatively minor uplift, "modern" rift-related basaltic andesites cover outflow facies Amalia Tuff of the Questa caldera. In the south, there has been approximately 7-8 km of uplift, and the pre-erosional base of the Oligocene volcanic section is projected to be at an elevation of greater than 7400 m. In the southern portion of the Questa caldera, intermediate amounts of uplift and subsequent erosion have exposed the middle and lower structural levels of the caldera system.

The tholeitic to alkalic Taos plateau volcanic rocks, which post-date much of the modern rift structural activity, range in age from 5 to 2 Ma and are comprised of a range of compositions and land forms from basaltic

shield volcanos to rhyolite and rhyodacite domes (Lipman and Mehnert, 1979). Similar-aged (10 Ma to present) alkaline volcanic activity occurs along the trend of the Jemez lineament from eastern Arizona to northeastern New Mexico.

LITHOLOGIC DESCRIPTIONS

The stratigraphy at Questa consists of a Precambrian basement overlain by early Tertiary sediments and the Oligocene volcanic sequence of the Latir volcanic field (Fig. 4; Tables 2a and b). The Latir volcanic field consists of a thick sequence of pre-caldera intermediate-composition volcanic rocks that are part of a calc-alkaline trend, followed by a peralkaline-affinity suite of volcanic units that culminated in formation of the caldera-forming Amalia Tuff. Intrusions are associated with pre- and syn- caldera volcanism. Post-caldera igneous activity consists of batholith-scale intrusions with only sparsely-preserved volcanic equivalents. Post-caldera intrusions migrated from north to south over a 7 m.y. interval (Czamanske et. al., 1990).

Precambrian units

The Questa mining district is at a major E-W striking boundary between Precambrian rock types with meta-sedimentary units to the north and meta-igneous units to the south. The contact between rock types is covered by Tertiary volcanic cover, but may represent a deep-seated Precambrian-aged fault zone that influenced later magmatic and structural events.

Precambrian units in the southern portion of the map area consist of mafic schist and gneiss, amphibolite, amphibolite schist, felsic schist and two wide-spread quartz monzonite to granitic plutons (Tab. 2a). Protoliths for the schists and gneisses are dominantly mafic volcanic and volcaniclastics (Lipman and Reed, 1989) with local diorites and gabbros. Foliation in this unit ranges from weak to strong and is steeply dipping, E-W to ENE striking (Plates 1 and 2; Lipman and Reed, 1989). A somewhat unique, highly foliated quartz, feldspar, ±biotite, ±hornblende, ±garnet, ± magnetite schist is exposed in and near the underground workings of the Southwest ore zone (Plate 1 and Fig. 5) near the contact with the meta-sedimentary package to the north. This unit is in high-angle fault contact with quartz monzonite to the south and appears to be a tectonically emplaced sliver of highly foliated rock at the meta-sedimentary / meta-igneous boundary. Amphibolites and amphibolite schists likely represent metamorphosed mafic plutonic rocks and local related volcanic and volcano-sedimentary units (Lipman and Reed, 1989). Felsic schists are highly foliated and contain quartz and feldspar phenocrysts indicative of a probable felsic volcanic protolith, possibly representing a metamorphosed tuff. U-Pb zircon analyses of similar units a few km to the south have upper concordia intercept ages of 1765 Ma (error not reported; Lipman and Reed, 1989).

The above units are extensively intruded by non- to strongly-foliated porphyrytic granite to quartz monzonite bodies that contain local pegmatites. The intrusive body in the region of the mine is the quartz

monzonite of Columbine Creek, while the intrusive mass near and east of the Red River town site is termed the quartz monzonite of Old Mike Peak (Lipman and Reed, 1989). The Old Mike Peak intrusive body near Red River is similar to the Columbine Creek body, but contains a high proportion of associated aplitic phases. Upper intercept concordia dates of 1730 ±10 Ma and 1699 ±2 Ma are reported for the Columbine Creek and Old Mike Peak intrusions respectively (Lipman and Reed, 1989; Reed et. al., 1987). The bulk of the Columbine Creek quartz monzonite in the mine area is non- to poorly foliated, but local regions of E-W oriented shear within this body contain mylonitic fabrics (Kirchner, unpublished report for Molycorp Inc., 1983).

Quartzites, mica gneisses and schists of metasedimentary provenance are in the northern portion of the mining district. A U-Pb date of 1713 (± error not reported) on euhedral zircons in a correlative quartzite in San Cristobal Canyon, about 10 km south of Questa, is interpreted to represent syn-sedimentary volcanic input (Aleinikoff et. al., 1985). If this represents the date of sedimentation, the metasedimentary package lies between the early and later phases of quartz monzonite intrusive activity. Mapping relationships between the Old Mike Peak quartz monzonite and quartzite in lower Mallette Canyon permissively support this interpretation (Plate 1).

All of the above units are overlain by, and included as clasts in, the locally-derived Eocene sediments described below.

Precambrian to Paleozoic intrusions

Local diabase dikes (Od of Plate 2 and Tab. 2a) tentatively dated at 500 Ma (Rb-Sr isochron on similar dikes to the north; Reed, 1984) intrude the Precambrian units immediately south of the Southwest ore body (Fig. 5). These dikes are volumetrically minor and have steep dips with E-W strikes.

Early Tertiary sediments

An early Tertiary red bed unit overlies the Precambrian basement in the western half of the mining district (Fig. 4; Plates 1 and 2; Tab. 2a). This unit is composed entirely of Precambrian source rocks and grades upward from a coarse grained conglomeratic base (Tcgc of Plate 2) into an upper sandstone with local siltstone beds (Ts of Plates 1 and 2).

Unit thicknesses range from 0-125 m. Individual clasts in the basal conglomerate are as large as one meter in diameter and angular clasts are common at the base, indicating that the sediment is locally derived. North of the mine, the sediment is dominantly composed of weathered products of the local quartzite and mica gneiss basement. South of the mine, the conglomerate is dominated by clasts derived from the underlying meta-igneous basement. Cross-bedding and imbrication indicate that the source region is to the east.

This sediment serves as an invaluable marker unit. Reliable stratigraphic-upward and paleohorizontal indications are provided by bedding, clast imbrication, grading, channelling and cross-bedding. Careful mapping of the distribution and bedding attitudes of this unit provide a

great deal of the control necessary to resolve the scale of mid-Tertiary tilting and extensional faulting at Questa.

Regionally, the early Tertiary sediment is red and poorly indurated, but in the vicinity of the mine the sediment is red to grey and is well indurated due to thermal metamorphism (Lipman, 1983a). The well indurated nature of this conglomeritic deposit in the mine area caused earlier workers to correlate this unit with the Permian-Pennsylvanian Sangre de Cristo formation to the south and east (McKinley,1957; Carpenter, 1968). Regional mapping by Lipman and others (Lipman, 1983a; Reed et. al., 1983; Lipman and Reed, 1989) however, has led to the correlation of this unit with the Eocene Vallejo Formation of Upson (1941) and other Eocene continental sediments of the Rocky Mountain region. In the mine area, the early Tertiary sediment was probably derived from basement-cored Laramide thrust faults immediately to the east (Fig. 3).

Early volcanic series (including related intrusions)

The earliest volcanic activity in the region consists of an intermediate composition, calc-alkaline field that extends throughout the mining district (Lipman, 1988). This early volcanic field ranges in age from approximately 28.5 to 26 Ma (K/Ar and fission track dates, Lipman et. al. 1986; and $^{40}Ar/^{39}Ar$ dates, Czamanske et. al., 1990) and pre-dates the eruption of the Questa caldera. Similar patterns of long-lived volcanic fields culminating in batholithic-scale pluton development and caldera eruption are observed in the nearby San Juan Mountains, as well (Lipman et. al., 1978).

The flows are massive and thick, indicating proximity to vents. Vent areas are interpreted to exist near the Red River town site, where sub-volcanic intrusions predominate (Plate 1). The early volcanic series consists of: 1) local volcanic-derived sediments; 2) a low-silica rhyolite tuff; 3) voluminous andesite to quartz latite porphyry flows; and 4) hypabyssal quartz latite intrusions (Fig. 4). Volcanic-derived sediments are volumetrically minor in the district (Plate 1) becoming more abundant in the outlying portions of the volcanic field.

low-silica rhyolite tuff

A tuff unit that is commonly lithic rich (Tlt) is often located near and/or at the base of the andesitic pile. This unit has a uniform low-silica rhyolite composition, but varies from lava flows to tuffs (Tab. 2b). Location of this unit at multiple levels within the volcanic stratigraphy and textural variability indicate that the Tlt represents more than one depositional unit, probably emanating from a volcanic source region that was active during the time of andesitic volcanism. Rhyolitic lava domes in the region of Tetilla Peak, immediately east of the margin of Plate 1, are likely sources of these deposits (Lipman, 1983a).

andesite to quartz latite porphyry flows

The vast majority of the pre-caldera volcanism is represented by a sequence of massively bedded andesite (Tan of Plate 1; Tab. 2b) overlain locally by massive quartz latite flows (Tql of Plates 1 and 2; Tab. 2b). K/Ar dates on these units range from approximately 27 to 28.5 Ma (Lipman et. al., 1986). For mapping purposes, any unit containing less than 2 mm

plagioclase phenocrysts is considered andesite porphyry. Compositionally, this grouping ranges from 54-68 % SiO_2 (Tab. 1), with the majority of the unit being andesitic. Thickness of the andesite porphyry unit (Tan and Tanq) is between 1 and 2 kilometers. Flow foliations and bedding contacts are scarce due to the massive, near vent nature of the deposits (Fig. 6).

Quartz latite porphyry flows (Tql of Plates 1 and 2) overlie andesite in much of the region, but are rare in the mining district, which may have been located between flow dome complexes. In the mining district, quartz latite porphyry only overlies the andesite in the extreme northern area, along the northern margin of Plate 1. These exposures likely represent the southern margin of a thick latite dome complex located further to the north in the Latir Mountains (Latir Peak Quartz latite of Lipman, 1983a; Reed et. al., 1984; Lipman and Reed, 1989).

Quartz latite porphyry megabreccia blocks are extremely abundant in the intracaldera fill of the overlying Amalia tuff (Fig. 6). These landslide blocks are interpreted to have slumped off of the southern caldera wall, implying northward transport of blocks on the order of a few kilometers. Although later obliterated by tectonic uplift and erosion, a pre-caldera quartz latite dome complex is interpreted to have existed south of the mine area along the southern margin of Plate 1. Some of these quartz latite composition megabreccia blocks may have been eruptive equivalents to the quartz latite porphyry intrusive complex observed near Red River (Plate 1). Texturally and compositionally, the quartz latite flow unit is very similar

to the quartz latite intrusive suite (Tables 1 and 2b) and the two are considered to be intrusive-extrusive equivalents.

Very local laharic breccia deposits are located in the volcanic stratigraphy and as local megabreccia blocks in the Amalia Tuff (Tlh of Plate 2). The extreme scarcity of deposits of this type attests to the near vent nature of the pre-caldera volcanic pile.

hypabyssal quartz latite intrusions

Quartz latite porphyry dikes are scattered throughout the mining district and a major quartz latite porphyry intrusive center exists in the area surrounding the Red River town site (Fig. 6)(Plate 1). This center is a high-level composite intrusive body consisting of stocks and composite dikes, probably representing the eroded sub-base of a volcanic center. Deeper-level portions of this composite intrusive body are coarser grained and more felsic, locally becoming a quartz monzonite porphyry. Sample 82QC44 from a quartz monzonite porphyry phase of the Red River intrusive system yields a biotite $^{40}Ar/^{39}Ar$ discordant plateau age of 26.1 ±0.3 Ma (Czamanske et. al., 1990).

All of the dikes in the western portion of the district and the major portion of the Red River intrusive body are quartz- and orthoclase- poor latite porphyries (Tqli of Plates 1 and 2; Tab. 2b), whereas stocks and dikes of distinctive quartz and orthoclase bearing latite (Tqlo and Tqlk) occur in addition to Tqli intrusions in the eastern portion of the district (Plate 1; Tab. 2b). Quartz latite porphyry stocks and dikes in the Hottentot scar area have distinctive resorbed quartz phenocrysts (Tqlo) and have previously

been considered to be rhyolites related to the post-caldera magmatic system (e.g. Carpenter, 1968; Lipman and Reed, 1989). Field relationships (Plate 1) and geochemical data (Tab. 1) suggest, however, that these intrusions are strongly altered phases of the pre-caldera quartz latite porphyry intrusive system.

pre-caldera basaltic andesites

Basaltic andesite and xenocrystic basaltic andesite (Txba; Tab. 2b) underlies outflow Amalia Tuff 20 km to the north of the mining district at Cedro Canyon. These basaltic andesites do not underlie the intracaldera tuff in the mining district, but are found locally as megabreccia blocks in the tuff (Txba of Plate 2). As was the case with the quartz latite porphyry flows above, the basaltic andesites are interpreted to have slumped into the caldera from south of the southern caldera wall. The source region currently has no basaltic andesite exposures because erosion has removed the Tertiary volcanic pile to the south of the caldera.

These basaltic andesites are similar to xenocrystic and non-xenocrystic basaltic andesites found in other regions of the Rio Grande rift (e.g. Hinsdale Formation of the San Juan Mountains, Lipman and Mehnart, 1975). The approximate 26 Ma age of the Questa basaltic andesites is similar to the age of the beginning of basaltic volcanism in the southern Rocky Mountain region (Lipman and Mehnart, 1975).

Later volcanic series (and related intrusions)

Following intermediate composition, calc-alkaline volcanism, magmatic activity became weakly peralkaline. In the mining district, this

activity consisted of Amalia Tuff and a tuff-related quartz latite to rhyolite porphyry dike suite (Fig. 4). In the greater Questa region, this activity also included pre-caldera commenditic lavas, (immediately east of Plate 1)(Lipman, 1983a) and epizonal peralkaline phases central to the caldera that are interpreted to represent resurgent non-erupted Amalia Tuff magma (Johnson and Lipman, 1988; Johnson et. al. 1989b).

The Latir volcanic field and the nearby San Juan volcanic field were similar in their magmatic development through time. In both systems, caldera-style volcanism and associated batholith-scale magmatism followed regional composite-style volcanism. Questa magmatism differs significantly from the San Juan Mountains, however, in that caldera-style volcanic activity did not remain calc-alkaline, but switched for a brief time to a bimodal peralkaline association. This switch in magmatic chemistry has been attributed to alkaline basalt injections related to the initiation of Rio Grande rift/Basin and Range-related extension (Lipman, 1983b; Johnson and Lipman, 1988).

Amalia Tuff

The Amalia Tuff is a >500km^3 high-silica peralkaline rhyolite (Tables 1 and 2b) that erupted from the Questa caldera at 25.7 ±0.1 Ma (sanidine $^{40}Ar/^{39}Ar$; one standard deviation error; Czamanske et. al., 1990; Meyer and Foland, 1991). The Questa caldera is shallowly eroded along its northern border and deeply eroded along its southern boundary; thus shallow volcanic to deeper plutonic levels of the same magmatic system are exposed. This wide range of exposure allows investigation of geochemical and

petrogenetic linkage between volcanic and cogenetic plutonic rocks (Johnson and Lipman, 1988; Johnson et. al., 1989b, 1990), and allows study of the structure and stratigraphy of the deeper-level portions of a caldera system.

Questa caldera

The Questa caldera is approximately 14 km in diameter as measured in a N-S direction, perpendicular to the axis of later extension (Fig. 2). Evidence for a caldera in this region includes the 2 km thickness of the densely welded tuff and the abundant megabreccia blocks characteristic of intracaldera units elsewhere (Lambert, 1974; Lipman, 1976, 1983a, 1984).

The southern structural margin is interpreted to be a linear fault zone, 1-2 km wide, that nearly straddles the course of the Red River for much of its length (Fig. 7). Evidence for the location of the southern margin in this area includes: 1) a southward thickening wedge of megabreccia blocks in the intracaldera fill, indicating proximity to the south caldera wall (Plate 1); 2) an E-W trending zone of distinctive peralkaline affinity dikes (Fig. 7); and 3) local E-W striking, high-angle faults that are interpreted to represent step-wise caldera ring structures (Fig. 7). The southern structural boundary appears to be linear, paralleling the E-W to NE trending Precambrian structural fabric in the southern portion of the mining district.

The northern structural boundary is defined by a 3-4 kilometer long segment of a peralkaline affinity ring dike that intrudes Precambrian units (Lipman and Reed, 1989). The lack of evidence for significant offset along

the northern ring fault and the extreme thickness of the intracaldera tuff within the mining district caused Lipman (1983a) to conclude that maximum collapse was along the southern caldera margin.

The eastern boundary of the caldera is poorly defined, but correlates with a thickening of the intracaldera unit. The western boundary of the caldera is hidden under lavas and sediments of the modern Rio Grande rift. If one assumes that the caldera was originally equidimensional and takes into account the >100% extension that post-dates eruption, the western margin of the caldera would be located immediately west of the modern course of the Rio Grande. The southwestern structural margin of the buried caldera may, in fact, be located in the Brushy Mountain horst block (Thompson et. al., 1986) where outcrops of Amalia Tuff and younger rhyolite porphyry domes lie on the southwestward projection of the southern caldera margin. If this is the case, the southern structural margin of the caldera would have originally been linear over a distance of 15-20 km.

Caldera floor exposures in the Questa region suggest that the floor did not drop as a completely coherent plate, as had previously been assumed (Lipman, 1984). The caldera floor is exposed in two places in the mining district due to 90º westward tilting of the volcanic stratigraphy by later extension (Fig. 7). The western exposure of the caldera floor appears to be relatively coherent, but the eastern exposure of the floor exhibits a cross-sectional outcrop pattern that suggests horst and graben structures (Fig. 7). Two lines of evidence support the idea that this outcrop pattern

represents faults that were active during or shortly after the time of caldera collapse: 1) Amalia Tuff immediately west of the faults (originally immediately above them) exhibits rheomorphic flowage (Fig. 7); and 2) caldera -related and younger dikes in the floor of the caldera are oriented ENE and parallel the projected continuation of these faults into the caldera floor (Fig. 7 and Plate 1).

Outflow tuff

The outflow sheet of the Amalia Tuff is a regionally distinctive high-silica rhyolite tuff that is weakly peralkaline (Tab. 1). This unit is found as far as 45 km to the SW, across the modern Rio Grande rift, and exists as both single and local compound cooling units. In an outcrop area 10 km south of Questa, an anomalously crystal poor, bedded unit, containing local accretionary lapilli has been interpreted as representing a co-ignimbrite ash deposit (Fig. 8). The great thickness of this deposit, relative to the ash flow, suggests that some fluvial reworking of the ash material is possible, as well. This unit overlies the Amalia Tuff and has the same distinctive incompatible trace element chemistry (Fig. 15). This ash deposit is currently preserved in half-graben structures (Fig. 8). In order to preserve these easily erodible ash deposits, these half-grabens were probably active during or slightly after the time of ignimbrite eruption.

Petrographic, geochemical and isotopic studies by Johnson (Johnson and Lipman, 1988; Johnson et. al., 1989b, 1990), particularly on well exposed vertical sections of the tuff to the NE of the caldera, demonstrate minor amounts of major element zoning and large amounts of trace element

and isotope zonations. The last erupted Amalia Tuff is geochemically equivalent to high-level intrusive phases exposed in the center of the caldera. These central intrusions are interpreted to represent unerupted Amalia Tuff magma that is subsequently being uplifted as resurgent intrusive phases (Johnson and Lipman, 1988; Lipman, 1988; Johnson et. al., 1989b,1990).

Exposures of the outflow unit in the map area (Plate 1) are poor and often structurally complex and non-diagnostic. The largest outcrop region of outflow tuff, located near the eastern margin of Plate 1, is problematical. High-angle normal faults (cross-section in Plate 1) have been inferred in order to keep the unit from approaching thicknesses that are typical of intracaldera units. These high-angle faults are not mappable on the surface, but are in keeping with the structural style of the region. It should be kept in mind, however, that should there be no fault repetition, the tuff in this region would be better interpreted as an intracaldera unit.

Intracaldera tuff

Post-caldera extension and tilting has resulted in 3 well-exposed cross-sectional views of the intracaldera tuff (Fig. 7 and Plate 1). The structurally corrected thickness of this intracaldera unit is at least 2.5 km in the western exposure, and the entire vertical extent of the tuff demonstrates no mineralogic or chemical zonations. Intracaldera tuff in the district is identical to the first-erupted tuff outside of the caldera, implying that collapse occurred early in the caldera eruptive cycle.

Welding and devitrification textures are dominated by proximity to megabreccia blocks, which have acted as heat sinks (Fig. 9; Lipman, 1983a). The majority of the intracaldera tuff is granophyrically devitrified and has pumice flattening ratios $\geq$10 to 1 (Figs. 9 and 10). Within the vicinity of megabreccia blocks, glassy-looking pumice is common and flattening rations are generally less than 10 to 1 (Figs. 9 and 10). Additionally, areas near megabreccia blocks are anomalously rich in lithic fragments. Typical outflow Amalia Tuff contains <0.5 percent lithic fragments, typical intracaldera tuff contains 0.5 to 1 percent fragments, and areas adjacent to blocks can contain up to 10 percent lithic clasts (Fig. 9).

Local areas of rheomorphic flowage within highly welded tuff may be spatially associated with underlying caldera-floor faults that were active during or slightly after caldera collapse (Fig. 7). This may be similar to areas of remobilized tuff interpreted to overlie caldera floor faults in the Bachelor caldera (Lipman, 1984).

Intracaldera megabreccia

Intracaldera megabreccia blocks form a significant volume of the caldera fill. These blocks are interpreted to represent landslide blocks that have slumped off of the oversteepened southern structural wall of the caldera (e.g. Lambert, 1974; Lipman, 1976, 1983a).

Variation in the distribution of the megabreccia blocks parallel to the south caldera margin is evident by comparing more easterly and westerly cross-sections of the intracaldera fill (Fig. 3; and Plate 1). In the SW section, megabreccia blocks are dominantly of andesite and quartz latite

flows and the blocks are concentrated near the base of the section. In the south-central portion of the caldera, intrusive quartz latite porphyry blocks are abundant as well, and the megabreccia facies is located higher in the intracaldera stratigraphy (Fig. 11).

The caldera block litholigies are presumed to record the wall-rock along the southern caldera margin at the time of collapse. Although source volcanic units to the south and west of the caldera margin have subsequently been eroded, an andesite and quartz latite flow stratigraphy can be assumed. To the south and southeast of the caldera, quartz latite intrusions were also abundant, probably representing higher-level portions of the intrusive complex that is centered near the red River town site. (Plate 1). This intrusive center may have been more massive and resistant to slumpage than more distal flows. Ring faulting through this resistant mass may have formed a structurally oversteepened wall that resisted slumpage until later in the caldera fill cycle, resulting in blocks that are located higher in the caldera-fill stratigraphy.

Radial variation in megabreccia block distribution and in facies of the megabreccia is evident, as well. Close to the southern caldera wall, the megabreccia unit thickens abruptly. Welding and devitrification in the intracaldera tuff become less well developed to the south, as well, presumably from the greater abundance of megabreccia block "heat sinks" (Lipman, 1983a). With increasing distance from the caldera wall, megabreccia blocks become smaller and more rounded, and a greater range of the available pre-caldera stratigraphy is found in the blocks.

In cross-sectional view, individual lenses of landslide megabreccia extend from the south caldera wall (Fig. 11). Preservation of these individual lenses at Questa and elsewhere (e.g. Hon, 1987) indicates that the megabreccia blocks do not fall into the middle of, or sink into the bottom of, an ignimbrite "soup", but float at or relatively near to the top of the partially inflated ignimbrite.

The breccia block sizes range from near 1 km diameter down to cm scale (compare large blocks in Plate 1 with Fig. 12a and b). Large megabreccia blocks (megabreccia of Lipman, 1976) are mapped by their individual rock types (Plates 1 and 2) and regions with smaller-than-outcrop sized blocks are mapped as rhyolite tuff breccia (Trtbx; Tab. 2b; mesobreccia of Lipman, 1976). Larger blocks can be seen in the process of breaking into smaller blocks during transport, and large blocks often are surrounded by aprons of Trtbx debris (Fig. 9b and Plate 2).

Abrasion between blocks during transport is believed to have been significant, as is evidenced by the lack of pumice in the tuffaceous matrix of the Trtbx unit (Tab. 2b). Different block types appear to have been able to resist abrasion during transport to various degrees. Basaltic andesite and minor interbedded volcanic sediments decompose readily during transport and contributed large components of less than mm sized material into the tuffaceous matrix (Fig. 12b). Locally, mechanical mixing of disaggregated block material with the tuff has occurred to such a degree that the original tuffaceous matrix is nearly unrecognizable.

Basal broken crystal zone

A distinctive unit termed the basal broken crystal zone (Trtb in Plate 2; Tab. 2b) has been identified in the intracaldera tuff. Descriptions of units similar to this have not been previously given in the literature. This unit consists of a massively bedded phase of the intracaldera tuff that is distinguished by containing anomalously high amounts of broken phenocrysts (Fig. 13) and by being located almost exclusively on the tops of megabreccia blocks and block lenses (Fig. 11). This unit contains anomalously low amounts of pumice (1-10%) and from 3 to 20% andesite porphyry, quartz latite porphyry and rhyolite porphyry xenoliths. The rhyolite porphyry xenoliths are variable in texture and are interpreted to have originally been high-level dikes related to the Amalia Tuff (Fig. 14). Contacts between this unit and the overlying tuff can be either sharp or gradational.

These deposits are interpreted to represent the initial vent clearing phases ignimbrite eruption following pauses in the eruptive cycle (Fig. 14). The mechanism of breakage of the phenocrysts is not clear. Breakage requires either steep gradients in pressure or temperature, an eruption with a high proportion of crystal-crystal impacts, or explosive fragmentation of an partially solidified mass. A hydrovolcanic component to the eruption might conceivable aid the above, however the high degree of hydrothermal overprinting on the deposits at Questa thwarts any attempts at classification by shard shape analysis.

The location of these deposits at various stratigraphic levels within the ignimbrite suggests ignimbrite eruption from various vent sources through time. Each new basal broken crystal unit *could* be correlative to a new stage of migration of the vent around the structural perimeter of the caldera (Fig.14a, b and c)(Hildreth and Mahood, 1986). The variously textured rhyolite porphyry xenoliths would then be best interpreted as early-stage ring-dikes that were subsequently entrained in the ring-vent eruptions (Fig. 14c).

Basal broken crystal zones are tentatively interpreted to represent deposition from the relatively high-concentration leading edge of a pyroclastic flow (Fig. 14c) rather than depositing from a pre-ignimbrite or ignimbrite-related low-concentration surge. This is supported by the relatively massive nature of the deposits, suggesting en masse emplacement from a high-concentration flow. Additionally, local gradational contacts with the main body of the overlying tuff suggests emplacement from the same depositional unit. Granularmetric analyses, which might conceivably aid in the classification of this deposit (e.g., Cas and Wright, 1987), have not been carried out due to induration and overprinting hydrothermal alteration.

The location of basal broken crystal zones on the tops of megabreccia blocks provides insights into the timing of the caldera-forming eruption relative to structural collapse and landsliding events. Discrete megabreccia block lenses in the tuff imply either: 1) steady-state (constant rate) eruption and non-steady-state collapse (and/or

landsliding), 2) non-steady state eruption and steady-state collapse, or 3) non-steady state eruption and non-steady-state collapse. The occurrence of basal broken crystal zone anywhere in the intracaldera fill indicates vent initiation and non-steady state eruption. The location of these basal broken zones on the top of megabreccia block lenses implies that vent initiation followed a period of time (*possibly* on the order of days) during which eruption had ceased and landslide debris from the oversteepened wall was allowed to accumulate on the partially welded tuff. Such time gaps *may* be correlatable to cooling breaks in compound cooling units of outflow sheets.

The preservation of basal broken crystal zones may only be possible in local domains within the caldera fill, as significant transport may result in mixing with the volumetrically dominant overlying tuff (Fig. 14d). Such deposits may not have previously been noticed in other caldera systems due to their relatively specialized mode of occurrence, their volumetric insignificance and to the scarcity of deep-level caldera-fill exposures in the geologic record. The recognition and study of less-altered equivalent deposits elsewhere, could provide a better understanding of the mechanisms of formation and significance of this unit and may aid in the understanding of caldera collapse processes in general.

Caldera-related intrusions

A suite of early intrusions ranging in composition from 65-77% SiO_2 is believed to be part of the same magma system that is responsible for eruption of the Amalia Tuff. Evidence for the association with the Amalia

Tuff is: 1) temporal - the intrusions pre-date later extension in the region and post-date intermediate composition pre-caldera magmatism; 2) spatial - the intrusions are concentrated along an E-W striking zone interpreted to correlate to the southern structural margin of the caldera; 3) geochemical - the intrusions have similar high incompatible trace element chemistries to the Amalia Tuff (Tab. 1 and Fig. 15); and 4) lithologic - one of the dike suite units (Trff of Plate 2) has a similar phenocryst population to the tuff, and one dike of this low-phenocryst unit exhibits eutaxitic foliation, suggesting that it vented to the surface (Kirchner, unpublished report for Molycorp Inc., 1983). As these dikes were presumably located along the southern margin of the caldera-forming intrusion, tapping from the sides of deeper-level, more mafic phases of the intrusion seems possible.

Caldera-related intrusions are found as E-W striking high-angle dikes in the Precambrian (Trf of Plate 1 and Trff of Plate 2), as N-S to NE striking sills in the Tertiary sediment(Trf of Plate 1 and Tqlf,Trdf, Tcrf and Trff of Plate 2), as E-W to NE striking dikes to small plutons in the andesite (Trf of Plate 1) and as NW striking dikes in the south-central portion of the map area (Plate 1 and Fig. 7). In detail, these intrusions are divided into four different rock types. A low phenocryst rhyolite porphyry (Trff of Plate 2) is texturally and chemically similar to the Amalia Tuff (Tables 1 and 2b; Fig. 15). This unit commonly intrudes early Tertiary sediment, originally as sills that were subsequently dissected and tilted 90 degrees westerly during regional extension.

Crystal rich rhyolite dikes (Tcrf of Plate 2; Tab. 2b) are found exclusively in complex composite dike relationships with rhyolite to dacite porphyry (Trdf; Tab. 2b; Fig. 15; Plate 2). The most mafic dikes of this family are quartz latite porphyry dikes (Tqlf of Plate 2; Tab. 2b) that have high incompatible trace element chemistries (Tab. 1 and Fig. 15) yet have SiO_2 values as low as 65 percent.

A few rhyolite porphyry intrusions in the center of the district near Cabresto Creek (Fig. 7) are texturally similar to the low phenocryst content rhyolite porphyries, yet have low incompatible trace element values. These have been tentatively grouped with the caldera-related suite of intrusions.

This study is the first to demonstrate intermediate composition units of peralkaline affinity related to the Amalia Tuff magma. The wide compositional range (65 to 76% SiO_2) of the peralkaline affinity dikes indicates that differentiation of >65% SiO_2 rocks occurred along an entirely peralkaline trend (Fig. 15a and b). Within this trend the incompatible trace element content of the 65% SiO_2 unit is low and incompatible trace elements systematically increase with fractionation (Fig. 15a and b). Derivation of the 65% SiO_2 unit from a less evolved, metaluminous magma seems likely. This is in agreement with the suggestion of Johnson and Lipman (1988) that silicic peralkaline rocks are the result of fractionation of metaluminous magmas. In contrast to Johnson and Lipman's model, however, the first peralkaline magma was intermediate in composition rather than granitic.

Post-caldera intrusive units

In the following discussion, "pluton" refers to the higher-level apical phases of the batholith-scale intrusion (e.g. Red River pluton) and "stock" refers to smaller intrusions that appear to cross-cut the top of the batholithic body (e.g. Goat Hill stock). Granite-aplite bodies termed the Bear Canyon, Sulphur Gulch, Cabresto Lake and Red River plutons represent high-level phases of a composite batholith that underlies an approximately 20 by 35 km region. Gravity, drilling information, porphyry dike distribution and mapping relationships all indicate that the entire Questa mining district is underlain by this composite intrusive body (Cordell et. al., 1985; Lipman and Reed, 1989; cross-sections of Plate 1).

Pulses of magmatism shifted to the south over time; initiating in the caldera-centered resurgent intrusions to the north of the mining district at between 25.7 and 24.6 Ma and culminating with 18.5 Ma phases 30 km to the south (Fig. 16; Czamanske et. al., 1990). The majority of the $^{40}Ar/^{39}Ar$ cooling dates for the plutonic bodies in the Questa area (at the southern margin of the caldera) cluster around 24.6 Ma, post-dating caldera formation by 1 m.y. (Meyer and Foland, 1991). An additional $^{40}Ar/^{39}Ar$ 24.7 Ma biotite cooling date in the center of the caldera (Fig. 16) indicates that the 24.6 Ma intrusive pulse included a large region within the caldera as well as the area along the southern caldera margin (Czamanske et. al., 1990). An approximately 0.4 m.y. younger $^{40}Ar/^{39}Ar$ biotite cooling date on a deep-level granite porphyry sample of the Bear Canyon pluton may represent a separate, slightly younger intrusive event (Czamanske et. al.,

1990). Similar cooling dates for biotite related to molybdenum mineralization (Czamanske et. al., 1990) indicate that molybdenum-related phases of the intrusion may post-date early intrusive phases by many 100's of thousands of years. In the immediate mine area, where the intrusive paragenesis is best constrained, porphyry diking both pre- and post- dates mineralization-related plutonism (Fig. 17).

Pre-mineral intrusions

Pre-pluton phases consist of an early series of compositionally-zoned dikes (Tqlcz of Plate 2) and an early sequence of dikes and plutonic phases that exhibit evidence of large-scale wall-rock contamination (Tqlc of Plate 2)..

Compositionally zoned dikes are located in an east-west striking, high-angle dipping belt (Plate 2) and range from latite porphyry (border phases) to rhyolite porphyry (core phases) (Jones, 1988). Contacts between more and less felsic phases are gradational. Mineralogic zonation studies and petrologic modelling of surface samples by Jones (1988) led him to conclude that these dikes represent mixing between a volatile-rich basalt end-member magma and a low-silica rhyolite to rhyodacitic magma. Consideration of similar dikes in underground mine and drill core exposures leads to an alternate interpretation that these early zoned dikes represent mixing caused by tapping of variably contaminated portions of the intrusions.

Early contaminated dikes and intrusions (Tclc; Tab. 2b) are best exposed in the open pit mine and in the underground workings of the

Southwest ore zone. Contaminated bodies range from rhyolite to aplite to granite porphyry and occur both as early phases in high-level portions of the pluton and as early porphyry dikes. Plutonic phases contain ubiquitous andesitic and local Precambrian xenoliths that are at various stages of assimilation. Texturally, these intrusive phases are extremely variable with phenocryst contents ranging from 10 to greater than 50 percent, and pegmatitic textures are common. Rapikivi orthoclase, biotite and hornblende phenocrysts are anomalously abundant. Spatial association of high phenocryst phases with assimilating xenoliths (many of which contain feldspar and mafic mineral porphyroblasts) leads to the suggestion that many of the unevenly distributed "phenocrysts" are, in fact, assimilated porphyroblasts. High fluorine and other volatile contents are probably needed in order to lower the melting temperature of the melt and prevent early solidification, and to allow metasomatic incorporation of the xenoliths into the melt.

Syn-mineral plutons

The plutonic bodies in the Questa mining district are epizonal, commonly intruding their own 3-5 km thick volcanic cover. As the volcanic stratigraphy was extended by approximately 200% previous to cooling of the batholithic-scale plutons, an intrusive depth of 1-3 km is likely. Features of plutonism that indicate epizonal emplacement include: 1) aplitic textures; 2) abundant porphyry dikes; 3) extreme variations in grain size of the aplitic units (interpreted to result from episodic volatile exsolution); 4) local micrographic textures, crenulate quartz veining and

magmatic-hydrothermal breccia formation (discussed in the section on Southwest ore zone mineralization); 5) extensive associated hydrothermal alteration; 6) common preservation of magmatic stope-blocks and xenoliths; and 7) tuffisite, a unit that is interpreted to represent the preserved vent phase of a rhyolite porphyry stock (Tt and Ttf of Plate 2).

Much of the variation in texture and composition of the different granite-aplite plutonic bodies in the mining district is due to their range in level of exposure. The Cabresto Lake and Red River plutons are extremely heterogeneous, contain abundant xenoliths, have high proportions of more mafic phases, and are largely exposed only within a few hundred meters of their upper contact. The Sulphur Gulch and Bear Canyon plutons contain deeper homogeneous granitic phases in addition to upper heterogeneous phases. These plutons connect in the subsurface and are exposed to 600 to 700 m depths below their uppermost contacts.

Internally, the textures of the mine area granite-aplite plutons are highly variable. In a general sense, however, individual granite-aplite plutons are composed in chronological order of: 1) local early contaminated phases; 2) local very fine-grained aplite phases; and 3) a thick rind of variably-textured aplite porphyry grading transitionally into porphyritic granite at greater depth. The early contaminated phases are found as stocks and local dikes and are discussed in the above section on pre-mineral intrusions.

The very fine-grained aplite phases occur as apexes to individual intrusive pulses of the composite granite-aplite plutons (Fig. 18). In the

vicinity of molybdenum mineralization, this unit is typified by low phenocryst contents, pervasive silicification, increasing-upward early barren quartz veining, and local crenulate quartz banding near the uppermost contact. Early barren quartz veins are interpreted to represent exsolution of magmatic fluids during episodic pressure releases that are believed responsible for the fine grained "chilled" nature of the aplite body. Magmatic fluids released from the apical phases of the aplite represent the major source of molybdenum mineralization at Questa.

The major volume of the granite-aplite plutons are made up of variably textured aplite porphyry (Tap of Plate 2; Tab. 2b) that contains from 5-50 percent phenocrysts and grades into granite porphyry and granite (Tgp of Plate 2; Tab. 2b) at depth. Thickness of the upper aplitic phase ranges from 0-500 m and the switch to granitic textures is transitional. Zones of different grain size and phenocryst contents are concentrically distributed within the intrusion, with finer-grained phases likely representing more rapid crystallization during episodes of volatile release and/or diking. Fluids released during crystallization of these deeper-level aplite phases may be responsible for additional amounts of molybdenum mineralization at Questa. Granitic phases of the plutons reflect slower cooling and relatively lesser amounts of volatile release and accompanying pressure-quenching at depth.

Post-mineral intrusions

A suite of post-mineral rhyolite to quartz latite porphyry dikes followed crystallization of at least the outer portion of the aplite body

(Trs through Tr in the mine area, Plate 2). In the mine area, cross-cutting relationships between dikes, wall rock alteration and mineralization indicate a younging-northward trend to the mine area dikes. The southernmost post-pluton dikes in the mine region (Trs of Plate 2; Tab. 2b) are in a one km wide belt intruding Precambrian basement. They are E-W-striking, high-angle dipping, and individual dikes are as much as 200 m thick. This intrusive phase is unique from the younger post-plutonic dikes in that it is restricted to the Precambrian and parallels the high-angle Precambrian structural grain.

Younger dike phases (Trl through Trq, Plate 2) are nearly restricted to the Tertiary sedimentary and volcanic cover and their intrusive pattern is strongly controlled by the structural grain of north-dipping low-angle fault planes. The faults that these dikes commonly follow are near 30° north-dipping faults that have pre-dike, upper-plate-to-the-east motions. Individual dikes intrude low-angle faults in some places, and occur as higher-angle north-dipping "ramp-ups" in others (Fig. 19). In this manner, individual dikes contain sections of low-angle and high-angle north dips, but their average overall dip is at a moderate angle to the north (cross-section B-B', plate 1). These younger dike phases (Trl through Trg) are dominantly rhyolite porphyry dikes that are subdivided based on phenocryst content, size, and abundance (Tab. 2b).

The northernmost unit of this intrusive suite consists of dikes and stocks (Trg of Plate 2; Tab. 2b) that have historically been termed Goat Hill porphyry because of their abundance on Goat Hill. Dikes of this phase are

north-dipping and the "stock" is an odd-shaped intrusion that commonly contains north-dipping contacts on its north and south margins (cross-section B-B', Plate 1). Although this stock appears to be rootless in cross-section B-B', it is likely that the missing root lies to the west of the cross-section. Overall, this intrusion appears to be a north-dipping structurally-controlled stock that locally demonstrates north-dipping composite dike-like features. This intrusion post-dates molybdenum mineralization as it contains local xenoliths of molybdenum mineralized andesite and crenulate quartz banded aplite.

The northernmost rhyolite porphyry stocks are slightly less differentiated than their dike counterparts to the south; they contain less quartz phenocrysts, more plagioclase and mafic mineral phenocrysts, lower silica values (70.5 percent versus 72 percent SiO_2) and elevated titanium (0.25 percent versus 0.15 percent TiO_2). As the northernmost stock (Trg) is interpreted to be the youngest phase of rhyolite porphyry intrusions in the mine area, deeper-level tapping of the more mafic portions of the cooling pluton is suggested.

Units termed tuffisite and fragmental tuffisite (Tt and Tft of Plate 2; Tab. 2b) are intimately associated with the northernmost (Trg) stock. The tuffisite units are interpreted to represent co-genetic, multiple-vented phases of the rhyolite porphyry stock. Tuffisite most commonly is located along the margins of the rhyolite porphyry stock, but is locally found interior to the stock (Plate 2). Tuffisite is made up of the same components that make-up the stocks (Tab. 2b), but the crystals are highly

anhedral/broken. The tuffisite units contain from near-zero to greater than 50 percent Tertiary xenoliths. Regions of greater than 10 percent xenolith content, termed fragmental tuffisite (Tft), are concentrically distributed in an irregular manner around the margins of the rhyolite porphyry stock (Plate 2).

Contacts between the tuffisite and the rhyolite porphyry stock are usually sharp, although one gradational contact exists on the south side of Goat Hill Gulch. In cases of sharp intrusive contacts between the stock and the tuffisite, the grain size of the rhyolite porphyry intrusions often gets finer as the tuffisite contact is approached.

Portions of the tuffisite are lithologically very similar to the basal broken crystal zone of the Amalia Tuff, described earlier. Similar processes are interpreted to have formed the tuffisite and the basal broken crystal zone, although they were separated by approximately one m.y.. In both cases composite dike-like intrusions have vented to form highly fragmental rocks that have incorporated a significant amount of the co-genetic dike material. Major differences are in the level of exposure of vent facies (tuffisite) versus near-vent eruptive facies (basal broken crystal zone), and in the association of the basal broken crystal zone as an initial phase in the eruption of an ignimbrite.

Three small pebble dikes are located in the immediate mine area (Plate 2) and contain rounded fragments of aplite and andesite in a silicified rock-flour matrix. These dikes post-date molybdenum mineralization and contain local fragments of quartz-veined aplite. No molybdenum-

mineralized fragments have been noted, however, indicating that these dikes probably did not pass through molybdenum mineralized areas.

Younger, mafic-suite diking

A suite of mafic dikes ranging from lamprophyre to quartz latite (Tqll of plate 2) post-date all other rock types, alteration and mineralization (Fig. 4). These dikes range from 1 cm to 4 m in width and appear to have been intruded with relatively low viscosities, irregularly filling all available faults. Silica contents range from 51-69 percent (Tab. 1), with most of the dikes having greater than 60 percent SiO_2. Some of the plagioclase phenocrysts and all of the orthoclase phenocrysts contain mineral inclusions and are metacrystic or xenocrystic (Tab. 2b). All of the quartz is strongly resorbed and some is multicrystalline, suggesting that the quartz is xenocrystic.

While deuteric alteration hinders attempts at isotopic dating of this unit, the mafic dike suite probably post-dates mineralization and cooling of the batholithic magma chamber by less than a few million years. Similar mafic intrusions are associated with molybdenum occurrences in Colorado and elsewhere, and in all cases the mafic dikes are intimately associated in space and time with leucocratic phases (Bookstrom et. al., 1985; Shannon et. al., 1984). Bookstrom and others suggested that these mafic magmas represent contaminated alkali-olivine basalts that underplated and melted the lower crust, generating leucocratic melts. At Questa, it is suggested that basaltic underplating generated the overlying granitic batholithic magma chamber and the late mafic dikes represent mafic magma inputs

after the overlying magma chamber had cooled sufficiently to prohibit underplating and allow dike propagation.

Evolution of the post-caldera magmatic system

Post-caldera igneous activity evolved through the following phases: 1) early compositionally zones dikes; 2) early contaminated dikes and pluton phases; 3) the main plutonic phases responsible for mineralization; 4) post-plutonic diking that became slightly more mafic through time; and 5) younger, mafic-suite diking. The above sequence *may* indicate the following processes: 1) *possible* growth and expansion of a post-caldera pluton due to basaltic end-member injections at depth (if 1 above is in fact related to basaltic end-member mixing); 2) early generation of volatile-rich, high-level plutonic phases (evidenced by 2 above); 3) attainment of a batholith-scale magmatic system with local volatile-rich apexes (evidenced by 3 above); 4) porphyry diking emanating from successively deeper levels of the magma chamber as the magmatic system cools (4 above); and 5) late-stage basaltic end-member intrusions after the batholithic chamber had cooled. The presence of basaltic end-member intrusions during the waning of the magmatic system (and possibly during its initiation, as well) suggests that basaltic injections provided the heat necessary for melting of the lower and middle crust and generation of intrusions. The lack of basalt-related rock types during the middle-stages of the system may be attributed to efficient density screening by the overlying batholith-scale magma body.

Quaternary deposits

Three types of Quaternary deposits are recognized in the area exclusive of waste dump deposits from the Questa molybdenum mine. These deposits are rift-fill alluvial sediments of the Rio Grande valley, local alluvium along modern drainages, and mud flow deposits located along the Red River and Bitter Creek drainages (Fig. 20). Mud flow deposits emanated from the numerous alteration scars in the district and are deposited as debris aprons at the intersection of the side canyons with major drainages (Meyer and Leonardson, 1990). Five major debris apron deposits have periodically impounded the major drainages, resulting in upstream stagnation and the development of a highly irregular down-river profile (Fig. 21).

STRUCTURAL GEOLOGY

Approximately 800 m of vertical relief within the map area and an additional 1000 meters of sub-surface mining and diamond drilling control allows investigation of the structural geology over a large structural range. Geologic mapping demonstrates a number of overall structural patterns: a) a strong ENE alignment in high-level plutons and dikes, molybdenum ore bodies and hydrothermal alteration zones (Plates 1 and 2; Fig. 5); b) an E-W to ENE-striking zone of dikes and faults indicative of the southern caldera structural boundary (Plates 1 and 2; Fig. 7); c) a near 90° westward tilt to the volcanic stratigraphy in the western 2/3 of the map area (Plates 1 and 2); d) a set of discontinuous low-angle faults with fault motion dominantly top-plate-to-the-east (Plates 1 and 2; Fig. 25); e) a set of throughgoing NNW-striking normal faults (dominantly down to the

east)(Plates 1 and 2; Fig. 25); and f) a N-S-striking set of normal faults (dominantly down to the west) along the modern rift front (Plate1; Fig. 25). Structures range in age from Precambrian to Tertiary.

Precambrian structures

A Precambrian-aged ductile shear zone is proposed in the Questa area separating metasedimentary units in the northern mining district from metaigneous units to the south (Plate 1). This shear zone is envisaged to be a broad, ENE to E-W trending structure that is centered underneath the ENE trending mineralized bodies and alteration (Plate 1 and Fig. 5). The central portion of this proposed shear zone is entirely covered by Tertiary units. On the southern flank of this proposed zone are local regions of lesser shear and fabric development that parallel the central portion of the structure.

This shear zone is believed to have exerted fundamental, deep-seated controls on structural and magmatic events in the district including: a) the trend and location of intrusion of pre-Mississippian diabase dikes (Plate 2); b) the trend and location of the southern caldera wall (Fig. 7); c) the linear nature of caldera ring fractures and dikes (Fig. 7); d) the location of high-level phases of the batholithic intrusion (Fig. 5); e) the E-W to ENE trend of pluton-related dikes (Plates 1 and 2); and f) the ENE trend of mineralization and hydrothermal alteration (Fig. 5).

Evidence for a structural boundary in this region includes: a) a major N-S change in Precambrian rock-types (Plate 1); b) local E-W to ENE striking, 90° dipping foliation in this area in contrast to regional patterns

(Lipman and Reed, 1989); c) local E-W trending cataclasite and mylonite zones in the Columbine Creek quartz monzonite (Kirchner, unpublished report for Molycorp Inc., 1983); and, d) a strongly E-W to ENE foliated quartz -feldspar ±biotite ±hornblende ±garnet ±magnetite schist exposed near the Southwest ore zone, near the tectonic boundary between these two rock types.

Evidence that this structure may have been active in the Precambrian includes: a) the ductile nature of the deformation, indicative of pressures and temperatures characteristically represented in Precambrian units; and, b) the sedimentary cover over both the southern and northern tectonic blocks, which contain locally-derived basement clasts that are dominantly metasediment in the north and dominantly metaigneous to the south. This relationship indicates that the juxtaposition of metasedimentary and metaigneous basement must have been at least as old as the early Tertiary sediment.

The metasedimentary units in the northern block are younger than the southern units and are believed to have initially been deposited at stratigraphically higher levels, but both the northern and southern blocks are of similar (amphibolite facies) metamorphic grade. Previous workers have recognized this boundary as a contact between the southern Taos terrain and northern Questa terrain (figure 1 of Grambling et. al., 1988), but have not commented on the nature of the terrain bounding structures. Other recognized terrain bounding structures in northern New Mexico include interpreted thrust faults and detachment-style structures (Grambling et.

al., 1988; Robertson et. al., in press) that juxtapose terrains of various crustal levels and metamorphic grade. The juxtaposition of units of similar metamorphic grade at Questa along with the high-angle to foliation, mylonitization and lithologic contacts implies juxtaposition of laterally adjacent terrains along a high-angle structural zone. A mid-crustal level strike-slip terrain boundary is *preliminarily* suggested at Questa.

Paleozoic-Mesozoic structures

Throughout much of Paleozoic and Mesozoic time the Questa mining district was located near the southeastern margin of the Uncompahgre-San Luis highland (Fig. 3)(Clark and Read, 1972; Dickenson, 1981). Although the eastern structural boundary of the Uncompahgre-San Luis highland may be located somewhere within the map area (Fig. 3) no field evidence of highland-bounding structures was found. If any Paleozoic or Mesozoic structures do exist in the area of Plate 1, they would be restricted to Precambrian rocks and therefore difficult to differentiate from earlier or later events.

Early Tertiary structures

The mining district is located in an area of Laramide uplift (Fig. 3) characterized by regionally east-vergent thrust and reverse faults. Evidence for this uplift is unequivocally preserved in the early Tertiary sedimentary record; thick foreland basin deposits to the east, and thin, locally derived deposits in the mining area. Although it is likely that structures responsible for this uplift exist in the mining district, none

were found. Again, the apparent absence of Laramide structures in the mining district may be due to difficulties of detection, rather than due to non-existence.

Mid-Oligocene to mid-Miocene structures

The mid-Oligocene to mid-Miocene structural history of the district is characterized by two contrasting styles of extensional faulting. Pre-caldera, syn-caldera and post-mineralization faulting was of a block-fault style consistent with extensional strain on the order of 10-30%. Extension during a one million year period of time following eruption of the caldera and synchronous with maximum igneous activity was of a style and scale found only in very highly extended regions of the Basin and Range province (Gans et. al., 1989). All of the mid-Oligocene and younger structures in the district are brittle and are interpreted to have been developed within the upper few kilometers of the earth's crust.

Pre-caldera extension (approximately 28 to 25.7 Ma)

Pre-caldera Oligocene volcanism in the region (approximately 28-25.7 Ma) was concurrent with extensional block faulting of probable minor total strain (Fig. 17). Co-volcanic normal faults are indicated by orientations of and internal deformations in pre-caldera porphyry dikes. North of the Questa caldera, in a region not overprinted by major amounts of younger extensional strain, quartz latite porphyry dikes are oriented at high angles, parallel to NNW-striking normal faults (Lipman, 1983a). This orientation is perpendicular to the proposed ENE-directed extensional field for that time (Lipman, 1983b).

Within the mine area, a few of the quartz latite porphyry dikes are strongly foliated. Foliation is localized along planar zones within individual regions of otherwise non-foliated porphyry dikes (Fig. 22). The foliated texture is interpreted to be related to normal-fault shearing while the quartz latite porphyry dike was still at or near it's solidus. These dikes are now oriented horizontally due to tilting by later extension, but when later tilting is subtracted, an original orientation of NNW strikes and high-angle dips is obtained.

Caldera-related structures (25.8 Ma)

The Questa mining district straddles the southern structural margin of the Questa caldera and contains fragmentary evidence of caldera-bounding and caldera floor faults. The structural boundary of the caldera is not a discrete fault, but is a 1-2 km wide E-striking zone of dikes and high-angle faults that have been largely dissected by later extension (Fig. 7 and Plate 1).

Three reasonably intact (but 90° westerly tilted) examples of the structural wall were originally E-striking, high-angle features that had relative down-drop of the northern intracaldera block (southernmost caldera-related faults of Fig. 7; Plate 2). All three of these faults are intruded by Amalia Tuff equivalent peralkaline affinity dikes, supporting the idea of their formation during the time of caldera collapse. These faults do not line up along a straight line, and are thought to represent individual strands in a linear zone of ring-faults.

Faults that are interpreted to bound caldera-floor horsts and grabens (subsequently 90° westerly tilted) are located in the Straight Creek-Bonita Canyon area (northern caldera-related faults of Fig. 7 and Plate 1). These faults offset the caldera floor and are intruded by dikes that are caldera-age and younger. Rheomorphic flowage of the overlying intracaldera tuff (Fig. 7) is due to motion on the caldera floor faults while part of the tuff was still plastic. This flowage implies syn- to slightly post-caldera collapse motion on the caldera floor faults.

Syn-caldera extension (25.8 Ma)

Extensional block-faulting continued during and immediately after the development of the Questa caldera at 25.8 Ma. A slow to moderate strain rate of extension is indicated by intracaldera slabby cooling joint patterns and by extracaldera half-graben structures that are syn- to slightly post-caldera in age (Fig. 8).

Closely spaced vertical joint patterns are common in caldera-fill ignimbrites (Lipman, 1984). At Questa, these vertical joints were initially oriented NNW, at 90° angles to the ENE-directed extensional field. This joint pattern is believed to have formed during cooling of the 2.5 km-thick intracaldera unit in an ENE-directed tensional stress field. Subsequent 90° tilting has resulted in the present-day relationship of sub-horizontal slabby cooling joints and sub-vertical NNW-striking eutaxitic foliation patterns (Fig. 23). Faults that are presently oriented at low angles often parallel this slabby-cooling joint set, indicating a significant influence of this early-formed jointing on subsequent structural development.

Half-graben structures in extracaldera ignimbrite provide additional information on caldera-aged extension. Outcrops south of Questa, near the town of San Cristobal, expose west-tilted fault blocks of outflow ignimbrite overlain by a fines-enriched ash bed (Fig. 8). The overlying ash bed has a distinctive trace element chemical signature similar to the Amalia Tuff (Fig. 15), and is interpreted to be a co-ignimbrite fallout deposit. The preservation of these easily erodible units in the half-graben structures at San Cristobal indicates extensional deformation during and/or immediately after formation of the caldera. The San Cristobal exposures provide evidence for moderate amounts of syn- to slightly post-caldera ENE-directed extension and indicate that the extensional field was regional, rather than restricted to the boundaries of the caldera interior.

Post-caldera extension (25.7-24.6 Ma)

Following caldera eruption, but preceding the cooling of 24.6 Ma plutonic phases, extreme extension occurred (Fig. 16; Meyer and Foland, 1991). The entire Tertiary stratigraphy and much of the Precambrian basement of the western 2/3 of Plate 1 (from approximately the town of Red River west to the rift front) was tilted near 90° westerly (Fig. 24a, b and c). This severe tilting is interpreted to have occurred in the roof of a partially molten batholithic magma chamber, with tilting being accomplished by the domino-style rotation of initially high-angle faults to near horizontal. Stratal tilts and non-rigorous palinspastic reconstruction of cross-section A-A' (Plate 1) indicates >200% extensional strain occurred at this time over the western 2/3 of the cross-section. The

rotated normal faults exerted primary controls on the pathways taken by later intrusions and hydrothermal fluids.

The timing of this extreme tilting event is well constrained. Tilting *post*-dated the cooling of the 2.5 km thick intracaldera tuff, as eutaxitic foliation is 90° tilted. Sanidine $^{40}Ar/^{39}Ar$ dates on the Amalia Tuff outflow sheet are 25.7 ±0.1 Ma (one standard deviation error; Czamanske et. al., 1990; Meyer and Foland, 1991). Extreme tilting *pre*-dated the cooling of the underlying magma chamber, pluton-related dikes and molybdenum mineralization. Paleomagnetic orientations in the Sulphur Gulch and Bear Canyon plutons, both biotite $^{40}Ar/^{39}Ar$ dated at 24.6 ±0.1 Ma (one standard deviation error; Czamanske et. al., 1990; Meyer and Foland, 1991), indicate no, or minimal post-cooling tilting (Hagstrum, et. al., 1982; Snyder, 1984; Hagstrum and Lipman, 1986). Both of these bodies intrude 90° tilted Tertiary stratigraphy. An especially instructive pluton-related dike intrudes 90° tilted Amalia Tuff near the head of Straight Creek. Biotite $^{40}Ar/^{39}Ar$ analysis indicates an age of 24.6 ±0.1 Ma (one standard deviation error; Meyer and Foland, 1991) for cooling of the dike below approximately 280°C. Alternating field demagnetization studies indicate that the dike is untilted below the magnetite Curie point of approximately 580°C. Tilting unequivocally followed the 25.7 Ma Amalia Tuff and preceded intrusion of this 24.6 Ma dike.

The alteration/mineralization zonations in the molybdenum ore body provide an additional line of evidence for the lack of post-intrusive tilting. The Southwest ore body is biotite $^{40}Ar/^{39}Ar$ dated at 24.1 to 24.2 Ma (±0.3

and ±0.2 respectively for two age dates, one standard deviation error; Czamanske et. al., 1990), and is about 2 km long in an ENE direction (Fig. 5). Along this entire length, the ore body is located at approximately the same elevation and mineralogic variations within the magmatic hydrothermal breccia and alteration above the ore deposit are vertically zoned. The location of the above features at nearly equal elevations along 2 km of strike-length suggests that no or minimal tilting has occurred parallel to the long axis of the ore body.

The faults that are responsible for the tilting initiated at high angles and have been rotated to low-angle orientations. These low-angle faults are distributed throughout the map area from Red River, westward to the Rio Grande rift front (discontinuous less than 45 degree dipping faults of Fig. 25). Commonly, these faults are located on both the north and south sides of the Cabresto Creek/Red River divide, approximately parallel to the line of cross-section A-A' (Plate 1). Faults on the north and south sides of the divide dip gently toward each other. Surface stratigraphy, as well as local underground drilling control, indicates that these faults connect at depth. The resulting pattern, when viewed parallel to the ENE transport direction, is one of U-shaped extensional "klippe", with higher-plate blocks in the highlands between the Cabresto Creek and Red River drainages (cross-sections B-B', C-C', D-D', Plate 1). This U-shaped geometry closely resembles mega-corrugation or fold patterns in low-angle fault zones in the Basin and Range province (Spencer, 1982; Frost, 1981). The fault plane corrugations may represent original undulations in the initially-formed

normal faults that have since been rotated to near horizontal. The recognition of this U-shaped fault geometry eliminates the need to call on an ENE-trending graben (the Red River trench of Carpenter, 1968; Clark and Read, 1972; Clark, 1968) to explain the location of stratigraphically high volcanic stratigraphy between the Cabresto Creek and Red River drainages.

The low-angle faults are variable in orientation, and average dips are less than 30° NE (Fig. 24d). Slickenside striation orientations indicate transport in an ENE direction (Fig. 24e and f), and stratigraphic offsets indicate upper-plate-to-the-east transport. All of the low-angle faults in the region are brittle and fault surfaces commonly contain clay and/or chlorite gouge.

Excellent exposures of low-angle faults exist south of the Southwest ore body along the northern wall of the Red River canyon (Fig. 26). Here, 90° tilted early-Tertiary sediments (Ts of Plate 1) are successively stair-stepped, upper-plate-to-the-east, along individual fault slices that are parts of a low-angle fault zone (Plate 2). Stratigraphic offsets of early Tertiary sediment on individual fault planes approach 1 km, and offset across the entire low-angle fault zone is on the order of several km.

Other excellent exposures of low-angle fault zones are found in regions of hydrothermal alteration scars east of the molybdenum mine area (Figs. 27 and 28) where fault zone thicknesses (measured perpendicular to the orientation of the fault zone) locally approach 500 m (Fig. 29). Mechanical weakening of the rock, due to pervasive shearing in these low-angle fault zones, is a major reason for subsequent slumpage and scar formation.

Low-angle fault zones provided permiability for hydrothermal fluids, which commonly altered fault zones (Fig. 30). Molybdenum mineralization and associated alteration in the Southwest ore zone was strongly controlled by low-angle, north-dipping faults (Plate 1, cross-section B-B').

Blocks between low-angle fault zones are internally deformed with structural relationships suggesting that internal deformation was syn-kinematic to motion on low-angle faults. Two types of internal deformation are observed, a "shear-couple" style, and an "upper-plate" style of deformation (Fig. 31a and b).

The "shear-couple" style of internal deformation typically occurs when block-bounding low-angle fault planes are spaced at meters to tens of meters apart. This style is characterized by internal cross-faults of minor offset that toe-in to low-angle upper and lower block-bounding faults (Fig. 32) with minor offsets on individual cross-structures. Locally, these cross-cutting structures can be extremely pervasive (Fig. 33 and 34) and may be responsible for significant bulk changes in the shapes of individual blocks.

The "upper-plate" style of internal block deformation occurs where parallel low-angle fault planes are hundreds of meters apart or an upper plate bounding structure is unknown. These structures are geometrically similar to faults found in the upper-plate of detachment structures in the Basin and Range province (Fig. 31b; Wernicke and Burchfiel, 1982; Gross and Hillemeyer, 1982; Davis et. al., 1986).

Contrasting examples of "upper-plate" style block deformation exist in the early Tertiary sediment outcrop region immediately north of the Sulphur Gulch pluton and in the western portion of the Hansen scar region (Fig. 5; Plate 1, map and cross-section A-A'). In the Sulphur Gulch exposures, intermediate-angle intra-block faults have repeated the Tertiary sediment about 10 times. These faults are interpreted to initially have rooted into a low-angle fault that now has been intruded by the underlying pluton. Stratal dips within this internal block are near 90° westerly, and the initiation of internal block deformation structures is believed to have been late in the tilting cycle. In the Hansen scar exposures, intermediate to high-angle intra-block faults root in an underlying fault and crosscut units that dip only moderately to the west. This moderately west-dipping zone in the Hansen scar area (represented by center of shallow dipping foliation in Fig. 24b) is an anomalous block surrounded by domains of greater tilt and probably represents an antithetically tilted block (initially tilted to the east) that has since been tilted to the west.

Post-mineralization faulting (24.2 Ma - earliest? Miocene)

Low-angle faults with minor-scale displacement post-date mineralization and alteration but pre-date late-stage dikes (Fig. 17). These faults are significant in that they exhibit top-to-the-ENE normal displacements on faults that were clearly active while they were oriented at angles less than 30°. Additionally, these faults caused minor offset of

molybdenum mineralized zones, and are therefore important to exploration and mining.

Faulting occurred both as reactivation of older low-angle fault planes and as generation of "new" low-angle faults. This fault set has associated propylitic (epidote-chlorite-clay alteration) and quartz-sericite-pyrite haloes, and the faults themselves can contain chlorite, pyrite and/or clay gouge. Late-stage low-angle faults post-date tilting and cross-cut the batholithic intrusion, rhyolite porphyry diking and mineralization-alteration. Examples of low-angle fault offsets on the batholith exist in the southern portion of the Sulphur Gulch pluton (immediately NW of the mill yard, Plate 1), and in subsurface exposures in the underground workings of the Southwest ore body. Low-angle faults in the batholith are generally restricted to the high-level positions of the intrusive system.

Examples of minor low-angle fault offsets of rhyolite porphyry dikes exist in the ore deposit region and to the east. One well-constrained dike near Straight Creek shows 125 m of ENE displacement of a 24.6 Ma ($^{40}Ar/^{39}Ar$ biotite date, Meyer and Foland, 1991) rhyolite porphyry dike along a gently east-dipping fault plane. Paleomagnetic orientations demonstrate that the dike itself is untilted. This indicates that: a) the offsets and tilting associated with the late-stage low-angle faults are minor; and b) extensional fault motion occurred while the fault was unequivocally oriented at a low angle.

Late low-angle fault offsets on molybdenum mineralization and related alteration are evident in the vicinity of the Southwest ore zone. Diamond

drilling of the western extension of the Southwest ore body demonstrates structural attenuation of the deposit by faults that dip shallowly to the east. Surface exposures of structural offsets of the molybdenum-related alteration haloes are common in the region of the mining shafts (Fig. 30). In this region, pre-mineral low-angle faults served as the conduit for altering hydrothermal fluids. These same low-angle faults were later reactivated, resulting in the structural juxtaposition of alteration types (Fig. 30).

Post-mineral low-angle faulting pre-dates the intrusion of a distinctive lamprophyre-latite porphyry dike suite. Due to strong deuteric alteration, this dike suite is undated, however, similarity to dike suites in other magmatic systems (Bookstrom et. al., 1985; Shannon et. al., 1984) suggests that it represents a late-stage pulse of the overall magmatic system that probably post-dates main-stage magmatic activity by less than a few million years.

It is significant that these faults were unequivocally oriented at low angles during their extensional fault motion. The mechanism of allowing motion on such "improperly" oriented faults is uncertain, but it is possible that motion was allowed because of a reduction of effective stress across the fault planes due to overpressured hydrothermal fluids. The demonstrated low-angle fault motion of this post-mineralization event supports the proposal that post-caldera/pre-mineral low-angle faults were active at angles less than 30°, as well.

Block-fault extension (earliest Miocene? to mid-Miocene)

A set of NNW-oriented extensional block faults formed during continued regional extension, after the batholith had completely cooled (Figs. 17 and 35). This normal fault set is throughgoing (Fig. 25 and Plate 1), has dominantly down to the east motion, and offsets the batholith and related molybdenum mineralization.

Block faulting post-dates emplacement of the lamprophyre-quartz latite porphyry dike suite and cross-cuts the deepest exposed levels of the underlying batholith (cross-section A-A', Plate 1). Faulting pre-dates the development of modern Rio Grande rift-front normal faults that dip westward and trend N-S along the eastern margin of the rift (western margin of mapping in Plate 1).

Vertical offsets on this fault set can be as much as 1 km although paleomagnetic evidence (Hagstrum et. al., 1982; Hagstrum and Lipman, 1986) indicates only minor, less than 10°, resultant tilting. Lateral changes in offset indicate that the faults are scissor-like. East- and west-dipping normal faults on either side of the Sulphur Gulch pluton lose their throw to the south (Fig. 25 and Plate 1), whereas east-dipping faults on the east side of the Bear Canyon pluton and in the Hottentot Canyon region lose their throw to the north (Fig. 25 and Plate 1). Individual strands of this fault set offset the Southwest ore body by as much as 30 m, down-to-the-east. This offset is sufficient to adversely affect the mining of this portion of the Southwest ore body.

Comparison of the highly rotational, syn-magmatic normal fault set with post-magmatic faulting, demonstrates a number of important points: 1) the continuance of lower strain-rate extension after the magmatic system cooled emphasizes that the earlier high-strain-rate extension was likely due to an interaction of regional extension with a magmatic system, rather than to magmatic forces alone; 2) the extreme lessening of strain-rate after the magmatic system had died emphasizes the control that the magmatic system had on concentrating extension into the area; and 3) the change in extensional style, from syn-magmatic, "thin-skinned" to post-magmatic deeply penetrative block faulting, demonstrates the significant effects of the magmatic system on the strength of the crust (e.g. Morgan and Golombek, 1984; Morgan et. al., 1986).

Discussion: geometric relationships of extensional faults at Questa

Although the overall pattern of low-angle faulting is readily apparent, the detailed kinematics of the structures remains problematic. Among the greatest structural dilemmas at Questa are the 90° to 110° angular relationships of low-angle fault planes to bedding attitudes (Fig. 24a, b, c and d), and the presence of 90° of extensional tilting with only one clearly defined generation of extensional faults.

Classical models predict initiation of extensional faults at angles near 60° to bedding (Anderson, 1951). With continued extension, these faults tilt in domino fashion to lower angles (near 30°) where they lock-up, and new 60° dipping normal faults (now at near 90° angles to 30° tilted bedding) become active until they, in turn reach critically low angles

(Morton and Black, 1975; Proffet, 1977; Chamberlin, 1983). Three generations of rotated planar faults are necessary to obtain 90° of stratal tilt.

At Questa, the near 90° angular relationship between low-angle faults and strata suggest that the first generation of extensional faults at Questa were active at near 90°. NNW-striking, vertically-oriented cooling joints in the thick intra-caldera tuff were ideally oriented to become activated as vertically-oriented normal faults. Alternatively, fault planes oriented at 90° to bedding may not have been active until after the favorably oriented joint surfaces had been rotated to 60°-80° attitudes by a currently unrecognized earlier normal fault set (e.g., Angelier and Colletta, 1983). If so, this earlier fault set might have escaped detection because of its relatively insignificant offset in comparison to later faults.

Second generation faults exist at Questa as throughgoing, east-dipping normal faults that cross-cut the batholith (discussed further in later structural sections) and cross-cut 90°tilted strata. Structural relationships as well as paleomagnetic evidence suggests that these faults were developed late in the structural sequence (after 80°-90° of stratal tilt) and caused minimal tilting. This implies that first generation structures, the major offset low-angle faults observed at Questa, were active during their inclination to angles significantly less than 30°. One explanation for this apparent fault motion down to exceedingly low angles is that overpressured fluids from the molybdenum-related hydrothermal system may have reduced the effective stress across the fault planes.

Mid Miocene - Recent rift-front faults

West-dipping normal faults at the base of the mountain front represent the eastern margin of the Rio Grande rift graben (western portion of Fig. 25 and Plate 1). The majority of the offset is believed to be on a fault that is buried just to the west of the mountain front, and lesser offsets occur on 3 splay faults that cross the mouth of the Red River canyon near Questa (Fig. 25 and Plate 1). The N-S trend of these rift-bounding faults, in contrast to NNW striking trends of earlier faults is believed to result from a mid-Miocene rotation of the least principle stress direction (Lipman, 1983b).

Motion on this fault set occurred from mid-Miocene to Holocene (Chapin and Seager, 1975; Menges, 1987, 1988) and offsets in this segment of the rift are as much as 7-8 km (Lipman and Mehnert, 1979). A possible period of increased uplift and erosion during the Pliocene (?) resulted in faceted spurs along the Rio Grande rift-front, such as the one between Red River and Cabresto Creek. Additionally, increased uplift caused entrenchment of the Red River and Cabresto Creek drainages resulting in development of "valley-in-valley" cross-canyon profiles (Fig. 20; Menges, 1987, 1988).

Quaternary landslides

Recent to active landslides range in size from 0.9 km^2 down to less than map-scale, and are scattered throughout the map area (Fig. 20 and Plate 1). A majority of the landslides are located at or below the slope-break at the boundary between the gentler outer and steeper inner canyons (Fig.20). Active landslides are located in many of the alteration scars and

landslide failure is an important process in the development of the badlands (scar) topography (Meyer and Leonardson, 1990).

Discussion: significance of caldera-related structures

With the recognition of the Questa caldera, recent authors have proposed relatively caldera-centered views of the regional geology. Lipman (1983a, 1988) suggested a model of extension in the caldera region that incorporates an interaction of regional extension with caldera resurgence. In this model fault blocks are symmetrically tilted away from a proposed resurgent axis of intrusions (figure 6 of Lipman, 1988). The western and eastern caldera walls are envisioned as acting as break-away zones to the extended caldera interior, and the southern structural margin is believed to act as a tear zone, allowing greater tilt of caldera-interior units. Other workers (e.g., Leonardson et. al., 1983) have emphasized the importance of southern caldera margin structures in localizing plutonism and controlling molybdenum mineralization in the district.

It is suggested herein that caldera structures are significant, but not as important as previously believed.

1) The importance of caldera resurgence is de-emphasized due to recognition of a lack of symmetry about possible resurgent intrusions in the southern caldera region (compare Plate 1, cross-section A-A' to figure 6 of Lipman. 1988). Although caldera resurgence occurred in a regional extensional field, resurgent intrusion did not have an active influence on the deformational style.

2) The idea of caldera walls acting as breakaway zones and tear zones is only weakly supported by detailed mapping of this area. The western and eastern caldera walls are not exposed in the region as the western wall is under the Rio Grande rift and the eastern wall is obscured by the Red River pluton. A major change in tilt direction and magnitude is located in the region where the eastern caldera wall is presumed to be (Plate 1, cross-section A-A'), providing permissive evidence that this margin may, in fact, have been a breakaway zone.

Southern caldera margin faults have been mapped in detail (Fig. 7 and Plates 1 and 2). There is no indication of differential tilt across these faults and the faults themselves are tilted and attenuated by post-caldera low-angle faulting. Additionally, 55° west-tilted sediment is exposed 2-3 km south of the caldera, indicating that much of the change in tilt magnitude lies south of the caldera margin in this area. It is suggested that low-angle faults such as the ones exposed in the region of the moly-mine shafts and mill area serve as major tilt-accommodation structures. These faults have demonstrated offset after caldera formation while mapped caldera-margin structures demonstrate no significant post-caldera displacements.

3) The idea of the southern caldera structural boundary being a primary control on plutonism and mineralization in the district is de-emphasized due to the recognition of pre-caldera structural elements of the same orientation in this area (discussed above in the section on Precambrian structure). Southern caldera margin ring-faults that were

along the same trend as the Precambrian structural zone were restricted to high-crustal levels and were strongly dissected and rotated by pre-mineral low-angle faults. Caldera-related structural remnants have had relatively little influence on the location of subsequent plutons and mineralization in comparison to the deep-level Precambrian structural grain and the shallow-level low-angle structures.

The above suggests that postpcladera plutons, rather than specifically caldera-related features, served to focus the regional extension into the Questa caldera area and greatly influenced the style of extensional deformation. Locallization of plutons and related mineralization along the southern caldera margin is largely due to deep-seated Precambrian structural controls, rather than due to caldera-margin fault control alone.

MINERALIZATION AND ALTERATION

Questa is a major molybdenum mining district that has been nearly continuously active since 1919 (Schilling, 1956,1990)(Fig. 36). Mineralization at Questa is located above the apex of individual intrusive pulses of the southern caldera margin plutons, and both the plutons and the mineralization are aligned along an ENE structural trend. This section will describe the regional alteration, district-wide molybdenum mineralization and details of the igneous, structural and mineralization history of the Southwest ore zone. Following this description a comparison is made to the typical "Climax" type molybdenum system, and finally a district-wide

model is presented emphasizing petrology, structure and alteration as primary exploration tools.

Regional Alteration and Alteration Scars

Intrusion of the southern caldera plutons into the overlying volcanic cover caused extensive hydrothermal fluid circulation and alteration in the Questa mining district. Nearly the entire region of the Questa mining district has experienced moderate levels of propylitic alteration (chlorite-epidote-calcite-pyrite/magnetite) with more restricted areas of biotization (quartz-biotite-orthoclase-magnetite) and pyritization (quartz-sericite-pyrite).

Numerous regions of high pyrite content (>2%) in the Questa district resulted from meteoric-hydrothermal systems that were often localized in permeable zones created by low-angle faults. Exposure of these high-pyrite zones to the surface resulted in oxidation of the pyrite and extensive clay alteration of the pyritized rock. Where regions of extensive clay alteration and tectonic preparation exist on significant slopes, rapid erosion occurs by processes of landsliding, slumpage and mud flow, and a badlands topography (or scar) develops (Figs. 5 and 28). These scars are the most visible geologic feature of the Questa mining district. The formation of scars is believed to depend on four factors, listed in order of decreasing significance (Meyer and Leonardson, 1990):

1) High slope angle (>25°), necessary in all cases for mass wasting processes to become significant. High-angle slopes are located at the Cabresto Creek-Red River divide, at the slope-break between the inner and

outer canyons, and along the fault scarp at the eastern margin of the Rio Grande rift graben (Fig. 20).

2) Extensive shearing and weakening of the rock, dominantly by low-angle angle faulting.

3) Strong pyritization of the rock, resulting in clay mineral formation during weathering and loss of shear strength during periods of water saturation.

4) Relatively sparse vegetative cover, as most of the scars are on less vegetated south-facing slopes.

Low-angle structural preparation without high pyrite content appears responsible for the formation of the Questa scar (Fig. 5), but in this case, an anomalously high slope angle (>30°) related to rift-front faulting may have aided mass-wasting processes as well. High-pyrite content, without associated low-angle shearing appears responsible for the June Bug, Hansen and Bitter Creek alteration scars (Fig. 5). High-pyrite content combined with low-angle structural preparation appears responsible for all of the rest of the alteration scars in the district.

In the past, these scars have been interpreted as resulting from clay alteration caused by low-temperature acidic hyrothermal solutions (e.g. Loucks unpublished report for Kennecott Corporation, 1977). These scars lack silica sinters or high-level sulfotaric hydrothermal alteration minerals, however, and their distinctive high clay and iron oxide content is mainly the result of supergene alteration of tectonically sheared, pyritized rock.

Molybdenum mineralization and related alteration

Known molybdenum mineralization of any significance is restricted to the western portion of the district, and consists of 6 defined mineralized bodies (Fig. 5). All of the mineralization is located <500 m above apical phases of individual pulses of the underlying, highly-evolved pluton. In all but one instance, mineralization is located in overlying volcanic rocks that were tilted 90° westerly prior to mineralization. Figure 37 demonstrates a strong spatial correspondence of the majority of mineralization with the intrusive-country rock contact. Molybdenum mineralization is structurally controlled with the mineralized zones lining up along a N75E trend and with some mineralized bodies being severely elongated in this direction, as well (Fig. 5 and Plate 1).

The Log Cabin, Spring Gulch and central mineralized zones (Figs. 5 and 37) represent spatially distinct intrusive-mineralization pulses. Identical 24.1 Ma biotite $^{40}Ar/^{39}Ar$ dates on central zone mineralization and the Bear Canyon pluton (Czamanske et. al., 1990) suggest that all of the mineralization post-dates the main phase of the Sulphur Gulch pluton by 0.5 Ma. Additionally, these dates indicate that Bear Canyon-aged intrusive pulses may partially underlie the Sulphur Gulch pluton and be responsible for all of the mineralized bodies in the district. More detailed $^{40}Ar/^{39}Ar$ dating of these mineralized bodies and their associated intrusive units is warranted in order to better understand their spatial and temporal relationships.

The Log Cabin deposit lies at the western margin of the Sangre de Cristo range and is the westernmost mineralized body at Questa (Fig. 5). Mineralization in the Log Cabin deposit is in tilted caldera-floor andesite immediately above the intrusive rock-volcanic rock contact (Fig. 37). The Spring Gulch zone is the easternmost known mineralized body in the district (Fig. 5) and mineralization here is located 250-500 meters below the intrusive rock-volcanic rock contact (Fig. 37).

The central mineralized zone lies between the Spring Gulch and Log Cabin zones and accounts for nearly all of the historical production in the district. The mineralized bodies of the central zone are arranged in a horseshoe shape, open to the west (Fig. 5). Clockwise, from the northern leg of the shoe, these deposits are the Northeast zone, the pit ore body, the old underground ore zone and the Southwest ore zone (Fig. 5).

The Northeast mineralized zone is similar in many ways to the Southwest ore body described in more detail below. The greater depth and less regular distribution of ore-grade mineralization in the Northeast zone has led to less drilling and development and hence, a less complete understanding of the Northeast zone system. Similarities to the Southwest ore body include: 1) an overall extremely elongate geometry (mineralization is approximately 2 kilometers long in an ENE direction), 2) extreme control by a major, moderate-shallow north-dipping fault zone, 3) fluid derivation from highly-evolved low-phenocryst source aplites and 4) early barren quartz veins and crenulate quartz banding in the source aplites. Northeast zone mineralization is located in a moderate-angle north-dipping fault zone

that has major offset of the upper plate to the east (cross-section B-B', Plate 1). For most of the E-W length of this structural zone, hanging-wall megabreccia is juxtaposed against caldera-floor andesite. Mineralization is located on either side of this pre-mineral structure.

Mineralization in the old open pit mine (Fig. 37 and Plate 2) is concentrated above the 30° west-dipping intrusive contact of the Sulphur Gulch pluton with caldera-floor andesites. Earlier workers have assumed that the source of mineralization was from fluids derived from the immediately underlying pluton. However, very fine grained aplitic textures, characteristic of "source rocks" in the most molybdenum-bearing systems, are rare in the pluton underlying open pit mineralization. Recent mapping and drilling has led to the recognition of low-angle west-dipping fault zones in the open pit mine (Fig. 38) and of very fine grained, low-phenocryst aplites down the dip of these structures, to the west of the pit. It is likely that much of the pit area mineralization may, in fact, have been derived from aplitic sources west of the pit, with mineralizing fluids following these faults up-dip to the east (Fig. 38).

The old underground mine lies between the Southwest ore body and pit mineralization (Plate 1) but is distinguished from them by the presence of mineralization in large veins, rather than in a porphyry-style stockwork. These veins fill 20-40° south-dipping faults that parallel the aplite-andesite contact and are located a few meters to a few tens of meters below this contact. Veins were filled with early quartz-biotite-molybdenite-orthoclase-fluorite, followed by quartz-molybdenite-base

metals-fluorite and later calcite-rhodochrosite (Schilling, 1956). Similarities in vein mineralogy and paragenesis between the old underground vein system and the adjacent Southwest ore zone lead to the conclusion that underground mineralization is a more structurally controlled portion of the Southwest zone mineralizing system.

Previous workers interpreted these low-angle, contact-parallel structures as being the result of plutonic-induced stresses (Shilling, 1956). By this theory, sheeted fracturing occurs in the chilled carapace of the pluton due to the continued upward pressures of the rising, still-molten core (Shilling, 1956). Recent recognition of the importance of low-angle faulting in the district, however, leads to the speculation that these low-angle veins may, in fact, be following south-dipping splays of the pre-mineral low-angle fault system.

Southwest ore body

The Southwest ore body (Figs. 5 and 39) has been extensively developed and mined over the last 15 years, and most of the recent progress in understanding molybdenum mineralization at Questa applies to this deposit. This deposit contains approximately 120 million tons of ore at a grade of 0.3% MoS_2, and has been mined by underground block-cave methods since 1983. The mineralized zone is long and slender, having an approximately 2 km long E-W dimension (Plate 1) and averaging 170m and 200m in height and width respectively. Mineralization is restricted to within a few hundred meters above the intrusive aplite-andesite contact, along the sub-

surface connection between the Log Cabin and Sulphur Gulch plutons (Figs. 37, 39, and 40).

Mineralization and intrusion are strongly controlled by two fault sets. One fault set strikes approximately E-W, dips to the north at low to moderate angles and is exposed at the surface 700 to 1000 m south of the deposit (Plate 2). The second fault set dips N55W at low to moderate angles and is recognized only in drill holes and underground mine exposures of the Southwest ore zone. The northwest dipping fault set controlled fluid pathways on a local scale, resulting N35E oriented zones of thick mineralization within an overall N75E oriented ore body. Both of the above fault sets, along with mineralization and alteration of the Southwest ore zone, are cross-cut by a third N-S striking set of normal faults (Fig. 39).

Details of the Southwest ore body are evident on Fig. 40, which is oriented perpendicular to the local-scale structural, lithologic and mineralogic grain of the deposit (Fig. 40). Fig. 40 demonstrates the limits of 0.2% MoS_2 mineralization, the distribution of the magmatic hydrothermal breccia (discussed in more detail below), the close spatial relationship of mineralization to low phenocryst content aplite phases, and the extreme degree of control the north-dipping faults impart on mineralization and intrusion.

host rock and intrusive phases associated with mineralization

The vast majority of the mineralization is hosted in caldera-floor andesite that has been tilted near 90° to the west prior to mineralization. Evidence for this tilting includes high-angle dips of stratigraphically

higher tuff and stratigraphically lower sediments in underlying and overlying tectonic blocks (Plates 1 and 2). Rare intercepts of foliated andesite in drill core contain 70 to 90° dips to foliation, as well. The low- to moderate angle north-dipping fault set has upper-plate-to-the-east offsets and is responsible for the extreme stratal tilts. The andesite is locally intruded by pre-caldera quartz latite dikes (Tqli) and caldera-related rhyolite porphyry dikes (Trff) that are often in fault contact with the andesites due to offsets on low-angle faults (Fig. 40).

The intrusive rocks consist of pre- and syn-mineral phases of the aplite followed by post-mineral rhyolite porphyry dikes and stocks and finally by quartz latite to lamprophyre porphyry dikes. The main syn-mineral pluton reaches its apex immediately north of the Southwest zone (cross-section B-B', Plate 1; Figs. 40 and 41). The north flank of this apex dips at a low angle and is smooth, while the southern flank dips at a medium to high angle and is highly irregular (cross-section B-B', Plate 1; and Fig. 40). This geometry is interpreted to be due to the structural grain of the low-angle north-dipping fault zone, causing smooth, fault-parallel northern contacts and irregular, diked, south-facing margins. Textural variability within the syn-mineral pluton is concentrically zoned relative to the irregular southern margin of the pluton. Much of this textural variability is interpreted to result from volatile exsolution, chilling of residual magma and reaction of volatile-rich phases with andesitic wall rock. Conformity of textural variability to the southern margin implies

that volatiles escaped at right angles to this margin, up the dip of the pre-existing structural grain.

The earliest intrusive phase is a texturally-variable rind of aplite porphyry (Tapp, of Fig. 40) that pre-dates mineralization and is interpreted to have reacted extensively with its andesitic host. Details of this unit, termed contaminated aplite, are discussed in the district-wide lithology section on pre-mineral intrusions.

A fine grained, low phenocryst content aplite porphyry (Tap of Fig. 40) intrudes the contaminated rind and is interpreted to represent the source of the molybdenum mineralizing fluids (Fig. 18). The fine grained aplite lies structurally down-dip of molybdenum mineralization and is extensively quartz veined immediately down-dip of the highest grade mineralization (Fig. 40). This veining, termed early barren quartz veining, locally makes up to 95% of the volume of the rock. Veining intensity diminishes to near zero about 50 meters down-dip (down and to the northwest) of the contact. The spatial association of early barren quartz veining with the fine-grained aplite suggests that these veins represent the exsolution of magmatic-derived fluids, causing the rapid quenching of the fine grained, aplitic phases. The location of early barren quartz veins immediately down-dip from the highest grade molybdenum mineralization suggests that these magmatic fluids were, in fact, a major source of molybdenum mineralization.

Unidirectional solidification textures are located in the fine grained source aplite as well as in coarser grained, more phenocryst rich units (Fig.

43). These features consist of crenulate quartz bands similar to that described by Shannon and others (1982) at the Henderson mine, Colorado. Shannon and others interpret these features to represent quartz precipitation on the physical wall of the magma chamber, during short-term pauses between volatile release-induced quenches of the magma (Shannon et. al., 1982). At Henderson, these features were used to distinguish between texturally and compositionally identical intrusive pulses.

At Questa, crenulate quartz banding is commonly located below ore indicating the paleo-margins of magma chambers that are spatially related to mineralization. Crenulate quartz banding is also found, however capping intrusive phases that have no associated molybdenum mineralization. Crenulate banding appears to be indicative of a volatile-rich magmatic system, but is not necessarily an indicator of molybdenum mineralization.

Rhyolite porphyry dikes and stocks follow the north dipping fault system (cross-section B-B', Plate 1; Fig. 40), and are interpreted to have emanated from deeper-level portions of the cooling granite-aplite pluton (Leonardson et. al., 1983). These rhyolite porphyry bodies post-date 90-100% of the molybdenum mineralization. Local quartz-molybdenite, quartz-molybdenite-pyrite and molybdenite paint veins cross-cut some of the rhyolite porphyry dikes, and some rhyolite porphyry stocks and dikes contain xenoliths with quartz-molybdenite veining, crenulate quartz banding and early barren quartz veins. Quartz latite to lamprophyre dikes

post-date all mineralization and alteration in the district and are volumetrically insignificant (Plate 2).

structures

Major structures in the Southwest ore body fall into 3 categories: 1) north-dipping, medium to low-angle faults with pre- and post- ore movements, 2) northwest dipping medium to low-angle faults, and 3) post-mineral, east-dipping normal faults. The north-dipping and east-dipping fault sets are part of the regional structural pattern previously described. The NW-dipping fault set is only evident in the sub-surface of the Southwest ore zone.

Relative motion on the north-dipping fault set is upper-plate to the ENE as indicated by: 1) ENE striking fault plane corrugations exposed in underground workings, 2) ENE offsets on dikes and marker units and 3) the severe WSW tilting of the Tertiary stratigraphy. Pre-intrusive and pre-mineral offset is indicated by the termination of faults at intrusive contacts and by the lack of evidence for tilting of the ore body or its associated intrusion (Hagstrum et. al., 1982; Hagstrum and Lipman, 1986). Motion on individual strands of this fault set is as great as 1 km as indicated by top-to the-ENE offsets on Tertiary sedimentary units exposed at the surface (Plate 2). Relative motion on the northwest-dipping fault set is unknown and the total offset appears to be minor.

In the Southwest ore zone, north-dipping and northwest-dipping faults create a zone greater than 100 meters thick of intense faulting and fracturing (cross-section B-B', Plate 1; Fig. 40). Deformation is brittle,

with fault zones containing breccia and localized chlorite-clay gouge . These fault zones exerted first-order controls on mineralization by: 1) constraining the apex of the intrusion, 2) tectonically shattering a zone that subsequently developed into the magmatic-hydrothermal breccia (Fig. 40), and 3) channeling molybdenum-related hydrothermal fluids. North-dipping fault zones appear to have controlled the overall shape of the apex to the intrusion (Fig. 41), the overall trend of the Southwest ore zone, and been the major conduits for E-W to ENE striking dikes that reached the surface. Northwest-dipping faults controlled intrusive apexes and fluid pathways on a local scale, resulting in local N35E striking intrusive apexes and N35E striking region of thick magmatic-hydrothermal breccia within the overall N75E trending ore zone (Figs. 39 and 40).

Post-mineral motion on low-angle faults occurs largely as reactivation of the north-dipping fault set. This late-stage fault movement locally cross-cuts the magmatic hydrothermal breccia, causing minor attenuation of the Southwest ore zone (Fig. 42). The upper and lower bounding contacts of the magmatic hydrothermal breccia often represent pre-mineral, fluid channelling faults that also demonstrate post-mineral offset. Surface exposures of these late-stage faults show offset of mineralization-related alteration (Fig. 30), and deep underground mine exposures demonstrate local continuance of these faults into higher-level portions of the underlying pluton (Fig. 40).

Post-mineral rhyolite porphyry dikes parallel the low-angle north-dipping structural grain and are locally offset by this late-stage

reactivation episode. Although the lack of sufficient markers hinders accurate determinations of offset amounts, mineralization, alteration, and dike attenuation suggest tens-of-meter scale and local >100 meter scale motions for this faulting event.

The last structural event to effect the Southwest ore body is the formation of a set of east-dipping normal faults that cross-cut the ore zone in two distinct zones near the western half of the ore body (Fig. 39, Plate 1). These faults cause as much as 80-100 meters of offset on mineralization down to the east, affecting the recovery of ore and causing regions of unstable rock within the underground mine.

mineralization-alteration

Mineralization and related alteration events for the Southwest ore zone are interpreted as follows: 1) pre-mineral biotization, 2) main-stage magmatic-hydrothermal breccia mineralization and associated alteration, 3) quartz-molybdenite-pyrite veining and associated alteration, 4) molybdenite paint deposition, 5) quartz-sericite-pyrite alteration associated with rhyolite porphyry diking, 6) quartz-fluorite-sericite-pyrite-base metal veining and 7) youngest calcite / gypsum veining (Fig. 17). The above are presented in a generalized chronological order, although significant temporal overlaps occur.

In many cases, the collapse of the hydrothermal system over time may result in apparent chronological relationships between alteration or veining types that are actually distal and proximal portions of the same mineralization-alteration episode. For example, quartz-pyrite veins cross-

cutting quartz-molybdenite veins may indicate that distal quartz-pyrite veining overprinted proximal quartz-molybdenite veining during collapse of the hydrothermal system.

pre-mineral biotization

Pervasive biotite-quartz-magnetite alteration of the andesite is located within 200-500 meters above the contact with the underlying intrusion. Outside of this region, pervasive chlorite-epidote-calcite±pyrite±magnetite alteration predominates. Geochemical analysis of biotized andesite indicates that relatively minor transport of whole rock components has occurred. Whole rock oxygen isotope ratios, and fluorine and phlogopite contents of biotite in the biotized zone are distinctly lower than later magmatic-related biotization and equilibration with meteoric water seems likely (Dave Jacobs, unpublished report for Unocal, 1984). This pervasive biotization, and possibly the more distal propylitic assemblage, is believed to have formed in the presence of meteoric fluids in the thermal aureole to the earliest intrusive phases.

magmatic-hydrothermal breccia and related alteration

A unit termed the magmatic-hydrothermal breccia (MHBx) makes up the core of the Southwest ore zone (Figs. 39 and 40) and is responsible for the majority of the molybdenum mineralization in the central and western portions of the deposit. The MHBx pinches out to the east, however a similar mineral assemblage occurs in veins of the eastern Southwest ore zone and in veins of the old underground ore body (Fig. 39). The MHBx

consists of centimeter to decimeter sized breccia fragments of andesite and local aplite in a pegmatitic matrix of quartz±orthoclase±biotite±molybdenite±rutile, in order of decreasing abundance. Country rock to matrix ratios range from about 70:30 to 90:10. This zone contains from 0.1% to greater than 1% MoS_2 with the molybdenite occurring both as euhedral crystals within the matrix (Fig. 44) and as disseminated molybdenite within the altered andesite fragments.

The term 'magmatic-hydrothermal' is applied to this breccia because the fluids depositing this unit are believed to be at the magmatic-hydrothermal fluid interface. Evidence that these fluids are magmatic-derived includes: 1) close spatial association of this unit to the underlying intrusion, 2) textures in the underlying intrusion that indicate volatile concentration and episodic volatile release, 3) continuity of the early barren quartz veining (formed by release of magmatic volatiles) with the matrix of the MHBx, 4) the pegmatitic nature of the deposit and 5) heavy oxygen isotope values in the MHBx, suggestive of a magmatic origin of the fluids (Dave Jacobs, unpublished report for Unocal, 1984).

The MHBx is bounded between upper and lower north-dipping faults that have both channelized MHBx related fluids, and later offset the MHBx to at least a small degree (Figs. 40 and 42). The region between these two faults, now occupied by the MHBx (Fig. 40), was probably tectonically shattered by low-angle faulting prior to mineralization. Similar zones of tectonic shattering are common throughout the Questa region. This initial

weakening would have aided later brecciation by fluids that were exsolved from the volatile-rich cap of the underlying magma body.

The MHBx is vertically zoned into three assemblages based on matrix mineralogy (Figs. 40 and 44). From the bottom-up, these assemblages are the quartz, quartz-orthoclase and quartz-biotite-orthoclase-molybdenite zones.

The lowermost portion of the MHBx contains 20-50 percent matrix of only quartz, 45-75 percent clasts of biotized and/or orthoclase flooded andesite and 5-8 percent aplite clasts (Fig. 44a). The contact of this zone with the down-dip source aplite is transitional within 1 to 2 m. At this point, early barren quartz veining in the source aplite is indistinguishable from the quartz matrix in the MHBx and the two are thought to be precipitated from the same magmatic-derived fluids.

Aplite clasts in the basal MHBx zone probably represent dikes in the andesitic wall rock that were subsequently brecciated during MHBx fragmentation. The preservation of domains of higher and lower aplite content within this zone indicate that mixing of clasts during brecciation probably occurred over distances of meters but not 10's of meters.

The quartz-orthoclase matrix MHBx overlies the quartz matrix unit and contains from 3-8 percent coarse grained orthoclase in the matrix. This unit has both orthoclase flooded and biotite stable andesite clasts, includes little or no aplite fragments, and contains minor amounts of molybdenite as books in the matrix (Fig. 44b).

The quartz-biotite-orthoclase-molybdenite unit of the MHBx overlies the quartz-orthoclase unit, although locally the boundary between this unit contains a parting of unbrecciated andesite. This part of the MHBx is by far the highest grade portion of the ore body. The matrix contains coarse grained molybdenite books and roses (known locally as clotty moly) in close spatial association with coarse grained biotite, and the orthoclase flooded fragments often contain significant disseminated molybdenite, as well (Fig. 44c). Quartz-biotite-molybdenite veins emanate up-dip from the top of the MHBx, and veining in the old underground mine also contains assemblages that indicate derivation from the MHBx system.

Andesite clasts in this zone are strongly orthoclase flooded in contrast to the andesite clasts in the underlying zone, which are commonly biotite stable. It is interesting that in the only portion of the MHBx where biotite is located in the matrix of the breccia, biotite is absent from the brecciated clasts.

Structurally up-dip from the MHBx is a zone approximately 100-150 m thick of pervasive orthoclase-quartz-sericite-green sericite-magnetite alteration. This alteration assemblage is mostly restricted to the region between the major, MHBx-bounding faults, but extends into the hanging wall block immediately above the top of the MHBx. Over 150 m up-dip from the ore body, the MHBx related alteration becomes partially structurally controlled and consists of quartz-sericite-green sericite-specular hematite (Fig. 45). Exposure of this more distal alteration assemblage

above and to the south of the ore body (Fig. 46) is the most accurate surface indication of Southwest ore zone mineralization.

quartz-molybdenite-pyrite veining and associated alteration

The MHBx is cross-cut by a veining assemblage that is zoned from proximal quartz-molybdenite, through quartz-molybdenite-pyrite, to distal quartz-pyrite. Mineralization of this episode makes up a significant part of the ore body beyond the boundaries of the MHBx, and adds to the already high-grade mineralization within the MHBx. Boundaries between the various vein assemblages are gradational and diffuse due to the multi-pulse nature of this mineralization episode and to the apparent overprinting effects of the distal vein assemblage as the hydrothermal system collapsed.

The outer limit of significant quartz-molybdenite or quartz-molybdenite-pyrite veining is less than 100 m beyond the 0.2 percent MoS_2 cutoff (Fig. 40). The inner portions of this zone consists of quartz-molybdenite and quartz-molybdenite-pyrite veins and veinlets with biotite alteration selvages and orthoclase-flooded haloes. Where vein and veinlet intensity is sufficiently dense, the alteration haloes coalesce to form a pervasively orthoclase-flooded rock.

molybdenite paint

Thin fracture fillings of pure molybdenite cross-cut all MHBx mineralization, and most of the quartz-molybdenite and quartz-molybdenite-pyrite veining assemblages. This final stage of

mineralization adds to the grade of the overall deposit and demonstrates the multi-phase nature of molybdenum mineralization at Questa.

quartz-sericite-pyrite alteration associated with rhyolite porphyry diking

Rhyolite porphyry dikes cross-cut all but the latest phases of molybdenum mineralization in the Southwest deposit. These dikes are nearly unmineralized and unaltered within the vicinity of the Southwest ore body. Dikes and minor stocks immediately to the north of the deposit, however, are strongly quartz-sericite-pyrite altered and have strongly altered their host rock.

quartz-fluorite-sericite-pyrite-base metal sulfide veining

Late-stage quartz-fluorite-sericite-pyrite-base metal sulfide veining and associated alteration is located distally to the ore deposit and cross-cuts rhyolite porphyry dikes. This mineralization-alteration is responsible for fluorite and base metal haloes above the deposit. The location of these anomalies vertically above the deposit, rather than structurally up-dip, may indicate a declining influence of the low-angle fault system on fluid migration as the hydrothermal system becomes less focused and more meteoric.

calcite / gypsum veining

Calcite and gypsum veining is the youngest molybdenum-related event to effect the region of Southwest zone mineralization. The majority of the region around the ore body, and much of the district as well, is significantly veined by calcite. Gypsum veining substitutes for calcite, however, in the region extending up-dip of the molybdenum ore body. As in

many hydrothermal systems, this late-stage event is interpreted to represent meteoric influx into the deposit as the hydrothermal system waned.

deuteric alteration

Deuteric alteration is associated with post-mineral latite porphyry and lamprophyre porphyry dikes (Fig. 17). Alteration is largely restricted to the dikes and consists of a classic propylitic assemblage of epidote, chlorite, calcite, and local magnetite.

Comparison to "Climax type" systems

The Questa molybdenum deposit can best be considered as a variant of the Climax-type system exemplified by the Climax and Urad-Henderson molybdenum ore bodies (Wallace et. al., 1968; Wallace et. al., 1978). Similarities include: 1) tectonic setting in an early-stage extensional environment, 2) geochemically equivalent high-silica, alkali-rich intrusions and 3) petrologic features in the source intrusions, including crenulate quartz banding, quench textures and early barren quartz veins.

Questa differs significantly from the typical Climax deposit in: 1) host-rock composition, 2) the degree of structural control on the intrusive rocks and mineralization and 3) the style of mineralization in the core of the deposit (the magmatic-hydrothermal breccia).

Although the intrusive rock chemistry and petrology differs very little from the typical Climax system, the effects of the overlying andesitic host rock on mineralization are marked. This more mafic host rock results in: 1) relatively telescoped geochemical haloes and alteration assemblages and 2)

early intrusive phases that are interpreted to have been significantly contaminated due to wall rock assimilation. Similar amounts of assimilation in Molybdenum-bearing igneous systems such as at Climax would not be easily recognizable, if they occurred, due to a lack of contrast in wall rock / host rock compositions.

The extreme amount of structural control of the north dipping fault system on the intrusions and mineralization at Questa is in sharp contrast to Climax type systems. Molybdenum mineralization in Climax type systems is generally centered in an upside-down teacup geometry, immediately over the apex of a stock (Wallace et. al., 1968; Wallace et. al., 1978). The symmetrical arrangement of the mineralization above the stock is interpreted to be due to hydrofracturing of the wall rock by over pressured magmatic volatiles (Wallace et. al., 1978). The influences of regional faults and stress on intrusive and mineralization geometries are minimal.

At Questa mineralization is distributed along the ENE trending axis of a pluton, and the structural controls on intrusions and mineralization are major. These influences include: 1) the ENE alignment of the mining district, 2) the ENE alignment of the pluton apex and subsequent ore body, 3) north-dipping structural controls on the shape of the pluton apex, 4) possible pre- to syn- mineral tectonic shattering to allow formation of the magmatic hydrothermal breccia, 5) north-dipping structural control of the mineralization and alteration and 6) north-dipping structural control on post-mineral diking.

The formation of a magmatic-hydrothermal breccia (MHBx) at Questa is very unique from the typical stockwork molybdenum deposits as at Climax. The development of the MHBx is a function of tectonic preparation of the rock at Questa and of the unique structurally controlled, pluton apex geometry. At Questa, exsolving fluids were not concentrated over a point source as at Climax, and the pre-existing structural preparation prevented pressures sufficient to allow concentrically-zoned hydrofracturing. Fluid pressures greater than lithostatic at Questa caused lifting and space formation in tectonically-prepared low-angle fault zones, resulting in brecciation. Open spaces within the breccia were subsequently infilled by pegmatitic minerals derived from the exsolving fluid.

District-wide exploration model

An improved model for molybdenum exploration in the district is now in place. Significant features of this model include: 1) recognition that apparently intermediate composition dikes can be emanating from highly-evolved, volatile-rich igneous bodies that have reacted in part with intermediate composition wall-rock; 2) recognition that low-angle faults play a critical role in channeling hydrothermal fluids, causing very significant lateral offsets to the alteration and geochemical haloes that would normally be expected to lie immediately above a molybdenum mineralized zone; and, 3) recognition of a low-angle, structurally controlled quartz-sericite-green sericite-specularite alteration assemblage that is structurally up-dip from molybdenum mineralization. Obvious targets in this model are regions of significant diking in low-

angle fault zones that contain quartz -sericite -green sericite ±orthoclase ±specular hematite ±magnetite alteration. Geochemical and geophysical methods may not be as reliable an exploration tool as the recognition of these mapable features.

REGIONAL MODELS FOR MAGMATIC-TECTONIC INTERACTION

The spatial and temporal overlap of the highly tilted terrain with caldera-related and post-caldera plutonism (Fig. 16) argue strongly that the tilting and plutonism are related. The exact nature of this relationship, however, is somewhat unclear. In this section a number of models will be considered and evaluated that demonstrate how magmatism and regional extension may interact.

A wide variety of processes and relationships may be considered to explain the concentration of extensional tilting at Questa. Tilting may be a function of magma chamber roof foundering (Fig. 47a and b), active stretching over the roof of an expanding magma chamber (Fig. 47c), interaction of a magma chamber with a regional detachment system (Fig. 47d) or focussing of regional extension into a magmatically active area (Fig. 47e and f).

The first two models (Fig. 47a and b) are variations on Lipman's original ideas (figures 7 and 9 of Lipman 1988) and call on block foundering over caldera-related or post-caldera plutons. Lipman's original model predicted symmetrical tilting away from a resurgent axis of intrusion, but this has been modified due to the west tilt of beds across the southern

Questa caldera area (compare figure 6 of Lipman, 1988 to cross section A-A' and Fig. 48 of this paper).

Both of these models (a and b) suggest minor amounts of extension (≤30%?) both within and outside of the extremely tilted region with the area of strongest tilt representing block foundering over the top of syn- to post-caldera plutons. Figure 47a implies block foundering above the post-caldera pluton and suggests that caldera ring structures acted as breakaway zones to the west and east and as tear faults to the north and south. This model is similar to that of Lipman (figure 6 of Lipman, 1988) except for the lack of symmetrical tilting. Figure 47b implies block foundering above the post-caldera pluton that cooled approximately 1 m.y. after caldera formation and implies no or minor use of caldera-margin ring structures. Model b (Fig. 47b) is preferred over model a (Fig. 47a) because of its non-reliance on caldera margin structures (not observed to be reactivated during tilting) and due to its slightly later time frame, allowing the 2.5 km thick intracaldera tuff and possible resurgent plutons to cool before tilting.

Special conditions that are not found at Questa would be required in order for foundering to produce the observed near 90° of tilt with ≤30% of extension (Wernicke and Burchfiel, 1982). Listric faults would need to have radii of curvature on the order of 1-3 km and some currently unknown mechanism would be necessary to allow independent motion of listric fault blocks. No strongly curved listric faults are observed at Questa, although faults with large radii of curvature may be locally present (Fig. 48 and

cross-section A-A' of Plate 1). Additionally, the general decrease in tilt of fault-blocks from west to east (Fig. 24a,b and c) suggests that the blocks were interrelated, but in a way that is counter to the additive increase in dip that would be expected if adjacent listric fault blocks had interacted (Wernicke and Burchfiel, 1982). This pattern suggests that listric faults are not significant at Questa.

Figure 47c indicates batholith-scale pluton emplacement into a block-faulted region in which the lateral expansion of an actively implaced pluton and/or the gravity effect of pluton-induced arching causes extreme extensional deformation above the pluton. Coupled with this pluton-capping extension is compression to the east and west caused by the forceful shouldering aside of the expanding pluton or by the weight of the sliding gravity block. In this model the net bulk strain of an ENE transect through the extended area over the pluton and the adjacent compressed region would be an increment of extension that is sub-equal in magnitude to extension in a parallel transect immediately north or south, in the non-pluton affected area. While the above model cannot be ruled out with certainty, there are no known mid-Tertiary compressional structures exposed to the east (or west) of the Questa mining district.

Figure 47d demonstrates a situation in which a detachment-style fault interacts with a magmatically active area in one of two ways. In one scenario, detachment faults developed in the time interval between intrusion of caldera-related and 1 m.y. younger plutons, yet the detachment faults had no physical relationship to them. This seems unlikely,

considering the significant spatial and temporal coincidence of extension and plutonism (Fig. 16). In another scenario, co-genetic detachment-style extension is modified laterally in the region of the pluton to a system that exhibits ductile deformation at depths below 3-5 km and brittle deformation in the upper crust. This implies the existence of a currently unrecognized detachment-style structure in the greater Questa region, which is not supported by regional tilting and structural mapping. An east-dipping low-angle fault system immediately east of the Red River town site, however, may be a candidate for a regionally extensive low-angle structure (Plate 1).

Figure 47e and f are the preferred models and imply that extensional deformation was concentrated into the area of post-caldera magmatism by fault bending (Fig. 47e) or along accommodation structures (Fig. 47f). By these models, the bulk extensional strain across a >100 km long, ENE trending cross-section through the highly extended region would equal the bulk extensional strain of a similar cross-section drawn through moderately extended regions to the north and south. The area of strong extensional strain at Questa would be balanced by regions of weak extensional strain to the ENE and WSW.

Regional mapping with the goal of finding regional structures related to the highly tilted region at Questa could certainly help reduce the above possibilities. Problems with such a project include abundant forest vegetation, the massive and discontinuous nature of the Tertiary stratigraphy and the lack of well-bedded units over much of the Questa

region. The current understanding of the regional geology favors fault bending or accommodation zone focussing (Fig. 47e and f), but aspects of block foundering (Fig. 47b) and of detachment style faulting (Fig. 47d) may also be present.

SOUTHERN CALDERA AREA MAGMATIC-TECTONIC HISTORY

Consideration of the regional constraints and integration of the igneous, structural and hydrothermal history of the southern caldera area results in the following schematic model (Fig. 48). The initial 2-3 m.y. of intermediate composition igneous activity preceding development of a caldera-related batholith was during a period of regional extension characterized by NNW striking normal faulting. Evidence for normal faulting during this time includes pre-caldera quartz latite porphyry dikes that are oriented parallel to NNW striking normal faults of (Lipman, 1983a), and "shear foliation" in some of the dikes that are interpreted to have intruded active NNW trending normal faults.

Eventually, the numerous magmatic centers of the intermediate composition field coalesced to form a granitic batholith (e.g. Lipman et. al., 1978), which erupted to form the Questa caldera. During the formation of the batholith and Questa caldera, and on the order of 10's of thousands of years afterward (enough time for the 2.5 km thick intracaldera tuff to solidify), extension continued in the Questa area at a moderate to slow pace (Fig. 48a). Evidence for extension during this time period includes rheomorphic flowage of the Amalia Tuff outflow sheet over active high-angle fault scarps (Lipman, 1983a), slabby jointing patterns in intracaldera

Amalia Tuff that are interpreted to have formed at right angles to extension, and half-grabens 10 km south of Questa, that preserve easily erodible, fines-enriched, co-ignimbrite fallout tuff (Fig. 8).

Following cooling of the intracaldera unit, the region approximately corresponding to the limits of the Questa caldera and to the limits of 24.6 Ma post-caldera plutons, was severely extended (Fig. 16). In the Questa mining district, extension was accomplished by domino-style tilting of initially high-angle faults and intervening stratigraphy near 90° to the west (Fig. 48b), resulting in low-angle extensional faults and 90° west dipping stratigraphy. The magmatic system is believed to have focussed regional extension into the specific area of post-caldera magmatism for a short time through the bending of normal faults or through accommodation structures (Fig. 47e and f). Batholith-capping brittle faults are believed to have rooted in the partially molten intrusions, and thermally weakened crust under the magma chamber is believed to have extended in a ductile manner.

Intrusive activity post-dating the majority of the low angle extensional faulting continued along the southern caldera margin. Intrusive phases were implaced at successively higher structural levels with the upper portions of the intrusive bodies, porphyry dikes, mineralizing hydrothermal fluids, and the character of the Southwest ore zone being strongly influenced by the previously formed low-angle structural grain (Figs. 40 and 48c).

Following the majority of the mineralization, low-angle faults with minor displacements locally cross-cut high-level portions of the intrusions (Fig. 48d). Activation of extensional structures at anomalously low angles is believed to be possible due to over-pressured hydrothermal fluids that demonstrably followed and brecciated low angle faults zones during the main mineralization epoch. Similarly, pre-mineral motions on low-angle faults (Fig. 48b) may have been aided by earlier over-pressured hydrothermal fluids.

Sometime after the intrusion had cooled, continued regional extension resulted in through-going normal faults that locally have significant offsets, but caused little rotation of intervening stratigraphy (Fig. 48d). This throughgoing block-fault structural style is typical of Oligocene to mid-Miocene extensional deformation in the majority of the southern Rocky Mountains (Tweto, 1979), where magmatic activity did not significantly influence the style of and magnitude of extensional deformation.

Finally, asthenospheric upwelling accompanied by only minor lateral extensional strain, caused formation of the modern Rio Grande rift and uplift and erosion of the rift-flanking Sangre de Cristo range (Fig. 48e).

COMPARISON TO OTHER EXTENDED REGIONS

Questa is an excellent example of high crustal level extension coincident with batholith-scale intrusion and thus invites comparison to other syn-magmatic extensional areas in the western North America. Questa is the northernmost of a number of highly extended areas along the Rio Grande rift that formed during the early phase of regional extension

(Baldridge et. al., 1984). Two of the best studied of these areas, the Lemitar and Organ Mountains, are associated with Oligocene-Miocene magmatism (Chamberlin, 1978, 1983; Seager, 1981; Seager and McCurry, 1988). The Lemitar Mountains exhibit syn-extensional growth fault relationships in sediments and outflow tuffs indicative of high-strain rate extension synchronous with large-scale magmatic activity that was centered to the south (Chamberlin, 1978, 1983). The Lemitar Mountains exhibit a *volcanic*-tectonic association, but any relationship between high extensional strain rate and *plutonism* is tenuous.

In the Organ Mountains a volcanic field with nested calderas is tilted to the west by east-dipping normal faults (Seager, 1981; Seager and McCurry, 1988). These faults are at angles < 50°, have stratigraphic offsets of 1.5 to 2.4 km, and are intruded by a batholith that is geochemically related to the overlying volcanic stratigraphy. Additionally, in the Organ Mountains the underlying, partially post-fault, batholith cooled within 1 m.y. after caldera formation (Seager, 1981; Seager and McCurry, 1988). As at Questa, there is debate as to whether syn-magmatic faulting is related to regional extension or to the local effect of caldera resurgence or roof foundering (Seager and McCurry, 1988). More detailed mapping, dating and paleomagnetic work in the Organ Mountains may help define the degree of locally-induced vs. regionally-related magmatic-tectonic interactions.

Other possible regions of syn-magmatic extension throughout the Basin and Range province include the Eldorado Mountains, Nevada (Anderson,

1971), the Castle Dome Mountains, Arizona (Gutmann, 1982), South Mountain, Arizona (Reynolds, 1985), Yerington, Nevada (Proffett, 1977), east-central Nevada and west-central Utah (Gans et. al., 1989) and Death Valley, California (Wright and Troxel, 1973). The Eldorado Mountains are similar to the Questa region as extension, volcanism and upper-crustal level plutonism all overlapped within an approximately 6 m.y. window during the mid-Miocene and the area of extreme extension is underlain by regionally extensive plutons. Anderson (1971) initially proposed that extension took place as a thin skin to a radially expanding pluton, but has subsequently de-emphasized the importance of plutonism as the regional detachment-style of the Colorado River extensional corridor came to be recognized (personal communication, Anderson, 1986). One wonders, however, if detachment style and pluton-capping styles of extension might not be able to co-exist along strike as part of the same overall extensional event (e.g. Fig. 47d).

Most highly extended regions in the Basin and Range province, including those with cogenetic magmatic activity, are considered to be related to regionally extensive detachment faults that root at mid-crustal or deeper levels (Wernicke, 1981, 1985; Davis and Lister, 1988). In contrast, the Questa model above (Fig. 48b) calls upon initially high-angle normal faults rooted in a partially molten batholith-sized intrusion and for the majority of the extensional deformation in and below the intrusion to have been ductile.

The timing of magmatic and structural events at Questa (Fig. 49) is in accord with a model presented by Gans and others (1989) for extension in the Basin and Range and Rio Grande rift provinces (Fig. 50). In this model, accelerated extension is preceded by a few m.y. of magmatic activity (Fig. 50), which thermally weakens the crust, allowing it to extend. Magmatism is fundamentally basaltic (Hildreth, 1981) and asthenospheric upwellings are envisioned as initiating an active rifting process (Gans et. al., 1989). This model is supported by mass-balance calculations for sections of the Basin and Range province that suggest addition of crustal material by magmatic intrusion and underplating of the middle and lower crust (Okaya and Thompson, 1987; Gans, 1987).

Although evidence at Questa supports a magmatic-tectonic linkage, a number of processes in the Questa region may be different than those suggested by Gans (Gans et. al., 1989). At Questa, thermal *and* mechanical weakening of the crust may have occurred in contrast to the purely thermal processes envisioned by Gans. This is likely due to the unusually shallow crustal-level of the intrusions at Questa, which may have acted as ductily deforming bodies.

Also at Questa, magmatism may be driven by basaltic injections, but it appears unlikely that asthenospheric upwellings related to the magmatic system are actively driving extension. The region effected by extension is much larger than the Questa magmatic system as the entire length of the Rio Grande rift began extending at approximately the same time, between 28-32 Ma (Chapin and Seager, 1975; Tweto, 1979; Price and Henry, 1984;

Chamberlin, 1978, 1983). Magmatism at Questa somewhat fortuitously overlaps with the initiation of extension over the entire region. This timing suggests that magmatism at Questa is not the cause of extension, but rather focuses regional extension into the thermally and mechanically weakened area.

Of importance is whether Questa represents a unique system in which regional extension only interacts with batholith-scale magmatism at extremely high crustal levels, or whether Questa represents a high-crustal-level end member of magmatic-extensional systems that occur at deeper crustal levels elsewhere (e.g. Gans et. al., 1989). In the first case, Questa represents a relatively insignificant geologic curiosity. In the second, Questa serves as a well constrained end-member example for comparison to systems that may be located throughout the Basin and Range province and elsewhere. Further studies of syn-magmatic/ extensional systems are needed to answer this question.

CONCLUSIONS

A number of interesting aspects of the magmatic, structural and hydrothermal history of the Questa mining district are summarized below:

1) A new volcanic rock-type, termed the basal broken crystal zone, has been described in the intracaldera Amalia Tuff. This unit is believed to represent the initial vent-clearing phase of ring vents to the Questa caldera following short-term pauses in the caldera eruption cycle. The location of this highly-fragmental deposit on top of megabreccia blocks and block trains is in keeping with a model of laterally migrating ring-vents.

By this model the megabreccia blocks are deposited on top of intracaldera tuff during pauses in the eruptive cycle that occur between the waning of one vent and the explosive initiation of the next ring-vent source. The explosive eruption of the new ring vent forms a fragmental deposit that is only locally preserved on top of irregular megabreccia block topography.

The basal broken crystal zone and its relationship to the megabreccia deposit implies non-steady state eruption and collapse of the caldera, even though the massive and unzoned nature of the interior of the intracaldera unit would otherwise lead one to believe that it was deposited in one eruptive pulse. Identification of basal broken crystal zones in other caldera settings may shed light on caldera collapse and eruption processes in general.

2) Structural re-interpretation of the district indicates that caldera-related faults and events are much less important in the control of extensional style, intrusion and mineralization than previouly believed (e.g. Lipman, 1983a; Leonardson et. al., 1983). Detailed mapping of the southern caldera area has demonstrated that tilting is not symmetrically aligned about a "resurgent axis" in this area and that southern caldera ring-faults did not act as tear zones. Rather, a picture is emerging where the concentration of extension is a function of the post-caldera batholithic intrusions interacting with a regional stress field and where "domain bounding" structures only locally correspond to earlier caldera-related faults.

Additionally, the recognition of Precambrian-aged E-W to ENE structural elements in the southern caldera region leads to the suggestion that this pre-caldera grain was the overriding control on later ENE oriented features. This grain is believed to have been a primary influence on the location and linearity of the southern caldera margin, later plutonism and pluton-related molybdenum mineralization.

3) Mapping relationships, age dating and paleomagnetic studies have demonstrated a close spatial and temporal relationship between extension and batholithic-scale intrusive activity. While the exact method of extensional focussing remains unclear, it appears that the region over a batholith-sized intrusion was preferentially extended due to thermal weakening by the long-lived magmatic system and due to mechanical weakening by the partially molten intrusive body itself.

4) Greater than 200% extension of the southern caldera region was accomplished by domino-style tilting of originally high-angle faults into low-angle orientations. The entire near-90° tilting of these faults and their intervening stratigraphy occurred in the one million year period between 25.7 Ma formation of the Questa caldera and 24.6 Ma cooling of the subjacent batholith to below the near 580°C curie point of magnetite and the near 280°C blocking temperature of biotite.

5) Extensional faults that are now at low angles were apparently active during their entire rotation from near-vertical to near-horizontal. Cross-cutting relationships and palomagnetic evidence unequivocally show that late-stage offsets on low-angle faults occurred when the faults were

oriented at low angles. High fluid pressures associated with the hydrothermal system are believed responsible for lowering the effective stress, allowing motion to continue through rotation to unusually low-angle orientations.

6) The Southwest ore zone deposit was formed by magmatic-derived fluids that were strongly controlled by a low-angle fault zone. The ore body, molybdenum mineralization, molybdenum-related alteration and rhyolite porphyry dikes are strongly distributed along a north-dipping low-angle fault zone. The magmatic-hydrothermal breccia, a unique pegmatite-like deposit that makes up the core of the molybdenum deposit, is believed to have formed because of intrusion of the volatile-rich aplite into a low-angle fault zone. Initially, the north-dipping fault zone controlled the geometry of the apex of the aplite body by differential stoping of the more broken fault material. Finally, invasion of the low-angle fault zone by over-pressured magmatic-derived fluids caused lifting and brecciation of the fault zone and deposition of a pegmatitic breccia infilling.

7) Questa presents an excellent example of interaction between magmatic, extensional tectonic and hydrothermal processes. Magmatic activity caused a concentration of regional extension into the Questa area. Resultant low-angle structures caused flat-topped intrusions, controlled porphyry dike intrusion, strongly channelized hydrothermal fluids, and allowed formation of a magmatic-hydrothermal breccia. Hydrothermal fluids allowed motion to occur on the low-angle fault planes long after they would have otherwise been "frozen".

ACKNOWLEDGEMENTS

Gail Kirchner, Mike Schulz, Dave Jones, Jim Shannon, Joel Metcalf, Jay Evans, Ralph Stegan, Less Osborne and Steve Atkin made significant contributions to the mapping. Gail, Mike, Dave and Steve were especially involved in the early stages and provided significant input of work and ideas. Peter Lipman's excellent regional work served as a springboard to our studies; his input and advice are appreciated. Gerald Czamanske and Ken Foland are thanked for sharing age dates analyzed in their laboratories. R. V. Fisher and Eric Frost were especially helpful as advisors to JWM during his dissertation research.

Management support by Gene Dewey is acknowleged. Significant financial assistance was given to JWM from the Union Oil Foundation, a Chevron Research Fellowship and a grant from the New Mexico Bureau of Mines and Mineral Research.

REFERENCES

Aleinikoff, J.N., Reed, J.C., Jr., and Pallister, J.S., 1985, Tectonic implications from U-Pb dating of detrital zircons from the early Proterozoic terrane of the central Rocky Mountains (abs.): Geological Society of America Abstracts with Programs, v. 17, p. 510-511.

Anderson, E.M., 1951, The dynamics of faulting (2nd edition); Oliver and Boyd, Edinburgh.

Anderson, R.E., 1971, Thin skin distension in Tertiary rocks of southeastern Nevada: Geological Society of America Bulletin, v. 82, p. 43-58.

Angelier, J., and Colletta, B., 1983, Tension fractures and extensional tectonics: Nature, vol. 301. p. 49-51.

Axelrod, D.I., and Raven, P.H., 1985, Origins of the Cordilleran flora: Journal of Biogeography, v. 12, p. 21-47.

Baldridge, W.S., Olsen, K.H., and Callender, J.F., 1984, Rio Grande rift: Problems and perspectives: New Mexico Geological Society Guidebook, 1984, p. 1-12.

Bookstrom, A.,A., 1981, Tectonic setting and generation of Rocky Mountain porphyry molybdenum deposits: Arizona Geological Society Digest, v. 14, p. 215-226.

Bookstrom, A.A., Shannon, J.R., and Smith, R.P., 1985, Bimodal rhyolite-kersantite suites of the Climax and Red Mountain porphyry molybdenum systems, Colorado (abs.): Geological Society of America, Abstracts with Programs, v. 17, no. 4, p. 210.

Carpenter, R.H, 1968, Geology and ore deposits of the Questa molybdenum mine area, Taos County, New Mexico; in Ore Deposits of the United States, 1933-1967: AIME Graton-Sales Volume, v. 2, p. 1328-1350.

Cas, R.A.F., and Wright, J.V., 1987, Volcanic successions: modern and ancient: Allen and Unwin, London, 528 p.

Chamberlain, R.M., 1978, Structural development of the Lemitar Mountains, an intrarift tilted fault-block uplift, central New Mexico (abs.): Program and Abstracts, 1978 International Symposium on the Rio Grand Rift, Santa Fe, p. 22-24.

Chamberlin, R.M., 1983, Cenozoic domino-style crustal extension in the Lemitar Mountains, New Mexico: a summary: New Mexico Geological Society, Guidebook 34, p. 111-118.

Chapin, C.E., 1979, Evolution of the Rio Grande Rift: a summary; in Rio Grande Rift: Tectonics and Magmatism, Riecker R.E. (ed.), American Geophysical Union, p. 1-5.

Chapin, C.E., and Seager, W.R., 1975, Evolution of the Rio Grande rift in the Socorro and Las Cruces area: New Mexico Geological Society Field Conference Guidebook no. 26, p. 297-321.

Christiansen R.L., and Lipman P.W., 1972, Cenozoic volcanism and plate-tectonic evolution of the Western United States. II. Late Cenozoic: Philosophical Transactions of the Royal Society of London, v. 271, p. 249-284.

Clark, K.F., 1968, Structural controls in the Red River district, New Mexico: Economic Geology, v. 63, p. 553-566.

Clark, K.F., and Read, C.B., 1972, Geology and ore deposits of Eagle Nest area, New Mexico: New Mexico State Bureau of Mines and Mineral Resources, Bulletin 94, 152p.

Coney, P.J., and Reynolds, S.J., 1977, Cordilleran Benioff zones: Nature, v. 270, no. 1, p. 403-406.

Cordell, L., Long, C.L., and Jones, D.W., 1985, Geophysical expression of the batholith beneath Questa caldera, New Mexico: Journal of Geophysical Research, v. 90, no. B13, p. 11,263-11,269.

Czamanske, G.K., Foland K.A., Hubacher, F.A., and Allen, J.C., 1990, The $^{40}Ar/^{39}Ar$ chronology of caldera formation, intrusive activity, and Mo-ore deposition near Questa, New Mexico: 41st Field conference guidebook, New Mexico Geological Society, Guidebook to 41st Field Conference, p. 355-358.

Davis, G.A., and Lister, G.S., 1988, Detachment faulting in continental extension: Perspectives from the Southwestern U.S. Cordillera: Geological Society of America Special Paper 218, p. 133-159.

Davis, G.A., Lister, G.S., and Reynolds, S.J., 1986, Structural evolution of the Whipple and South mountains shear zones, southwestern United States: Geology, v. 14, p. 7-10.

Dickinson, W.R., 1981, Plate tectonic evolution of the southern Cordillera: Arizona Geological Society Digest, v. 14, p. 113-135.

Eaton, G.P., 1979, A plate-tectonic model for late Cenozoic crustal spreading in the western United States; in Riecker, R.E. (ed.), Rio Grande

rift-tectonics and magmatism: American Geophysical Union, Washington, D.C., p. 7-32.

Eaton, G.P., 1986, A tectonic redefinition of the Southern Rocky Mountains: Tectonophysics, v. 132, p. 163-193.

Eaton, G.P., 1987, Topography and origin of the Southern Rocky Mountains and Alvarado ridge; in Continental Extensional Tectonics, Coward, M.P., Dewey, J.F. and Hancock, P.L. (eds.): Geological Society of London Special Publication no. 28, p. 355-369.

Elston, W.R., Rhodes, T.C., Coney, P.J., and Deal, E.B., 1976, Progress report on the Mogolon Plateau volcanic field, southwestern New Mexico, No.-3 Surface expression of a pluton: New Mexico Geological Society Special Publication No. 5, p. 3-28.

Epis, R.C. and Chapin, C.E., 1968, Geologic history of the Thirtynine Mile volcanic field, central Colorado; in Epis, R.C., ed., Cenozoic volcanism in the Southern Rocky Mountains: Colorado School of Mines Quarterly, v. 63, p. 51-86.

Epis, R.C. and Chapin, C.E., 1975, Geomorphic and tectonic implications of the post-Laramide, late Eocene erosion surface in the southern Rocky

Mountains; in Cenozoic history of the southern Rocky Mountains, Curtis, B.F. (ed..): Geological Society of America Memoir 144, p. 45-74.

Foland, K.A., Linder, J.S., Laskowski, T.E., and Grant, N.K., 1984, $^{40}Ar/^{39}Ar$ dating of glauconites: measured ^{39}Ar recoil loss from well-crystallized specimens: Isotope Geoscience, v. 2, p. 241-264.

Foland, K.A., Chen, J.-F., Linder, J.S., Henderson, C.M.B., and Whillans, I.M., 1989, High-resolution $^{40}Ar/^{39}Ar$ chronology of multiple intrusion igneous complexes: Applicatioon to the Cretaceous Mount Brome complex, Quebec, Canada: Contributions to Mineralogy and Petrology, v. 102, p. 127-137.

Frost, E.G., 1981, Mid-Tertiary detachment faulting in the Whipple Mountains, California, and Buchskin Mountains, Arizona, and its relationship to the development of major antiforms and synforms (abs.): Geological Society of America Abstracts with Programs, v. 13 no. 2, p. 57.

Gans, P.B., 1987, An open-system, two-layer crustal stretching model for the eastern Great Basin: Tectonics, vol. 6, no. 1, p. 1-12.

Gans, P.B., Mahood, G.A., and Schermer, E., 1989, Synextensional magmatism in the Basin and Range Province: A case study from the

eastern Great Basin: Geological Society of America Special Paper no. 233, 53p.

Grambling, J.A., Williams, M.L., and Mawer, C.K., 1988, Proterozoic tectonic assembly of New Mexico: Geology, p. 724-727.

Gross, W.W., and Hillemeyer, F.L., 1982, Geometric analysis of upper-plate fault patterns in the Whipple-Buckskin detachment terrane, California and Arizona; in Frost, E.G., and Martin, D.L. (eds.), Mesozoic-Cenozoic tectonic evolution of the Colorado River region, California, Arizona, and Nevada: Cordilleran Publishers, San Diego, p. 257-265.

Gutmann, J.T., 1982, Geology and regional setting of the Castle Dome Mountains, southwestern Arizona; in Frost, E.G., and Martin, D.L. (eds.), Mesozoic-Cenozoic tectonic evolution of the Colorado River region, California, Arizona, and Nevada: Cordilleran Publishers, San Diego, p. 117-122.

Hagstrum, J.T., and Lipman, P.W., 1986, Paleomagnetism of the structurally deformed Latir volcanic field, northern New Mexico: relations to formation of the Questa caldera and development of the Rio Grande rift: Journal of Geophysical Research, v. 91, no. B7, p. 7383-7402.

Hagstrum, J.T., Lipman, P.W., and Elston, D.P., 1982, Paleomagnetic evidence bearing on the structural development of the Latir volcanic field near Questa, New Mexico: Journal of Geophysical Research, v. 87, p. 7833-7842.

Hagstrum, J.T., and Johnson, C.M., 1986, A paleomagnetic and stable isotope study of the pluton at Rio Hondo near Questa, New Mexico: implications for CRM related to hydrothermal alteration: Earth and Planetary Science Letters, v. 78, p. 296-314.

Hildreth, W., 1981, Gradients in silicic magma chambers: Implications for lithospheric magmatism: Journal of Geophysical Research, v. 86, no. B11, p. 10153-10192.

Hildreth, W., and Mahood, G.A., 1986, Ring-fracture eruption on the Bishop Tuff: Geological Society of America Bulletin, v. 97, no. 4, p. 396-403.

Hon, K.A., 1987, Geologic and petrologic evolutio of the Lake City caldera, San Juan Mountains, Colorado: University of Colorado, PhD thesis, 162p.

Ishihara, S., 1967, Molybdenum mineralization at Questa mine, New Mexico, U.S.A.: Geological Survey of Japan, report 218, 68 p.

Izett, G.A., 1975, Late Cenozoic sedimentation and deformation in northern Colorado and adjoining areas; in Cenozoic history of the southern Rocky Mountains, Curtis, B.F. (ed..), Geological Society of America Memoir 144, p. 179-209.

Jiracek, G.R. , Gustafson, E.P., and Mitchell, P.S., 1983, Magnetotelluric results opposing magma origin of crustal conduction in the Rio Grande Rift: Tectonophysics, v. 94, p. 299-326.

Johnson, C.M., 1986, The Questa magmatic system: petrologic, chemical and isotopic variation in cogenetic volcanic and plutonic rocks of the Latir volcanic field and associated intrusives, New Mexico: PhD dissertation, Stanford, 322p.

Johnson, C.M., and Lipman, P.W., 1988, Origin of metaluminous and alkaline volcanic rocks of the Latir volcanic field, northern Rio Grande rift, New Mexico: Contributions to Mineralogy and Petrology, v. 100, p. 107-128.

Johnson, C.M., Shannon, J.R., and Fridrich, C.J., 1989a, Roots of ignimbrite calderas: batholithic plutonism, volcanism, and mineralization in the southern Rocky Mountains, Colorado and New Mexico: International Association of Volcanology and Chemistry of the Earth's Interior, Field Excursion 15B: New Mexico Bureau of Mines and Mineral Resources Memoir 46, p. 275-302.

Johnson, C.M., Czamanske, G.K., and Lipman, P.W., 1989b, Geochemistry of intrusive rocks associated with the Latir Volcanic Field, New Mexico, and constrasts between evolution of plutonic and volcanic rocks: Contributions to Mineralogy and Petrology, v. 103, p. 90-109.

Johnson, C.M., Lipman, P.W., and Czamanske, G.K., 1990, H, O, Sr, Nd, and Pb isotope geochemistry of the Latir Volcanic Field and cogenetic intrusions, New Mexico, and relations between evolution of a continental magmatic center and modifications of the lithoshpere: Contributions to Mineralogy and Petrology, v. 104, p. 99-124.

Jones, D.M., 1988, Compositionally zoned dikes of the Questa mine area, New Mexico: evidence for magma mixing and crystal fractionation, and implications for the evolution of the Questa magmatic system: M.S. thesis, University of Arizona, 116 p.

Lambert, M.B., 1974, The Bennett Lake cauldron subsidence complex, British Columbia and Yukon Territory: Geological Survey of Canada Bulletin, 227, 213p.

Leonardson, R.W., Dunlop, G., Starquist, V.L., Bratton, G.P., Meyer, J.W., Osborne, L.W., Atkin, S.A., Molling, P.A., Moore, R.F., and Olmore, S.D., 1983, Preliminary geology and molybdenum deposits at Questa, New

Mexico; in The genesis of Rocky Mountain ore deposits - changes with time and tectonics: Society of Exploration Geologists, Denver Region, Symposium Proceedings, p. 151-155.

Lipman, P.W., 1976, Caldera-collapse breccias in the western San Juan Mountains, Colorado: Geological Society of America Bulletin, v. 87, p. 1397-1410.

Lipman, P.W., 1981, Volcano-tectonic setting of Tertiary ore deposits, southern Rocky Mountains: Arizona Geological Society Digest, v. 14, p. 199-213.

Lipman, P.W., 1983a, The Miocene Questa caldera, northern New Mexico: relation to batholith emplacement and molybdenum mineralization; in The genesis of Rocky Mountain ore deposits - changes with time and tectonics: Society of Exploration Geologists, Denver Region, Symposium Proceedings, p. 133-148.

Lipman, P.W., 1983b, Tectonic setting of the mid to late Tertiary in the Rocky Mountain region - a review; in The genesis of Rocky Mountain ore deposits - changes with time and tectonics: Society of Exploration Geologists, Denver Region, Symposium Proceedings, p. 125-131.

Lipman, P.W., 1984, The roots of ash flow calderas in western North America: windows into the tops of granitic batholiths: Journal of Geophysical Research, vol. 89, no. B10, p. 8801-8841.

Lipman, P.W., 1988, Evolution of silicic magma in the upper crust: the mid-Tertiary volcanic field and its cogenetic granitic batholith, northern New Mexico, U.S.A.: Transactions of the Royal Society of Edinburgh, v. 79, p. 265-288.

Lipman, P.W., Prostka, H.J. and Christiansen R.L., 1972, Cenozoic volcanism and plate-tectonic evolution of the Western United States. I. Early and Middle Cenozoic: Philosophical Transactions of the Royal Society of London, v. 271, p. 217-248.

Lipman, P.W. and Mehnert, H.H., 1975, Late Cenezoic basaltic volcanism and development of the Rio Grande depression in the southern Rocky Mountains: Geological Society of America Memoir 144, p. 119-154.

Lipman, P.W., Doe, B.R., Hedge, C.E., and Steven, T.A.,1978, Petrologic evolution of the San Juan volcanic field, southwestern Colorado: Pb and Sr isotope evidence: Geological Society of America Bulletin, v. 89, p. 59-82.

Lipman, P.W. and Mehnert, H.H., 1979, The Taos plateau volcanic field, Northern Rio Grande Rift, N.M., in Rio Grande Rift: Tectonics and Magmatism, Riecker R.E. (ed.), American Geophysical Union, p. 289-311.

Lipman, P.W., Bowman, H.R., Knight, R., Millard, H.T., Pallister, J.S., Street, K.,Wollenberg, H., and Zielinski, R.A., 1982, Instrumental neutron activation analyses of Cenozoic volcanic rocks, phenocrysts, and associated intrusions from the southern Rocky Mountains and adjacent areas: United States Geological Survey Open File Report 82-1069.

Lipman, P.W., Mehnert, H.H., and Naeser, C.W., 1986, Evolution of the Latir volcanic field, northern New Mexico, and its relation to the Rio Grande rift, as indicated by potassium-argon and fission track dating: Journal of Geophysical Research, v. 91, no. B6, p. 6329-6345.

Lipman, P.W., and Reed, J.C.,1989, Geologic map of the Latir volcanic field and adjacent areas, northern New Mexico: U.S. Geological Survey Miscellaneous Investigation Map I-1907.

McKinlay, P.F., 1956, Geology of the Costilla and Latir Peak quadrangles, Taos County, New Mexico: New Mexico State Bureau of Mines and Mineral Resources, Bulletin 42, 32 p.

McKinlay, P.F., 1957, Geology of the Questa quadrangle, Taos County, New Mexico: New Mexico State Bureau of Mines and Mineral Resources, Bulletin 53, 23 p.

Menges, C.M., 1987, Temporal and spatial segmentation of Plio-Quaternary fault rupture along the base of the western Sangre de Cristo Mountain front, northern New Mexico; in Menges C. (ed.) Quaternary Tectonics, landform evolution, soil chronologies and glacial deposits - northern Rio Grande rift of New Mexico, p. 71-93.

Menges, C.M., 1988, The tectonic geomorphology of mountain-front landforms in the northern Rio Grande rift near Taos, New Mexico: PhD thesis, University of New Mexico, 339 p.

Meyer, J.W., and Leonardson, R.W., 1990, Tectonic, hydrothermal, and geomorphic controls on alteration scar formation near Questa, New Mexico: New Mexico Geological Society, Guidebook to 41st Field Conference, p. 417-422.

Meyer, J.W., and Foland, K.A, 1991, Magmatic-tectonic interaction during early Rio Grande rift extension and Questa, New Mexico: Geological Society of America Bulletin (in press).

Molling, P.A., 1989, Applications of the reaction progress variable to hydrothermal alteration associated with the deposition of the Questa molybdenite deposit, NM: PhD thesis, The Johns Hopkins University, 249 p.

Morgan, P., and Golombek, M.P., 1984, Factors controlling the phases and styles of extension in the northern Rio Grande Rift: New Mexico Geological Society, Guidebook to 35th Field Conference, no. 35, p. 13-19.

Morgan, P., Seager, W.R., and Golombek, M.P., 1986, Cenozoic thermal, mechanical, and tectonic evolution of the Rio Grande Rift: Journal of Geophysical Research, v. 91, no. B6, p. 6263-6276.

Morton, W.H., and Black, R., 1975, Crustal attenuation in Afar, in Pilger, A. and Rosler, A., eds., Afar depression of Ethiopia: Struttgart, Schweizerbart, p. 55-61.

Okaya, D.A., and Thompson, G.A., 1986, Involvement of deep crust in extension of Basin and Range province: Geological Society of America Special Paper 208, p. 15-22.

Parker, E.C., Davis, P.M., Evans, J.R., Iyer, H.M., and Olsen, K.H., 1984, Upwarp of anomalous asthenosphere beneath the Rio Grande rift: Nature, v. 312, p. 354-356.

Price, J.G, and Henry, C.D., 1984, Stress orientations during Oligocene volcanism in Trans-Pecos Texas: Timing the transition from Laramide compression to Basin and Range tension: Geology, v. 12, p. 238-241.

Proffett, J.M., Jr., 1977, Cenozoic Geology of the Yerington district, Nevada, and implications for the nature and origin of basin and range faulting: Geological Society of America Bulletin, v. 88, p. 247-266.

Reed, J.C., Jr., 1984, Proterozoic rocks of the Taos range, Sangre de Cristo Mountains, New Mexico: New Mexico Geological Society, Guidebook to 35th Field Conference, p. 179-186.

Reed, J.C., Jr., Lipman, P.W., and Robertson, J.R., 1983, Geologic map of the Latir Peak and Wheeler Peak wildernesses and Columbine-Hondo wilderness study area, Taos County, New Mexico: U. S. Geological Survey Miscellaneous Field Studies Map MF-1570-B, scale 1:50,000.

Reed, J.C., Bickford, M.E., Premo, W.R., Aleinikoff, J.N., and Pallister, J.S., 1987, Evolution of the Early Proterozoic Colorado province: Constraints from U-Pb geochronology: Geology, v. 15, p. 861-865.

Rehrig, W.A., 1969, Fracturing and its effects on molybdenum mineralization at Questa, New Mexico: PhD dissertation, University of Arizona, 194 p.

Reynolds, S.J., 1985, Geology of the South Mountains, central Arizona: Arizona Bureau of Geology and Mineral Technology, Bulletin 195, 61 p.

Robertson, J.M., Grambling, J.A., Mawer, C.K., Bowering, S.A., Williams, M.L., Bauer, P.W., and Silver, L.T., 1991, Precambrian geology of New Mexico; in Decade of North American Geology volume: Geological Society of America (in press).

Schilling, J.H., 1956, Geology of the Questa molybdenum (Moly) mine area, Taos County, New Mexico: New Mexico Bureau of Mines and Mineral Resources, Bulletin 51, 87p.

Schilling, J.H., 1991, A history of the Questa molybdenum (Moly) mines, Taos County, New Mexico: New Mexico Geological Society, Guidebook to 41st Field Conference, p. 381-386.

Seager, W.R., 1981, Geology of Organ Mountains and southern San Andres Mountains, New Mexico: New Mexico Bureau of Mines and Mineral Resources, Memoir 36, 97p.

Seager, W.R., and McCurry, M., 1988, The cogenetic Organ cauldron and batholith, south central New Mexico: Evolution of a large-volume ash flow cauldron and its source magma chamber: Journal of Geophysical Research, v. 93, no. B5, p. 4421-4433.

Shannon, J.R., Walker, B.M., Carten, R.B., and Geraghty, E.P., 1982, Unidirectional solidification textures and their significance in determining relative ages of intrusions at the Henderson Mine, Colorado: Geology, v. 10, p. 293-297.

Shannon, J.R., Bookstrom, A.A., and Smith, R.P., 1984, Contemporaneous bimodal mafic-felsic magmatism at Red Mountain, Clear Creek county, and Climax, Colorado (abs.): Geological Society of America, Abstracts with Programs v. 16, no. 4, p. 254.

Smith, R.W., 1983, Aqueous chemistry of molybdenum at elevated temperatures and pressures with applications to porphyry molybdenum deposits: PhD thesis, New Mexico Institute of Mining and Technology, 311p.

Snyder, G.A., 1984, Paleomagnetism of the Questa mine area, Taos County, New Mexico: M.Sc. thesis, Colorado School of Mines, Golden.

Spencer, J.E., 1982, Origin of folds of Tertiary low-angle fault surfaces, southeastern California and western Arizona; in Frost, E.G., and Martin, D.L. (eds.), Mesozoic-Cenozoic tectonic evolution of the Colorado River region, California, Arizona, and Nevada: Cordilleran Publishers, San Diego, p. 123-134.

Steven, T.A., 1975, Middle Tertiary volcanic field in the southern Rocky Mountains, in Curtis, B.F. (ed.), Cenozoic history of the southern Rocky Mountains: Geological Society of America Memoir 144, p. 75-94.

Steven, T.A., and Lipman, P.W., 1976, Calderas of the San Juan volcanic field, southwestern Colorado: US Geological Survey Professional Paper 958, 35p.

Thompson, R.A., Dungan, M.A., and Lipman, P.W., 1986, Multiple differentiation processes in early-rift calc-alkaline volcanics, northern Rio Grande rift, New Mexico: Journal of Geophysical Research, v. 91, no. B6, p. 6046-6058.

Tweto, O., 1979, The Rio Grande rift System in Colorado; in Riecker, R.E. (ed.), Rio Grande rift-tectonics and magmatism: American Geophysical Union, Washington, D.C., p. 35-56.

Upson, J.E., 1941, The Vallejo Formation: New early Tertiary red-beds in southern Colorado: American Journal of Science, v. 239, p. 577-589.

Vanderwilt, J.W., 1938, Geology of the "Questa" molybdenum deposit, Taos County, New Mexico: Colorado Scientific Society Proceedings, v. 13, p. 599-643.

Wallace, S.R., Muncaster, N.K., Jonson, D.C., MacKenzie, W.B., Bookstrom, A.A., and Surface, V.E., 1968, Multiple intrusion and mineralization at Climax, Colorado; in Ridge, J.D., (ed.), Ore deposits of the United States, 1933-1967 (Graton-Sales Volume): New York, American Institute of Mining, Metallurgical, and Petroleum Engineers, p. 606-640.

Wallace, S.R., MacKenzie, W.B., Blair, R.G., and Muncaster, N.K., 1978, Geology of the Urad and Henderson molybdenite deposits, Clear Creek County, Colorado, with a section on a comparison of these deposits with those at Climax, Colorado: Economic Geology, v. 73, p. 325-368.

Wernicke, B., 1981, Low-angle normal faults in the Basin and Range province: Nappe tectonics in an extending orogen: Nature, v. 291, p. 645-648.

Wernicke, B., 1985, Uniform-sense normal simple shear of the continental lithosphere: Canadian Journal of Earth Sciences, v. 22, p. 108-125.

Wernicke, B., and Burchfield, B.C., 1982, Modes of extensional tectonics: Journal of Structural Geology, v. 4, no. 2, p. 105-115.

Williams, M.L., 1990, Proterozoic geology of northern New Mexico: Recent advances and ongoing questions: New Mexico Geological Society, Guidebook to 41st Field Conference, p. 151-159.

Wright, L.A., and Troxel, B.W., 1973, Shallow-fault interpretation of Basin and Range structure, southwestern Great Basin; in DeJong, R., and Scholten, R. (eds.): Gravity and Tectonics, Elsevier, p. 397-407.

FIGURES, TABLES AND PLATES

Figure 1 Aerial view of the Questa mining district looking ENE, up Red River canyon, along the structural grain of the district. Waste dumps derived from open pit molybdenum mine located behind, and to the left of, dumps. Outcrops in front of waste dump demonstrate km-scale top-to-the-ENE displacement along low-angle normal faults (Figs. 26 and 33). Alteration scars visible in background are in altered Tertiary volcanic rocks.

Figure 2 Regional location map showing late Tertiary volcanic fields, late Tertiary normal faults and the Questa caldera. Modified from Lipman (1981).

Figure 3 Phanerozoic structures of the northern Rio Grande rift region. Note the expanded eastern boundary of the Uncompahgre-San Luis highland of this report (new margin) versus the old margin as given in Chapin and Seager (1975). Modified from Chapin and Seager (1975) and Lipman (1981).

Figure 4 Schematic cross-sectional representation of the stratigraphic and intrusive relationships in the Questa mining district: pCa, schist, gneiss, amphibolite schist and felsic schists; pCqm, quartz monzonite of Columbine Creek; pCq, quartzite; pCmg, mica gneiss; pCom,

quartz monzonite of Old Mike Peak; Od, diabase; Ts, continental sediments; Tlt, lithic tuff; Tan, andesite flows; Tql, quartz latite flows; Tqli, quartz latite intrusions; Txba, basaltic andesite; Trt, intracaldera Amalia Tuff with associated megabreccia blocks; Trtb, basal broken crystal zone; Trf, intrusions associated with Amalia Tuff; Tap/Tgp, post-caldera molybdenum-related intrusions; Tqll, quartz latite to lamprophyre dikes.

Figure 5 Geographic features in the Questa mining district.

Figure 6 Textural variations of the andesite pile volcanic units. Top row, middle and right-hand units are quartz latite porphyry flows, which occur as megabreccia blocks in the intracaldera Amalia Tuff. Bottom row, middle sample is homogenous andesite, which makes up the majority of the andesite pile.

Figure 7 Schematic map of selected features related to the Questa caldera. Note the pattern of three major exposures of intracaldera tuff that are tilted steeply to the west. This allows cross-sectional views of the intracaldera fill as presented schematically in Figure 11. Also note that the southern structural margin of the caldera, as defined by patterns in the intracaldera fill, interpreted ring dikes and interpreted ring faults, is an approximately 2 km wide ENE trending zone. Rock unit contacts interpreted by Lipman and Reed (1989) to represent a caldera margin "unconformity" are reinterpreted by the authors to represent low-angle

fault zones. Northern and southern contacts of the intracaldera fill are low-angle fault-bounded as well.

Figure 8 Sketch geologic map and cross-section of outflow Amalia Tuff and overlying fallout deposit located south of the Questa caldera. Note the 1/2 graben cross-sectional geometry. The preservation of such easily erodible units as the Amalia Tuff fallout unit indicates moderate amounts of syn-caldera to immediately post-caldera extension.

Figure 9 Distribution of pumice flattening ratios and devitrification in intracaldera Amalia Tuff (shaded) in relation to megabreccia blocks (white). Note the significant effect of the caldera megabreccia block "heat sinks" on welding and devitrification in the surrounding tuff: a) devitrification; Tmb, megabreccia blocks; Trtbx, rhyolite tuff breccia (mesobreccia of Lipman, 1976); Trtg, glassy-pumice tuff; Trtfg, fine grained, devitrified tuff; Trtcg, coarse grained, granophyrically devitrified tuff; b) pumice flattening; Tmb and Trtbx, same as above; Trtw, <1:5 pumice flattening ratio; Trtdw 1:5 - 1:12 flattening ratio; Trtvdw >1:12 flattening ratio. Tuff between the hatchured line and associated megabreccia block contains >1% lithic fragments in the tuff, indicating incorporation of fragments from megabreccia blocks.

Figure 10 Textures of the intracaldera Amalia tuff. Lower sample is vitric tuff with 5:1 to 10:1 pumice flattening ratios, typical of tuff located

near megabreccia block "heat sinks". Note lithic fragments interpreted to be derived from the adjacent megabreccia block. Middle sample is densely welded, devitrified tuff. Pumice flattening ratio is 8:1 to 12:1, although face cut parallel to foliation has the appearance in the photo of being less welded. Upper sample is very densely welded, granophyrically devitrified tuff. Pumice flattening ratios are >15:1.

Figure 11 Schematic cross-section of intracaldera structure and stratigraphy: a) westernmost exposure of intracaldera Amalia Tuff; b) central exposure of intracaldera Amalia Tuff (see Fig. 7 for location of Amalia Tuff exposures). Precambrian units are located low in the southern structural margin of the caldera and do not occur as intracaldera megabreccia blocks. Andesite flows are located in the caldera floor, in the upper portions of the structural margin of the caldera, and as megabreccia blocks in the intracaldera Amalia Tuff. Amalia Tuff is the most interior unit inside the caldera fill. View is looking west. Note the concentration of blocks against the southern caldera wall, the general correspondence between wall-rock and megabreccia block lithologies, and the location of most of the blocks in the lower vs. middle parts of the stratigraphy for the western and central exposures respectively.

Figure 12 a) Outcrop-scale megabreccia blocks exposed in Hansen scar.

b) Hand sample-scale megabreccia blocks; or mesobreccia of Lipman, 1976 (Trtbx of Plate 2). Tuffaceous matrix is lighter colored in all cases, although often the tuffaceous matrix is highly diluted by mechanically decomposed block material. Center sample shows gradational contacts between matrix and clasts demonstrating mechanical decompostition.

Figure 13 Photomicrograph of basal broken crystal zone (Trtb of Plate 2) showing breakage of quartz phenocrysts. Larger phenocryst appears to be fragmenting due to impact with smaller phenocryst. Such relationships, and the abundance of broken phenocrysts, suggest fragmentation during highly explosive eruption.

Figure 14 Schematic model demonstrating formation of megabreccia blocks and of the basal broken crystal zone at the southern caldera margin. Cross-sectional view (left) is of the southern caldera wall looking east. Aerial view (right) demonstrates the location of ignimbrite eruption in relation to the cross-section: a) partial filling of the caldera with congruent collapse and minor megabreccia formation; b) short-term pause in the eruption (possibly on the order of days) resulting in the build-up of a lense of megabreccia talus on the partially compacted intracaldera fill; c) caldera ring dikes propagate to the surface and a new phase of ignimbrite eruption begins. The initial vent clearing blast is highly explosive and fragments portions of the pre-cursor ring dike. The leading edge of the

ignimbrite deposits the basal broken crystal layer; d) as ignimbrite eruption continues, portions of the basal broken crystal zone not protected by megabreccia block-induced topography are reincorporated and disseminated into the main body of the ash flow.

Figure 15 Trace element variation diagrams of pre-, syn- and post-caldera units at Questa: a) Y vs. Zr.; b) Y, Zr, Nb. Square symbols represent caldera-related intrusive units in order from lower (filled square) to higher (open square) silica content (see legend of Plate 2 for unit names). Note that latitic phases are intermediate between pre-caldera units and Amalia Tuff, and that rhyolitic phases are similar to the Amalia Tuff. This suggests generation of the rhyolites from the same magma system as the Amalia Tuff and generation of the intrusive units from a less evolved Amalia Tuff system or a hybrid Amalia Tuff - pre-caldera igneous system. Major fields (dashed, outlined areas) are generated from numerous geochemical analyses (>15 analyses per field) of Lipman (1983 and unpublished) and data collected by Questa mine geologists (including data from Tab. 1). Asterisks denote two samples of co-ignimbrite fallout of the Amalia Tuff, that are preserved in 1/2 grabens along the rift-front, 10 km south of the Questa caldera (located in Fig. 8).

Figure 16 Tilt domain boundaries and $^{40}Ar/^{39}Ar$ cooling dates of selected intrusive phases of the composite Questa batholith. Note the decrease of intrusive ages to the south and the correspondence of maximum

tilting to the regions of the Questa caldera and post-caldera >24.6 Ma intrusive phases. Tilt domain data from Lipman and Reed (1989) and this study, Ar/Ar dates from Czamanske and others (1990).

Figure 17 Paragenetic summary of intrusive, alteration-mineralization and structural relationships in the region of the Southwest ore body. Note the broad overlap between intrusive, alteration-mineralization and structural events. Also note that early high-angle NNW striking faults are rotated to low angles during peak extension.

Figure 18 Fine-grained aplite porphyry with early barren quartz veining. Unit is located at the apex of the intrusion, down-dip from molybdenum mineralization, and represents the source of mineralizing fluids. Scale at base is in inches.

Figure 19 Approximately 50° north-dipping dike of post-mineral rhyolite porphyry.

Figure 20 Location of large landslide blocks, alteration scars and debri aprons in the Questa mining district. Dashed line indicates a prominent slope-break between the steeper inner and gentler outer canyons of the Red River and Cabresto Creek drainages: A, Goat Hill Gulch debris apron; B, Sulfur Gulch debris apron; C, Hansen scar debris apron; D, Hottentot/Straight Creek debris apron; E, Bitter Creek debris apron; F,

Cottonwood Park meadowland; G, Moly mill meadowland; H, Fawn Lakes meadowland; I, Red River town site; J, Bitter Creek Guest Ranch meadowland.

Figure 21 Profile of the Red River drainage looking north. Note the significant effect of the debri aprons on the gradient of the stream, which forms small-scale concave upward profiles above each obstruction.

Figure 22 Foliated quartz latite porphyry dike. Note regions of homogenous porphyritic texture at top and bottom of photo with transition into highly foliated texture in center, near pencil. Foliation dips at a low angle, parallel to the pencil.

Figure 23 View to the NNW of horizontal slabby cooling joints at right angles to vertically dipping eutaxitic foliation in intracaldera Amalia Tuff. Structural correction indicates an original NNW striking vertical orientation of slabby joints. This originally vertical joint set was utilized by normal faults, which may have initiated at near vertical angles.

Figure 24 Lower hemisphere equal-area plots of structural features of the Questa mining district: a) pole-normals to eutaxitic foliation in Amalia Tuff for western tectonic block (west of Sulphur Gulch pluton); b) pole-normals to eutaxitic foliation in Amalia Tuff in the central tectonic block (near Straight Creek and Hansen Scars); c) pole-normals to eutaxitic

foliation in Amalia Tuff in the eastern tectonic block (in and immediately east of Hansen scar); d) pole-normals to all faults; e) pole-normals to faults with measured striation or corrugation orientations; and f) orientation of slickenside striations and/or fault plane corrugations (one fault plane contained two lineation directions). Note the very steep dip of beds, low-angle orientation of faults and the well-clustered ENE trend to fault plane striations. Refer to Figure 7 for location of western, central and eastern tectonic blocks.

Figure 25 Structural map of the different generations of, and styles of faulting in the Questa mining district.

Figure 26 Sketch map of the region south of the central mineralized zone (immediately east of underground mine shafts). Note the large-scale top-to-the-ENE displacement of the 90° tilted sedimentary unit along low-angle normal faults.

Figure 27 East wall of Hottentot scar. Flat-topped outcrops in foreground represent a low-angle fault plane that crosses the entire scar. Fault can been seen in middle of picture across top of prominent cliffs.

Figure 28 View to the WSW of upper Straight Creek scar showing resistant bench of an east-dipping low-angle fault plane. Slickenside striations and "steps" in fault plane are oriented ENE. All outcrops in photo

are steeply-dipping Amalia Tuff that is pervasively cross-cut by low-angle faulting.

Figure 29 Thick zone of east-dipping low-angle faulting in southwest Hansen scar. Zone is approximately 500 meters thick. View is to the southeast.

Figure 30 Outcrop between #1 and #2 mine shafts demonstrating surface alteration related to the Southwest ore zone. Hydrothermal fluids were structurally controlled by a north-dipping low-angle fault zone that channelized fluids to the south. Note offset of two alteration types (light to dark color change) in center of photo due to minor post-alteration movement along these same low-angle faults. View is to the north.

Figure 31 Styles of internal block deformation at Questa: a) simplified diagram of "shear couple" style; b) simplified diagram of "upper plate" style. Note the difference in scale.

Figure 32 "Shear couple" fault style in upper Straight Creek scar. View is to the southwest and distance between block bounding faults (top and bottom) is approximately 3 meters. All rocks are strongly tilted Amalia Tuff: a) photograph; b) illustration of structures.

Figure 33 View to the north of internal block deformation between two major low-angle faults. Block bounding faults are at base of photo and immediately above bold outcrops. Block corresponds to small Tertiary sediment outcrop of Figure 26, located between labelled 14° and 25° dipping fault planes: a) photograph; b) sketch of internal block deformation showing rock types and faults; pCqm=Precambrian quartz monzonite; Tcgc=Tertiary conglomerate (vertically dipping and cut-off by basal fault); Trff=rhyolite porphyry intrusion (caldera-related). Rhyolite porphyry intrusion was originally a sill into Tertiary sediments and was subsequently tilted 90° westerly along with enclosing sediments. Location of boulder in Figure 34.

Figure 34 Pervasively sheared boulder within internally deformed fault block bounded by low-angle structures. Location shown in Figure 33.

Figure 35 High-angle normal fault that post-dates intrusion and mineralization. Corresponds to N-S striking fault of Figure 26. View is to the north.

Figure 36 Aerial view looking northeast of shafts and support buildings for the Southwest ore zone underground mine. Concrete tower in foreground is service shaft (#1 shaft), metal head frame in upper left is ventilation shaft (#2 shaft). Southwest ore zone is located nearly 1 km north of the service shaft, but mineralization-related alteration is best

exposed in the surface outcrops of this area (e.g. Fig. 30). Compare to Figures 5 and 46.

Figure 37 Generalized cross-section looking north at the Log Cabin zone, Central mineralized zone and the Spring Gulch zones. All of the Questa mineralized zones except Spring Gulch are located at and immediately above the intrusive rock contact. Mineralization shown in stippled pattern; Ti=Tertiary intrusion, Tv=Tertiary volcanic units, Qal=Quaternary alluvium. No vertical exaggeration.

Figure 38 The southern wall of the pit demonstrating the low-angle structural control on molybdenum-related hydrothermal fluids. Light colored portion of pit wall is quartz-sericite-green sericite-specular hematite alteration following a west-dipping, low-angle fault.

Figure 39 Cross-section of the Southwest ore body looking approximately N20W. Note the extremely long E-W dimension of the ore deposit and the restriction of mineralization to the area immediately above the aplite-granite intrusion. Magmatic-Hydrothermal Breccia is the dominant molybdenum bearing phase in the central and western portion of the ore body but pinches out to the east, where vein-controlled mineralization predominates. Note significant offsets by post-mineral normal faults. Control for this cross-section includes surface mapping, rotary and diamond drill holes, and extensive underground mine workings.

Numerous north-dipping low-angle faults control mineralization and intrusion. These faults are parallel to the surface-exposed low-angle faults of this section but are left out, in the vicinity of the ore zone, for simplicity. Figure 40 gives an indication of the abundance and complexity of these structures. No vertical exaggeration.

Figure 40 Cross-section of the Southwest ore zone looking N35E. Section shows details of the mineralization including relationship of 0.2% MoS_2 to: a) the magmatic-hydrothermal breccia; b) structures; and c) intrusive phases. Note the vertical zonation of the magmatic-hydrothermal breccia and how contacts between zones are fault bounded. Minor post-mineral offsets on these low-angle faults are suggested (Fig. 42). Cross-section is oriented S55W, parallel to the presumed direction of fluid migration from the source aplite intrusion (quartz-veined aplite along margin of section). Compare the 2300 meter elevation of source aplite to the intrusive ridge north of the ore body on Fig. 41).

Figure 41 Structure contour map of granite intrusion - host rock contact in the vicinity of the central mineralized zone. Note how the Southwest ore zone lies immediately south of an ENE trending high in the intrusive rock - host rock contact.

Figure 42 Schematic representation of the Southwest ore zone before and after post-mineral faulting: a) Pre-mineral and mineral-related

intrusions invade low-angle fault zone. Fluids from mineral-related intrusion react with faulted rock to form vertically zoned magmatic-hydrothermal breccia and related molybdenum mineralization; b) Post-mineral, N70E-directed faulting causes minor tectonic thinning of magmatic-hydrothermal breccia and related mineralization. View is looking N35E; section b corresponds to Figure 40. Evidence for post-mineral faulting in this cross-section includes: 1) basal termination of source aplite by a fault; 2) fault-contact boundaries at the top and bottom of, and between internal zones of the magmatic-hydrothermal breccia; and, 3) stringers of andesite along low-angle faults that cut the pre-mineral intrusion. Other evidence for post-mineral faulting, not displayed here, includes faulted contacts between disparate alteration assemblages both in subsurface and surface exposures.

Figure 43 Fine-grained aplite porphyry with well developed crenulate quartz banding. Note free (euhedral) crystal faces point to the bottom of sample (toward the penny) indicating that crystallization proceeded from top to bottom.

Figure 44 Sketch of the three assemblages of the Magmatic Hydrothermal Breccia (MHBx): a) lowermost assemblage; quartz matrix MHBx, b) middle assemblage; quartz-orthoclase matrix MHBx, c) top assemblage; quartz-biotite-orthoclase-molybdenite matrix MHBx.

Figure 45 Sketch showing variations of quartz-sericite-green sericite-specular hematite alteration typical at distances greater than 150 meters up-dip from the Magmatic Hydrothermal Breccia: a) pervasive quartz-sericite-specular hematite alteration with partial replacement by structurally-contolled quartz-sericite alteration, b) structurally controlled to pervasive quartz-sericite alteration that has largely replaced pervasive quartz-sericite-specular hematite alteration, c) quartz-sericite-green sericite alteration in fractures, structurally controlled to pervasive quartz-sericite alteration adjacent to fractures, and pervasive specular hematite alteration nearly completely replaced by quartz-sericite assemblage.

Figure 46 Location of surface quartz-sericite-green sericite-specular hematite alteration in relation to the surface projection of the Southwest ore zone. This alteration assemblage is interpreted to represent distal alteration related to the mineralization, with mineralization-related altering fluids having traveled 2 km up low-angle north-dipping fault zones. Major low-angle north-dipping faults are shown with dashed lines. Superimposed high-angle faults are shown with heavy solid lines.

Figure 47 Schematic representation of possible methods of concentration of extensional faulting into the Questa caldera area: a) block foundering into the caldera-related magma chamber and associated tilting with no or minimal increased extension in the caldera ; b) block foundering

into the post-caldera magma chamber and associated tilting with no or minimal increased extension above the post-caldera magma chamber; c) expansion and extensional faulting above the magma chamber with co-genetic contraction and compressional faulting off of the flanks; d) extension is part of a regional detachment system (currently unrecognized) with magmatism at Questa causing a local change in the extensional style; e) regional extension is concentrated into the magmatically weakened area by the bending and focussing of regional normal structures; and f) regional extension is concentrated into the magmatically weakened area along strike-slip accommodation structures. Note that all of the above models predict an ENE to E-W trending accommodation zone slightly north of the geographic center of the caldera separating regions of oppositely-directed bedding tilt. This zone is poorly constrained as it is located in a region of relatively poor stratigraphic control.

Figure 48 Model for interaction of extension, intrusion and hydrothermal fluids in the Questa mining district. A-A' refers to the development of cross-section A-A' of Plate 1: a) pre-caldera volcanism, caldera collapse and related magmatism with block-faulting indicative of a weakly extensional field (28-25.7 Ma); b) extreme extension and 90° tilting over the top of post-caldera plutonic phases (25.7-24.6 Ma); c) continued pluton emplacement and low-angle fault controlled molybdenum mineralization (24.6-24.1 Ma); d) minor low-angle faulting followed by

throughgoing normal faults after the magmatic system waned (24.1-±15 Ma); e) modern rift formation (<15 Ma).

Figure 49 Schematic representation of the timing and relative intensity of structural, magmatic and hydrothermal events at Questa. Structure curve shows an extensional maximum between 25.7 and 24.6 Ma and a late peak indicating post-mineralization low-angle fault reactivation. Volcanic curve indicates pre-caldera activity, caldera eruption (highest point) and two minor peaks indicating minor post-caldera volcanism preserved in the Rio Grande rift. Plutonism curve indicates pre-caldera intrusions, two main peaks corresponding to caldera-related intrusion and southern caldera margin intrusions, and finally lesser peaks corresponding to plutonic phases south of the Questa mining district. Mineralization pulse corresponds to the age of major molybdenum mineralization. Age date information from Czamanske and others (1990).

Figure 50 Generalized representation of the timing of magmatic and extensional tectonic events of selected areas of the Basin and Range and Rio Grande rift provinces. Note that Questa follows the general pattern of a maximum in extensional tectonism following a maximum in magmatic activity by 1-3 m.y. Modified after Gans and others (1989).

Table 1 Major and trace element composition of selected rock units of the Questa mining district, New Mexico. Due to wide-spread

hydrothermal alteration in the district, nearly all samples exhibit at least minor alteration (extent of alteration noted for each sample). Strongly altered samples were analyzed mainly for diagnostic immobile trace elements. Rock type symbols match legend for Plate 2. Analyses by Bondar Clegg, Vancouver, British Columbia. Whole-rock oxide values by D.C. plasma method, trace element analyses by x-ray fluorescence except for fluorine, which was analyzed by specific ion exchange. Errors are considered to be less than 5 percent.

Table 2a Petrographic description of pre-Oligocene units of the Questa Mining District. Rock type symbols match legend for Plate 2.

Table 2b Petrographic description of Tertiary volcanic and intrusive units of the Questa Mining District. Rock type symbols match legend for Plate 2.

Plate 1 Geologic map and cross-sections of the Questa mining district.

Plate 2 Geologic map of the Questa mine area.

Fig- 1

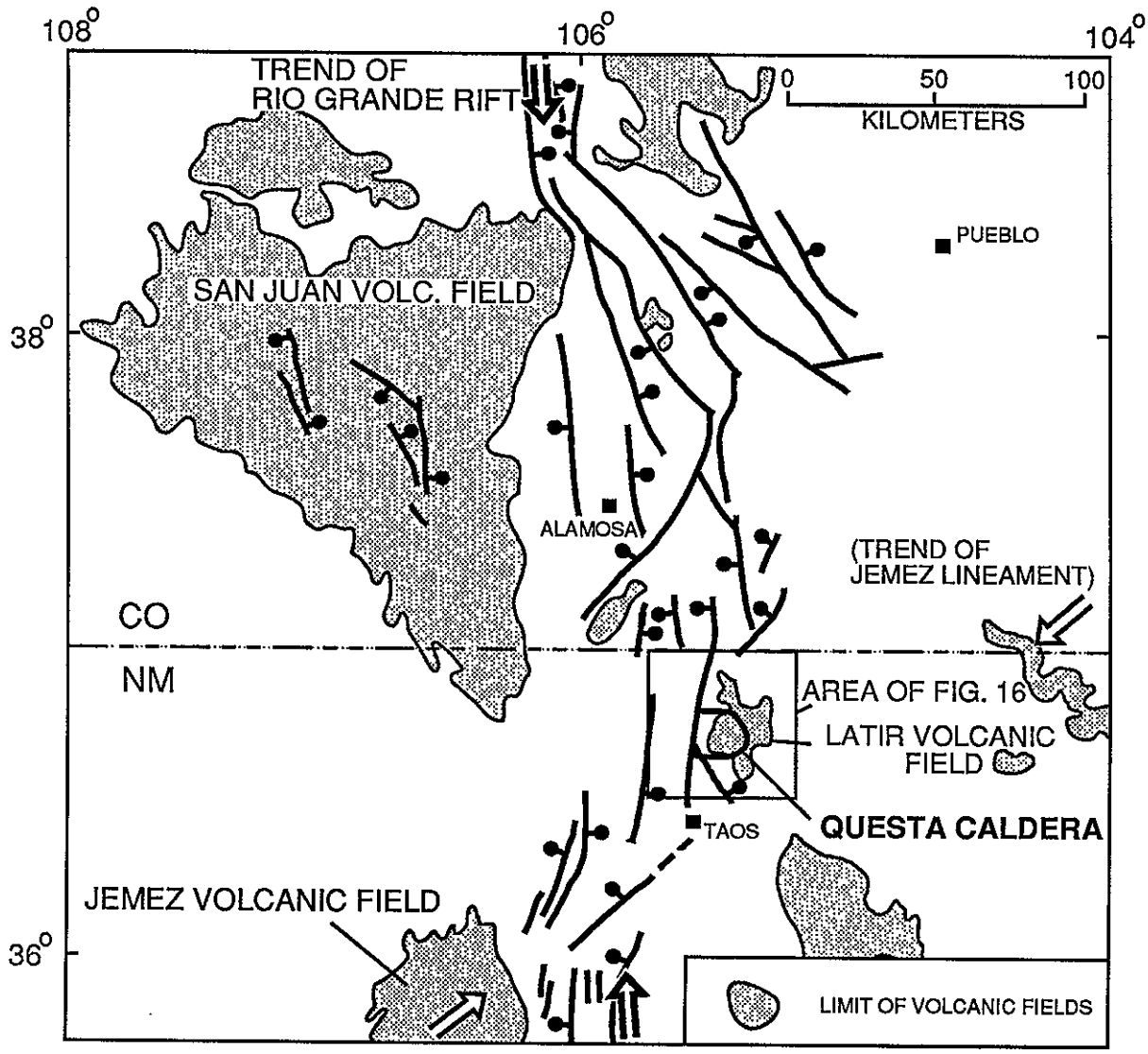
108°
106°
104°
38°
36°
TREND OF
RIO GRANDE RIFT
0
50
100
KILOMETERS
PUEBLO
SAN JUAN VOLC. FIELD
ALAMOSA
(TREND OF
JEMEZ LINEAMENT)
CO
NM
AREA OF FIG. 16
LATIR VOLCANIC
FIELD
TAOS
QUESTA CALDERA
JEMEZ VOLCANIC FIELD
LIMIT OF VOLCANIC FIELDS

Fig. 2

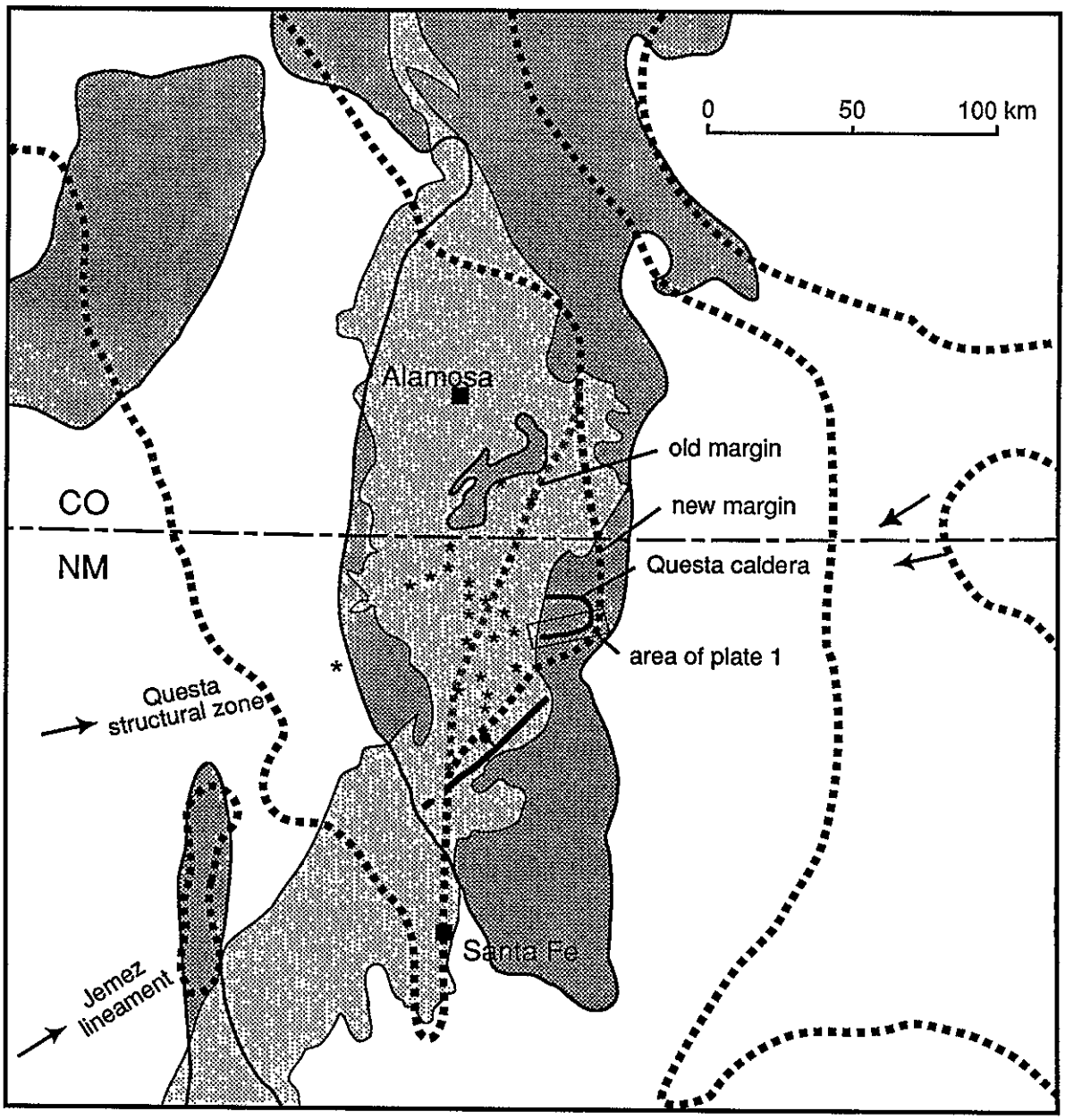
0
50
100 km
Alamosa
old margin
new margin
CO
NM
Questa caldera
area of plate 1
Questa
structural zone
Jemez
lineament
Santa Fe
- Paleozoic highlands
- Laramide uplifts
- Rio Grande rift fill
* - Taos volcanic field vents
(Pliocene to Holocene)

Fig. 3

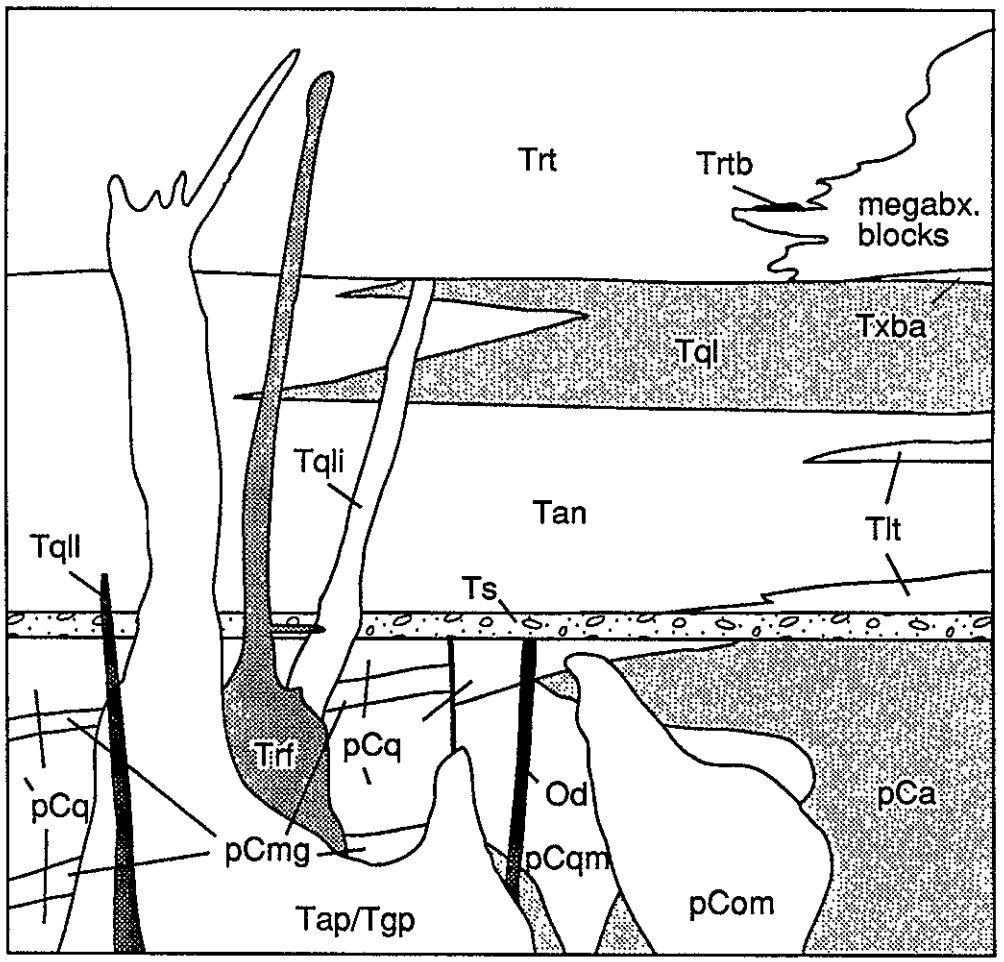
Trt
Trtb
megabx.
blocks
Txba
Tql
Tqli
Tan
Tlt
Tqll
Ts
Trf
pCq
pCq
Od
pCa
pCmg
pCqm
Tap/Tgp
pCom

Fig. 4

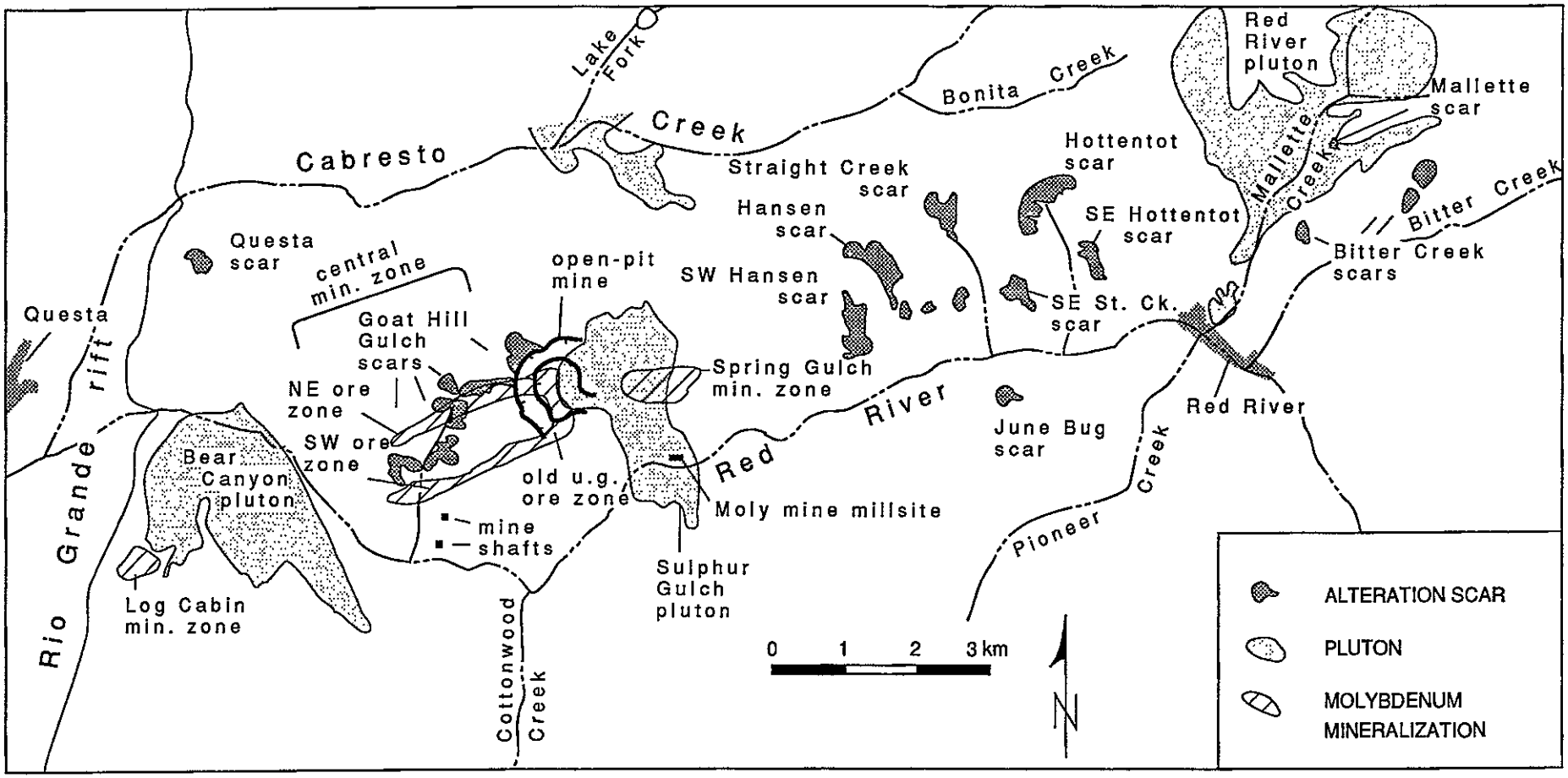
Lake Fork
Creek
Bonita Creek
Red River pluton
Mallette scar
Mallette Creek
Hottentot scar
SE Hottentot scar
Bitter Creek
Bitter Creek scars
Cabresto
Straight Creek scar
Hansen scar
Questa scar
central min. zone
open-pit mine
SW Hansen scar
SE St. Ck. scar
Questa
Goat Hill Gulch scars
Spring Gulch min. zone
NE ore zone
SW ore zone
Red River
June Bug scar
Red River
Rio Grande rift
Bear Canyon pluton
old u.g. ore zone
Moly mine millsite
mine
shafts
Pioneer Creek
Sulphur Gulch pluton
Log Cabin min. zone
Cottonwood Creek
0 1 2 3 km
N
ALTERATION SCAR
PLUTON
MOLYBDENUM MINERALIZATION

Fig. 5

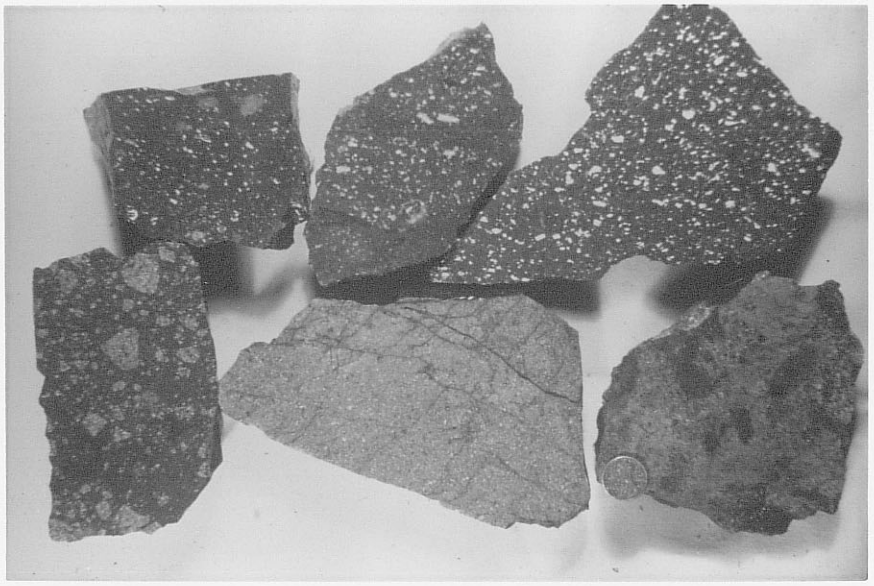

Fig. 6

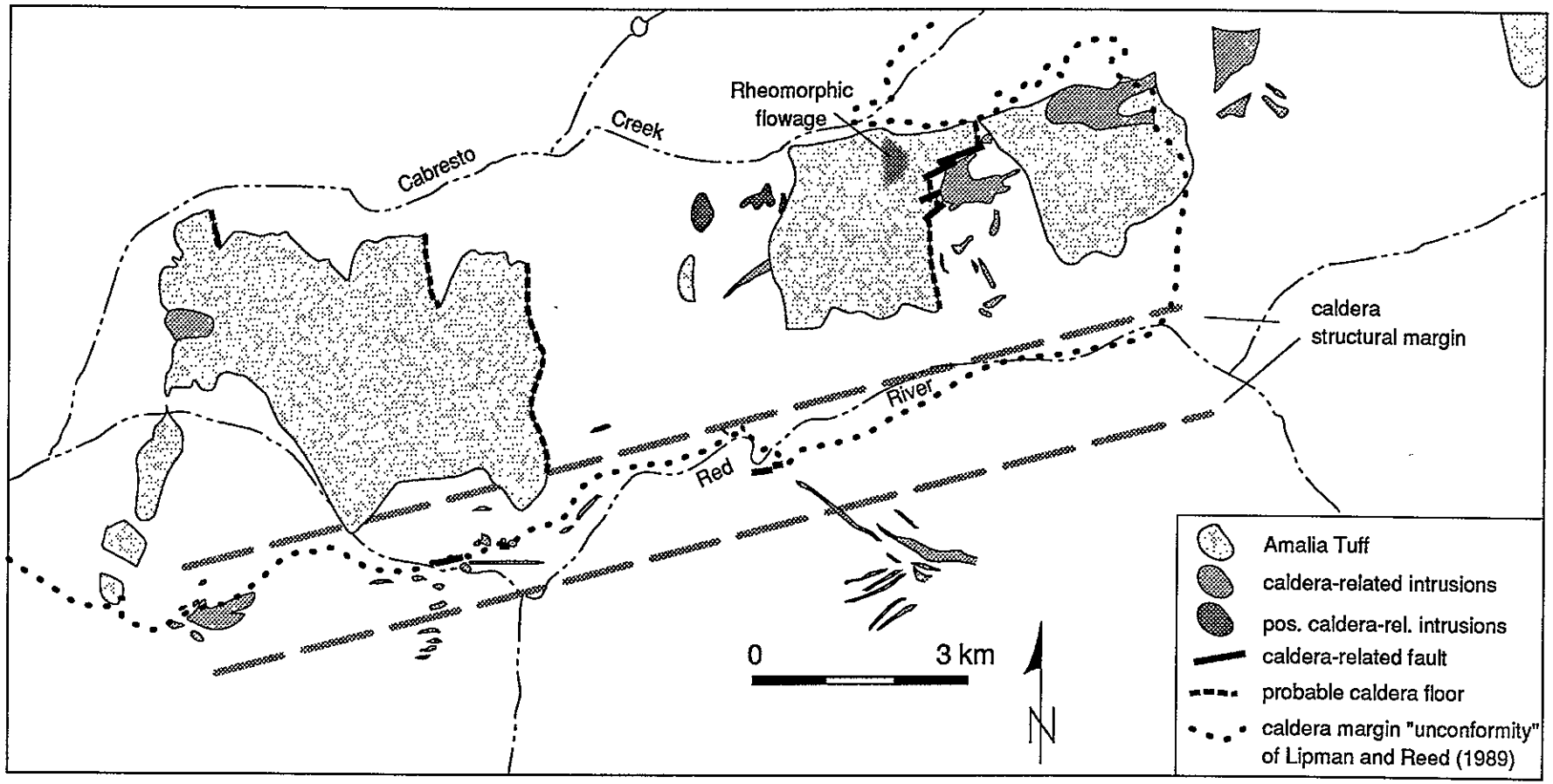
Rheomorphic
flowage
Creek
Cabresto
caldera
structural margin
River
Red
0
3 km
N
Amalia Tuff
caldera-related intrusions
pos. caldera-rel. intrusions
caldera-related fault
probable caldera floor
caldera margin "unconformity"
of Lipman and Reed (1989)

Fig. 7

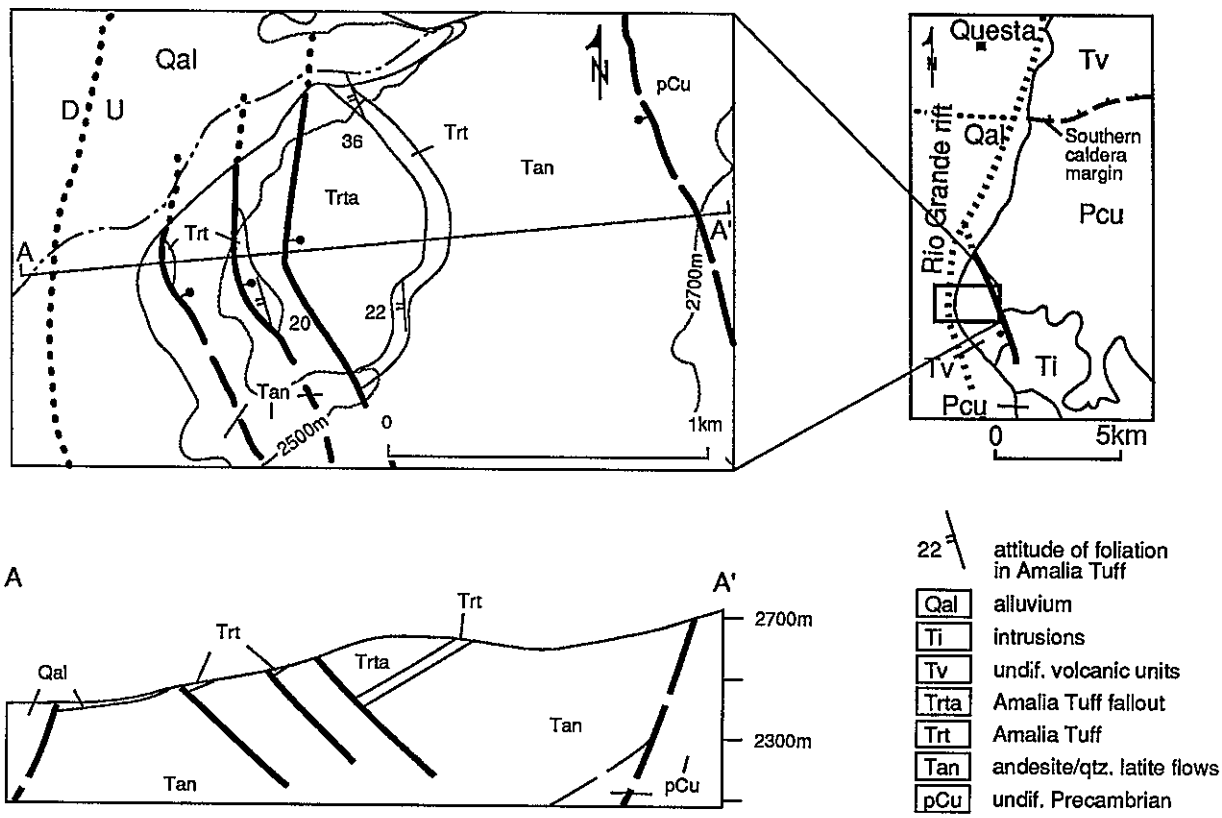
Qal
D
U
N
pCu
36
Trt
Tan
Trta
A
Trt
A'
2700m
20
22
Tan
2500m
0
1km
Questa
Tv
Rio Grande rift
Qal
Southern caldera margin
Pcu
Tv
Ti
Pcu
0
5km
A
A'
Trt
Trt
Trta
Qal
Tan
2700m
2300m
Tan
pCu
22
attitude of foliation in Amalia Tuff
Qal
alluvium
Ti
intrusions
Tv
undif. volcanic units
Trta
Amalia Tuff fallout
Trt
Amalia Tuff
Tan
andesite/qtz. latite flows
pCu
undif. Precambrian

Fig. 8

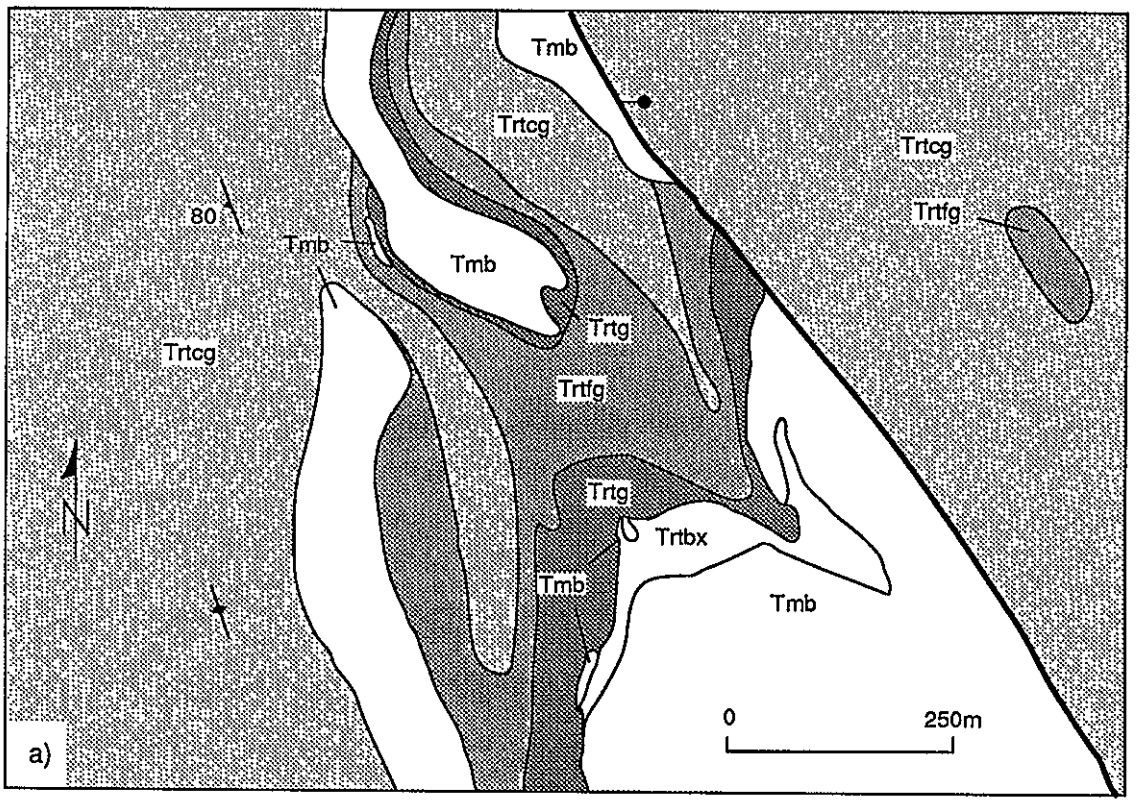
Tmb
Trtcg
Trtcg
Trtfg
80
Tmb
Tmb
Trtg
Trtcg
Trtfg
N
Trtg
Trtbx
Tmb
Tmb
0
250m
a)

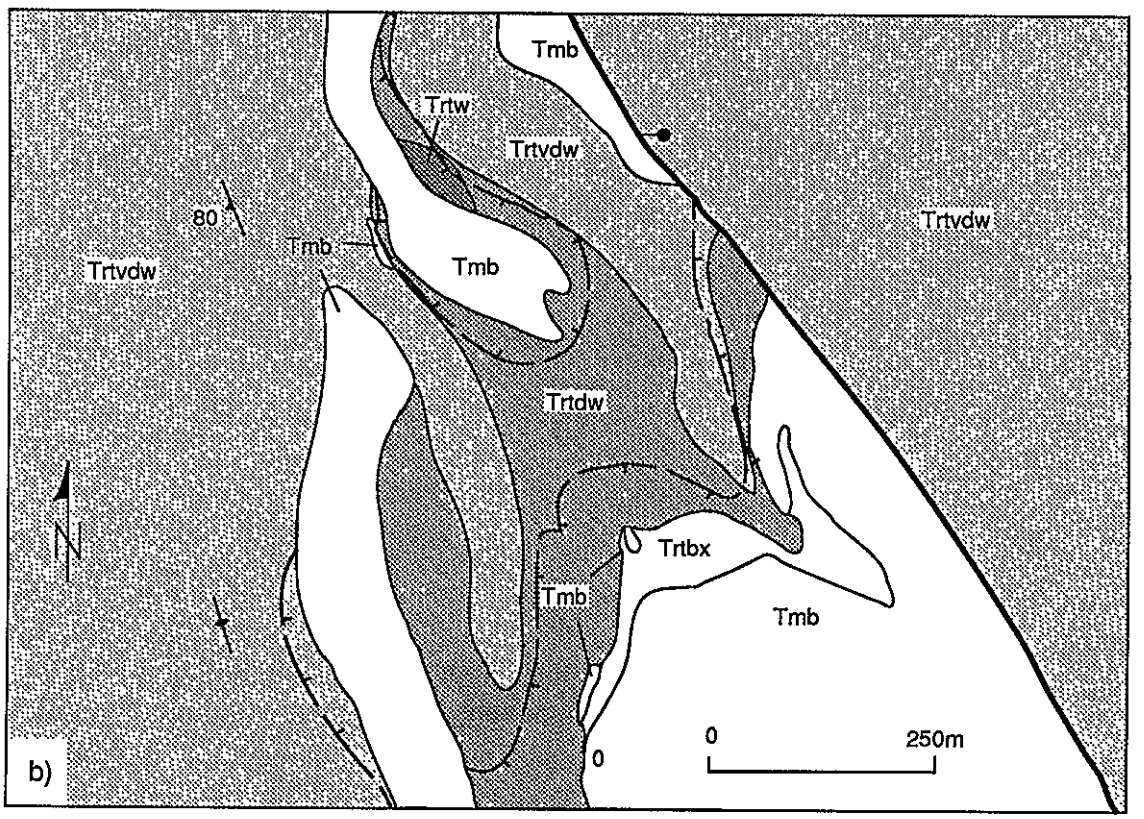
Tmb
Trtw
Trtvdw
Trtvdw
80
Tmb
Tmb
Trtvdw
Trtdw
N
Trtbx
Tmb
Tmb
0
0
250m
b)

Fig. 9

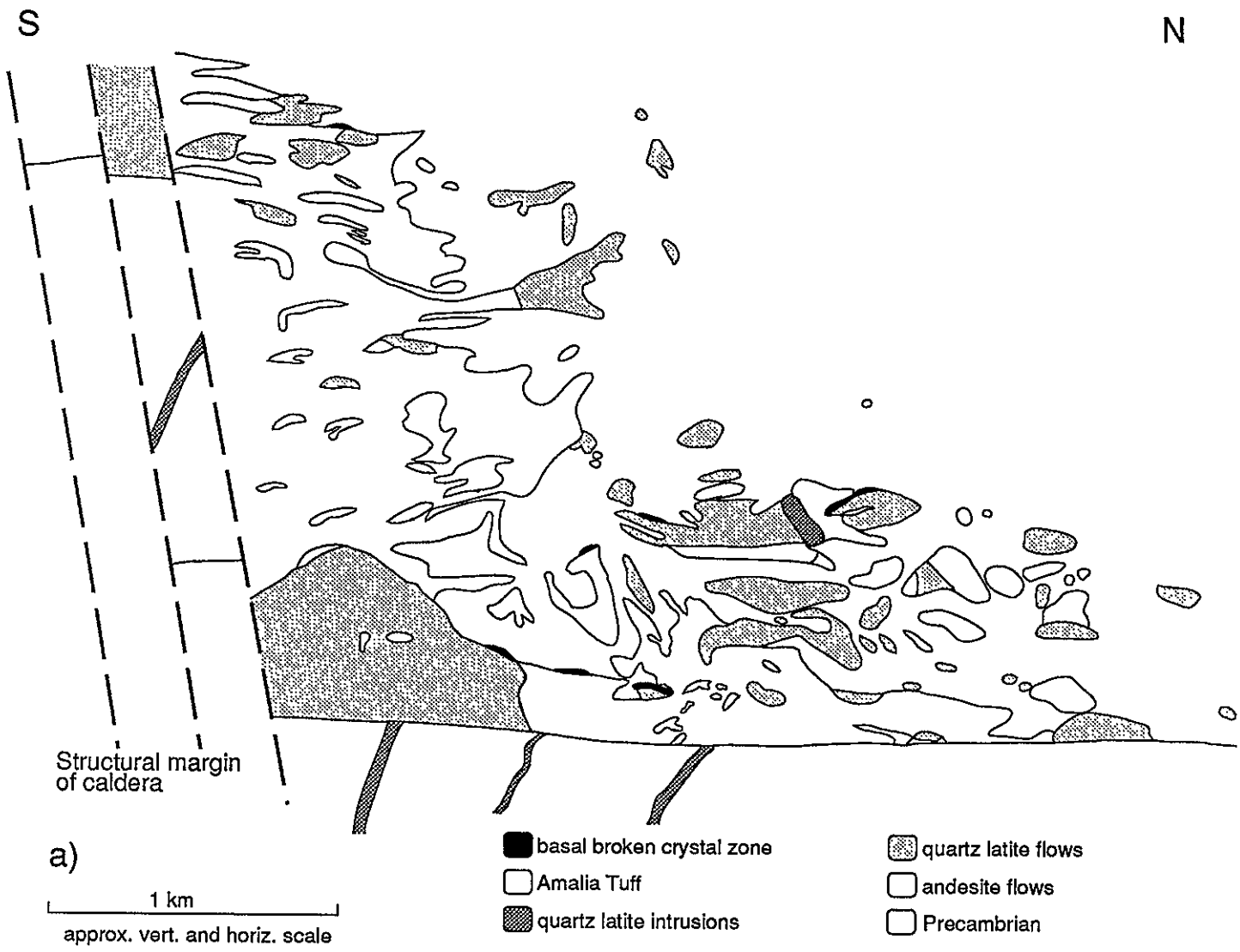
S
N
Structural margin of caldera
a)
1 km
approx. vert. and horiz. scale
basal broken crystal zone
Amalia Tuff
quartz latite intrusions
quartz latite flows
andesite flows
Precambrian

Fig. 11a

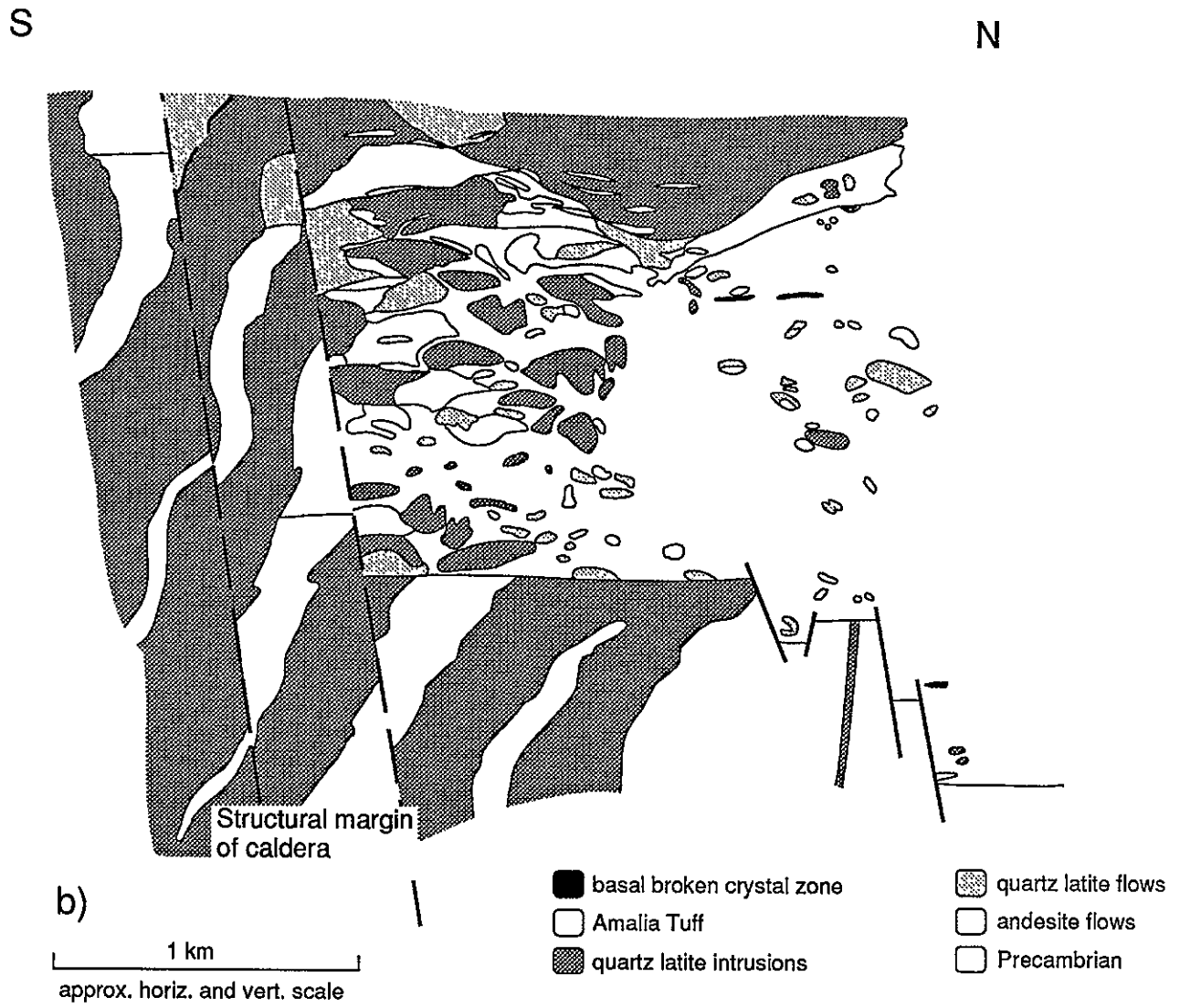
S
N
Structural margin of caldera
b)
1 km
approx. horiz. and vert. scale
basal broken crystal zone
Amalia Tuff
quartz latite intrusions
quartz latite flows
andesite flows
Precambrian

Fig. 11b

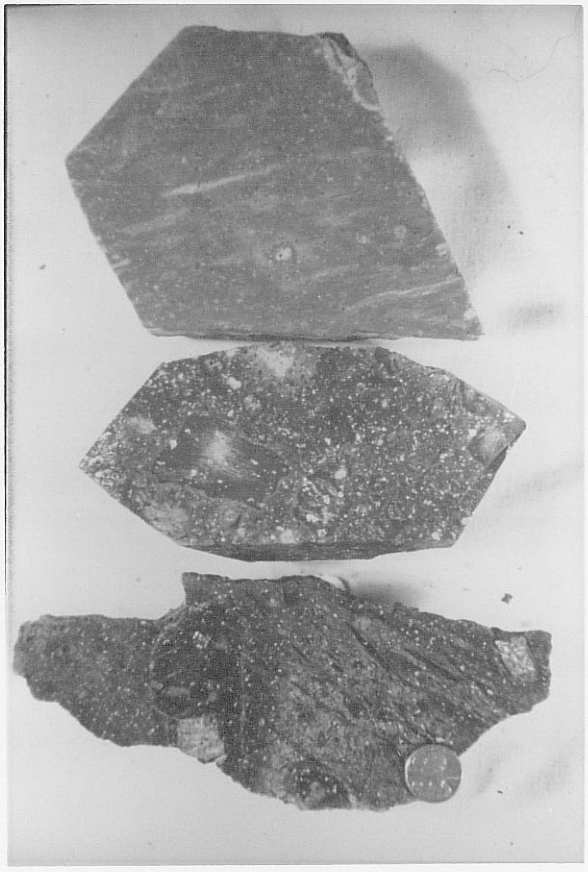

Fig. 10

Fig. 12a

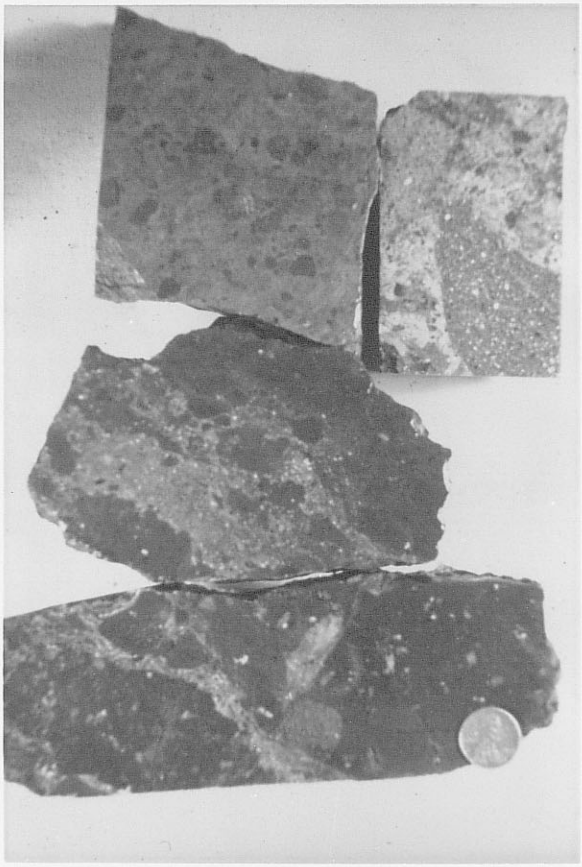

Fig. 12b

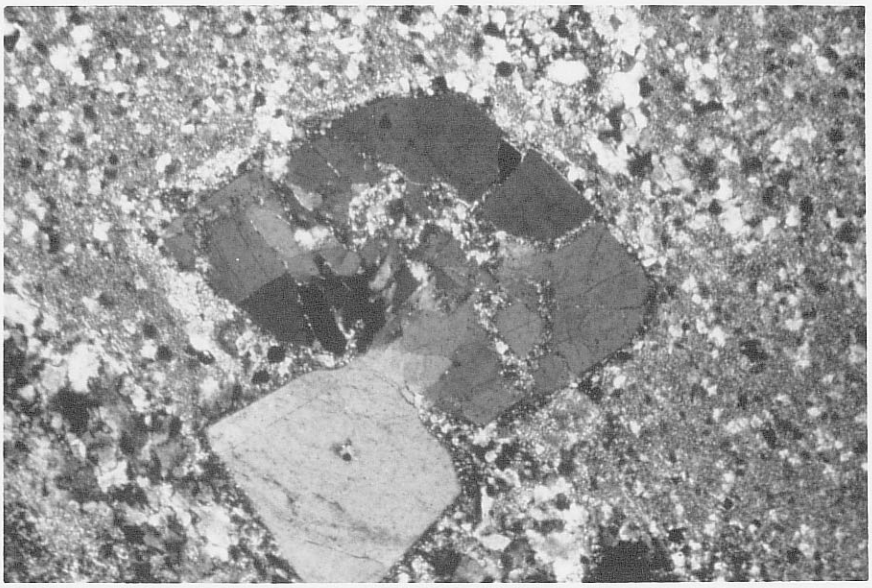

Fig. 13

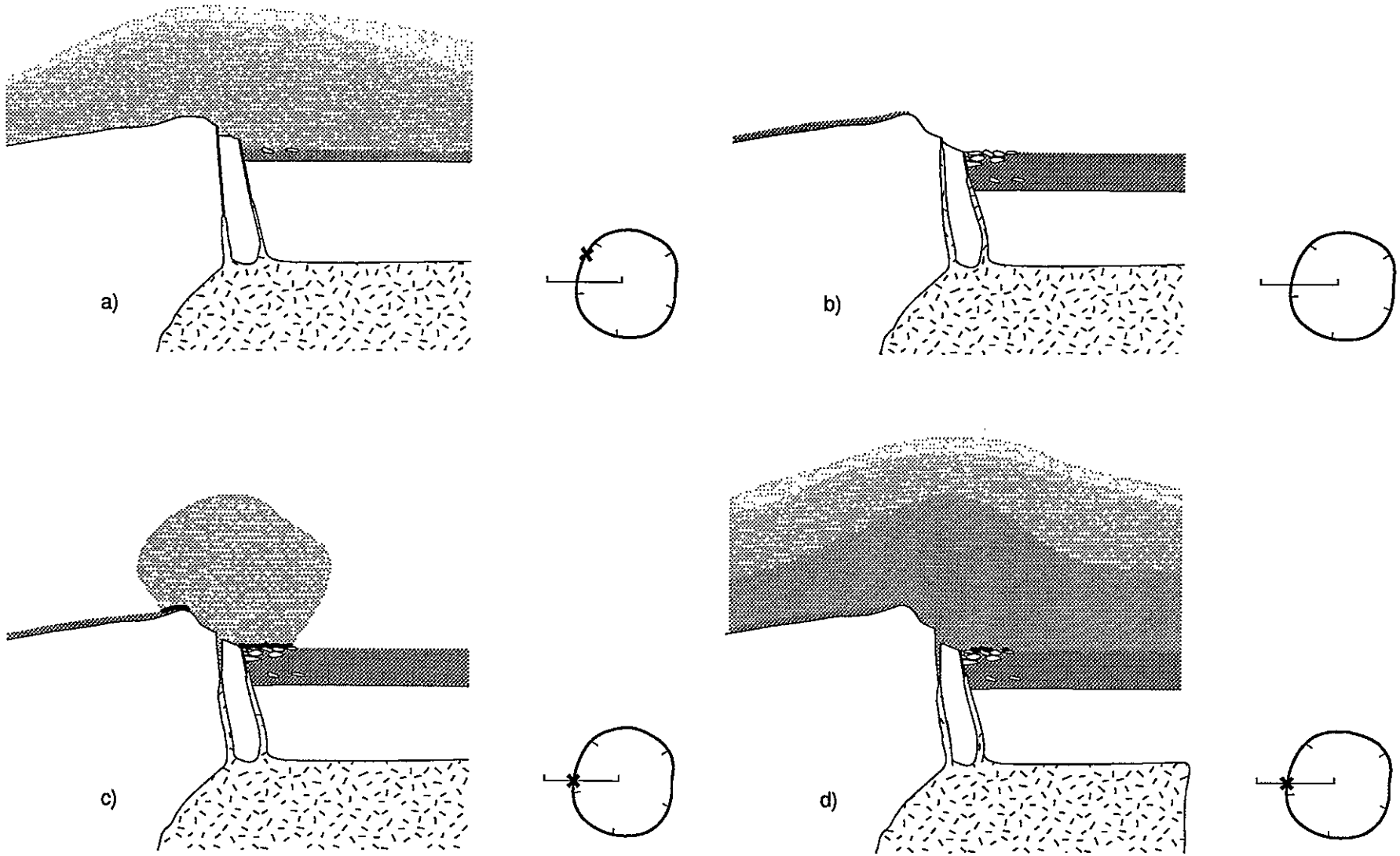

Fig. 14

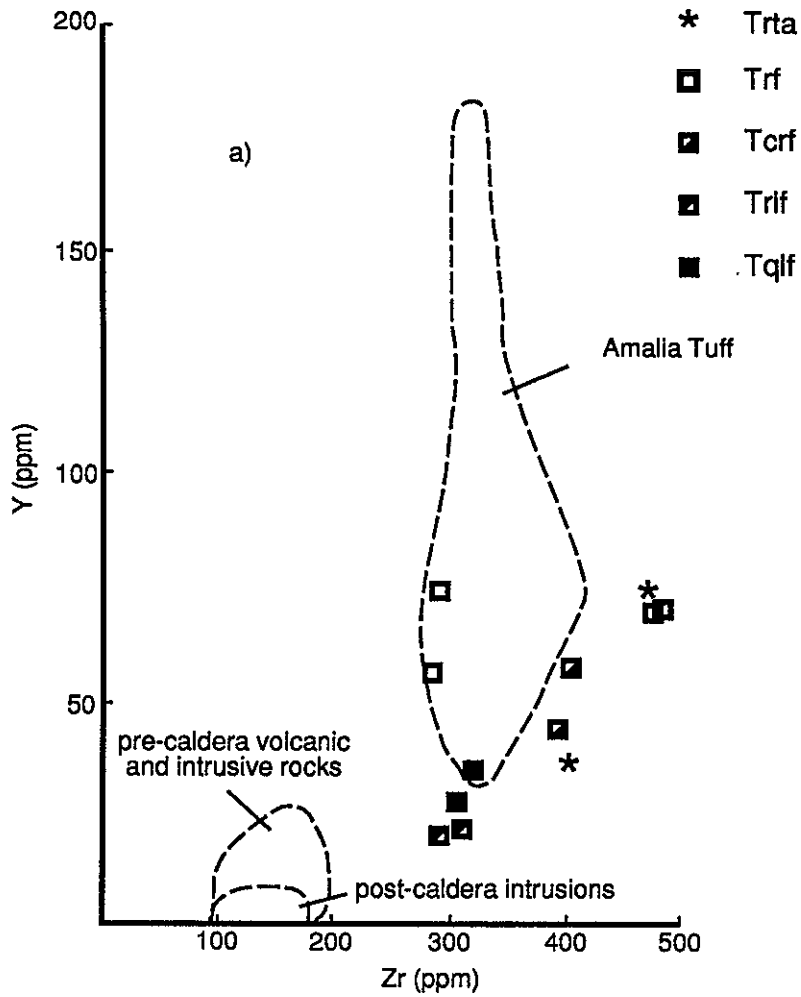
a)
Trta
Trf
Tcrf
Trlf
Tqlf
Amalia Tuff
pre-caldera volcanic and intrusive rocks
post-caldera intrusions
Y (ppm)
Zr (ppm)
200
150
100
50
100
200
300
400
500

Fig. 15a

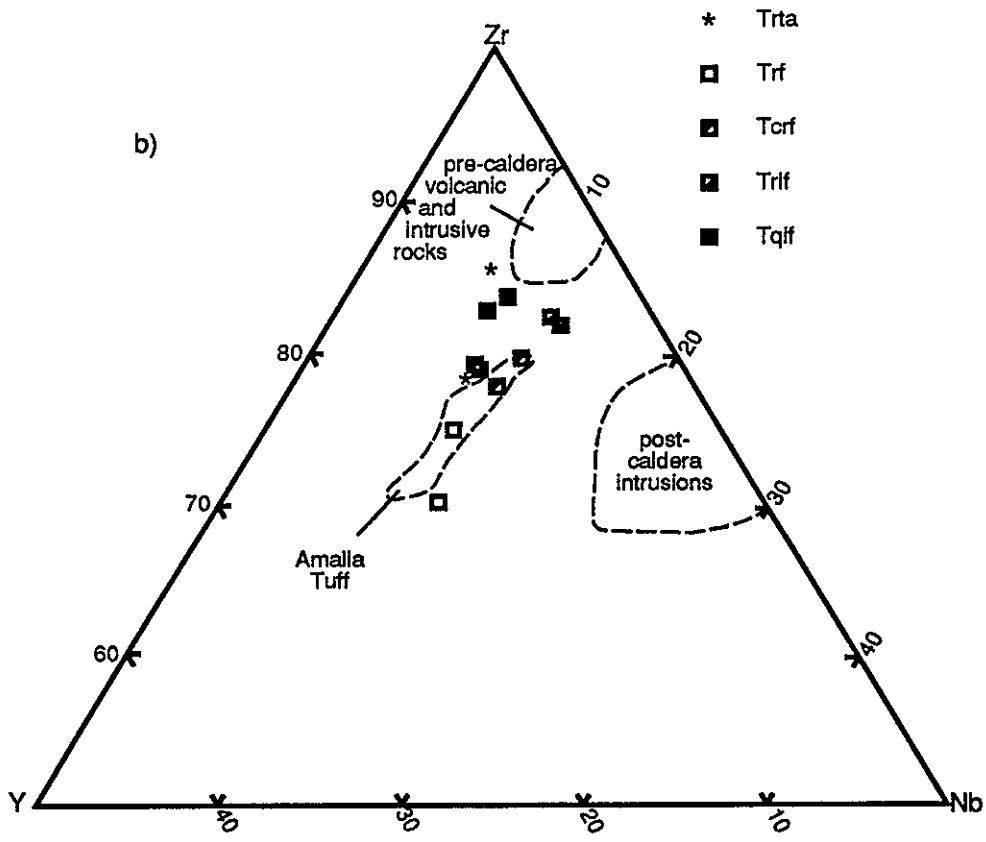
b)
Zr
Y
Nb
90
80
70
60
10
20
30
40
40
30
20
10
pre-caldera volcanic and intrusive rocks
post-caldera intrusions
Amalia Tuff
Trta
Trf
Tcrf
Trlf
Tqif

Fig 15 b

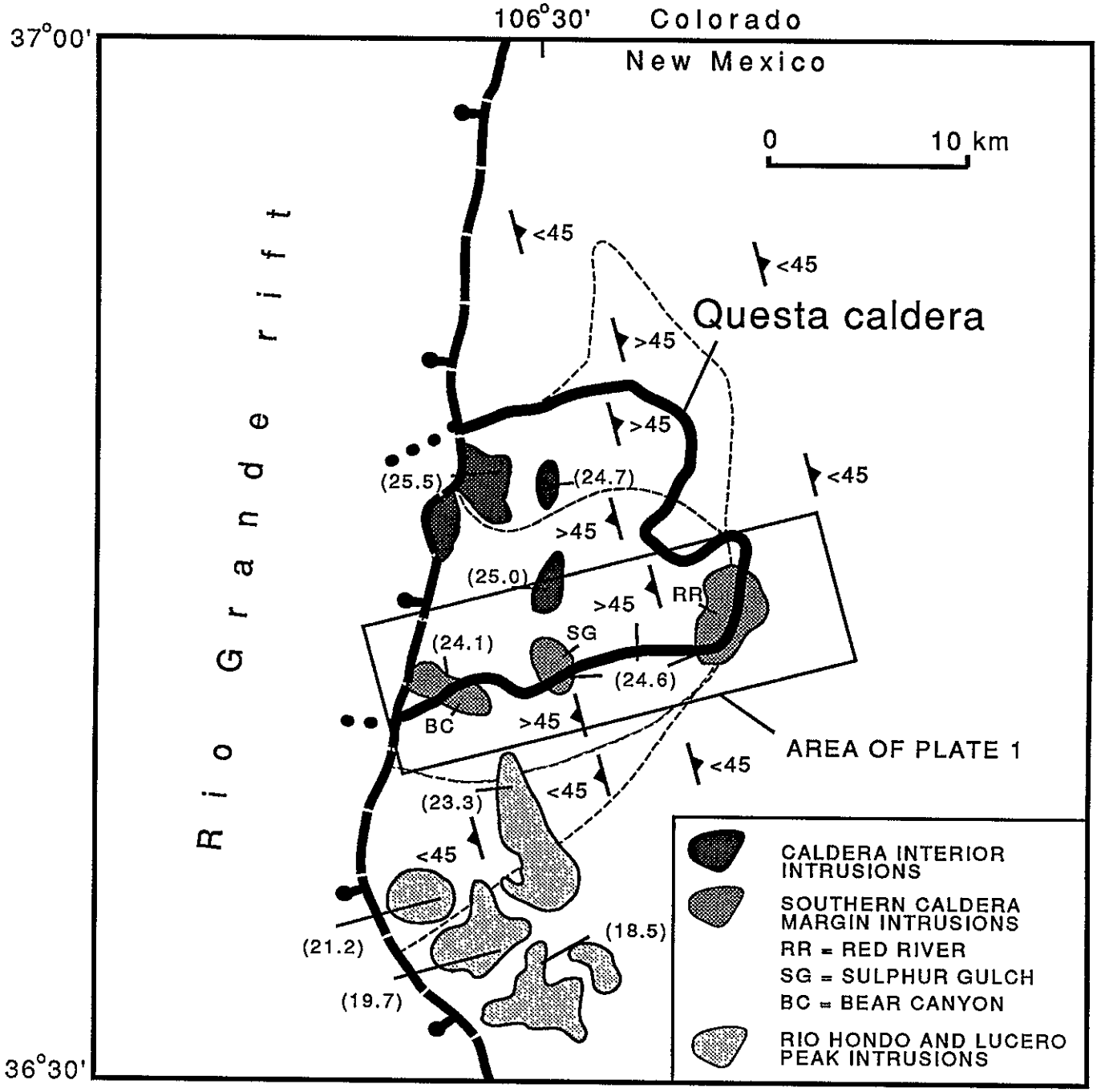
106°30'
Colorado
New Mexico
37°00'
36°30'
0
10 km
Rio Grande rift
Questa caldera
<45
>45
(25.5)
(24.7)
(25.0)
(24.1)
(24.6)
(23.3)
(21.2)
(19.7)
(18.5)
RR
SG
BC
AREA OF PLATE 1
CALDERA INTERIOR INTRUSIONS
SOUTHERN CALDERA MARGIN INTRUSIONS
RR = RED RIVER
SG = SULPHUR GULCH
BC = BEAR CANYON
RIO HONDO AND LUCERO PEAK INTRUSIONS

Fig. 16

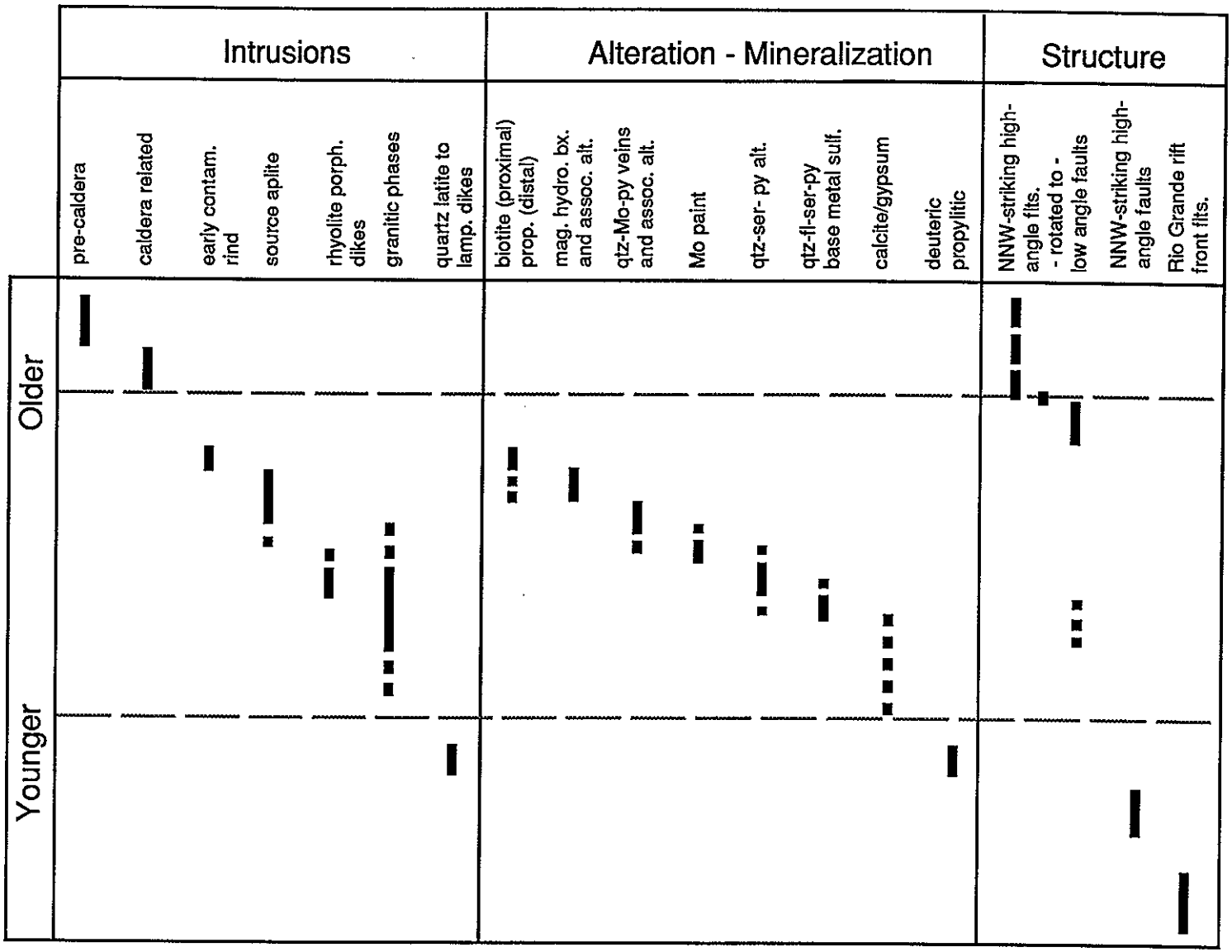
Intrusions
Alteration - Mineralization
Structure
Older
Younger
pre-caldera
caldera related
early contam. rind
source aplite
rhyolite porph. dikes
granitic phases
quartz latite to lamp. dikes
biotite (proximal) prop. (distal)
mag. hydro. bx. and assoc. alt.
qtz-Mo-py veins and assoc. alt.
Mo paint
qtz-ser- py alt.
qtz-fl-ser-py base metal sulf.
calcite/gypsum
deuteric propylitic
NNW-striking high-angle flts.
- rotated to - low angle faults
NNW-striking high-angle faults
Rio Grande rift front flts.

Fig. 17

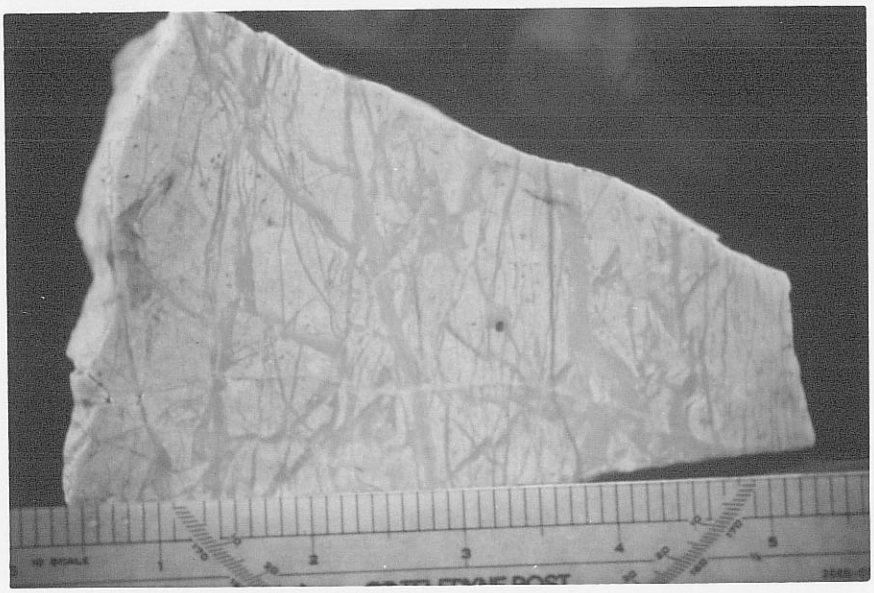

Fig. 18

OFR 431 # 109

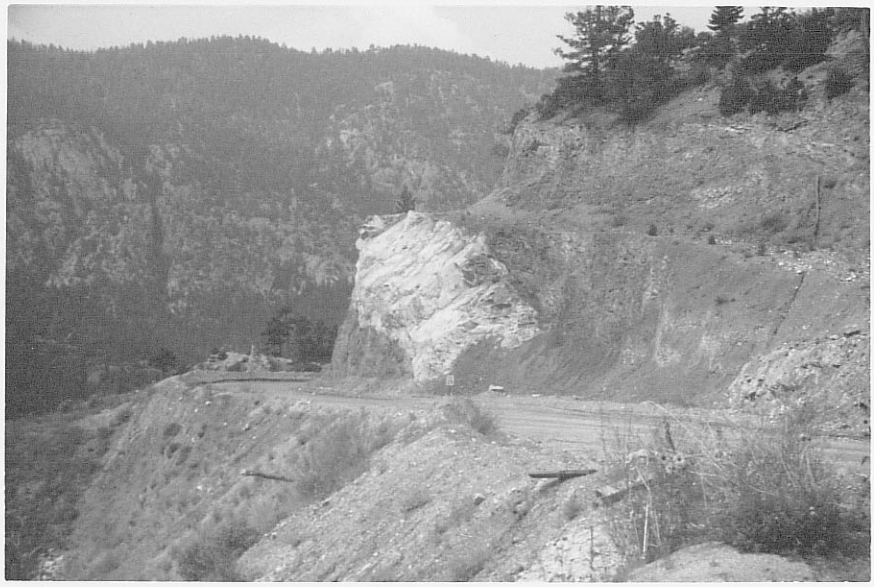

Fig. 19

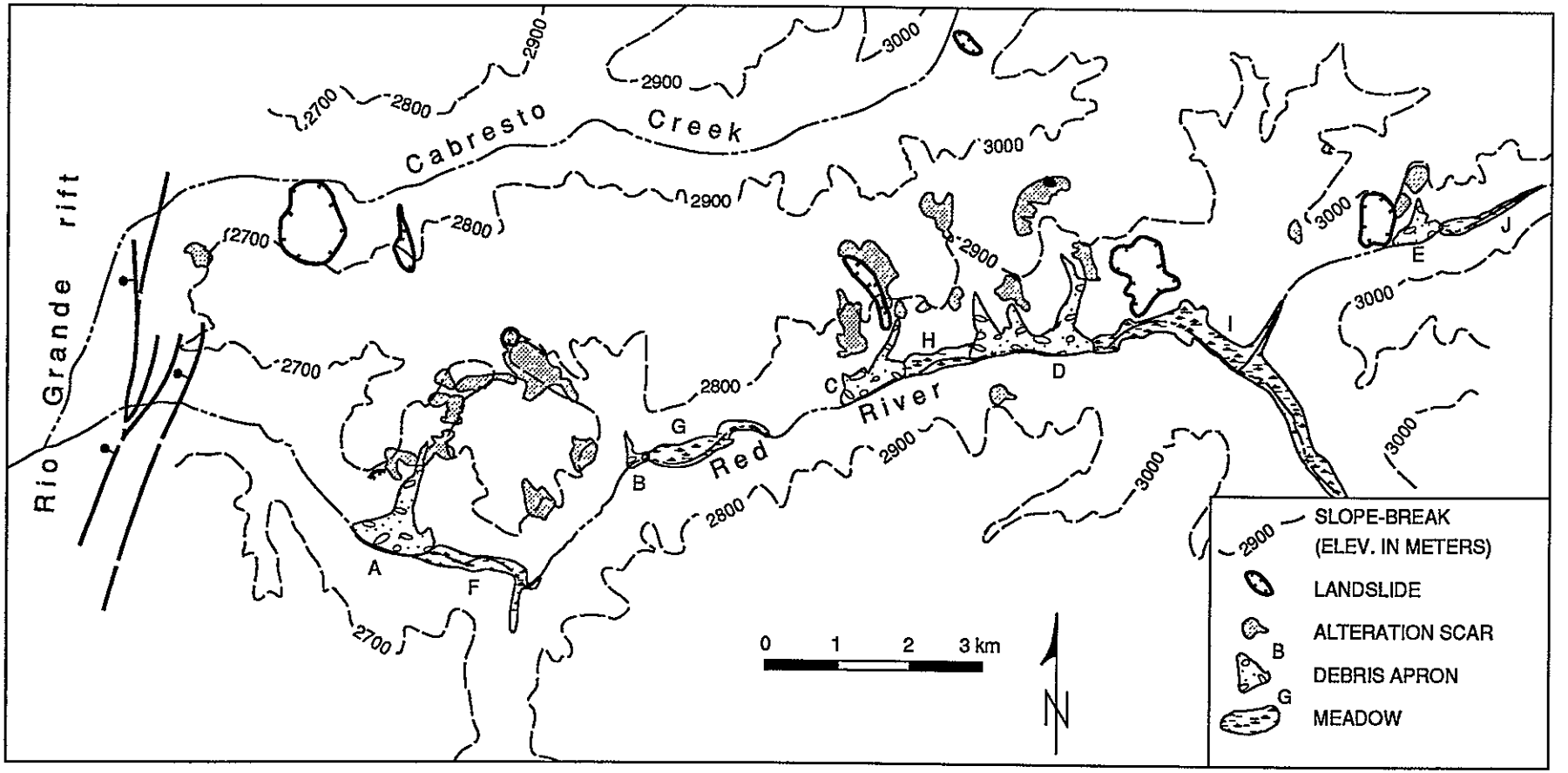
Rio Grande rift
Cabresto Creek
Red River
2700
2800
2900
3000
A
B
C
D
E
F
G
H
I
J
0 1 2 3 km
SLOPE-BREAK (ELEV. IN METERS)
LANDSLIDE
ALTERATION SCAR
DEBRIS APRON
MEADOW

Fig. 20

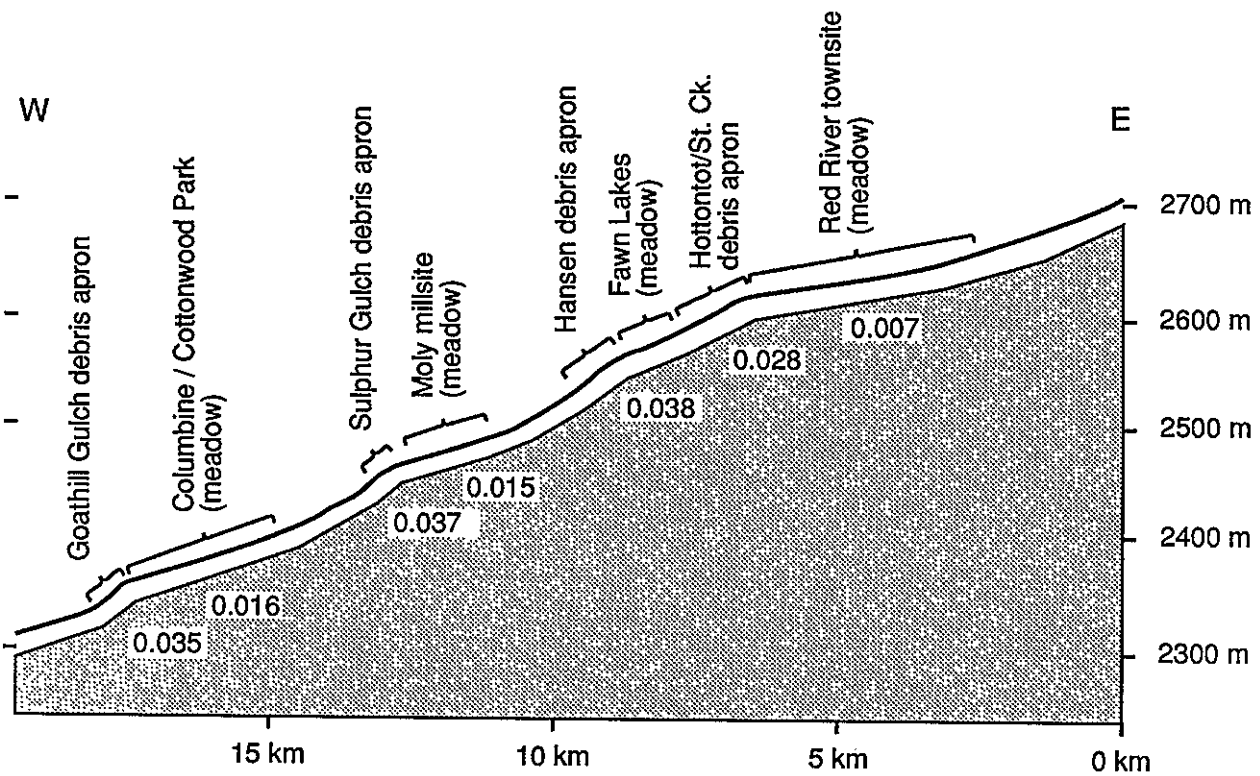
W
E
Goathill Gulch debris apron
Columbine / Cottonwood Park (meadow)
Sulphur Gulch debris apron
Moly millsite (meadow)
Hansen debris apron
Fawn Lakes (meadow)
Hottontot/St. Ck. debris apron
Red River townsite (meadow)
0.035
0.016
0.037
0.015
0.038
0.028
0.007
2700 m
2600 m
2500 m
2400 m
2300 m
15 km
10 km
5 km
0 km

Fig. 21

Fig. 22

Fig. 23

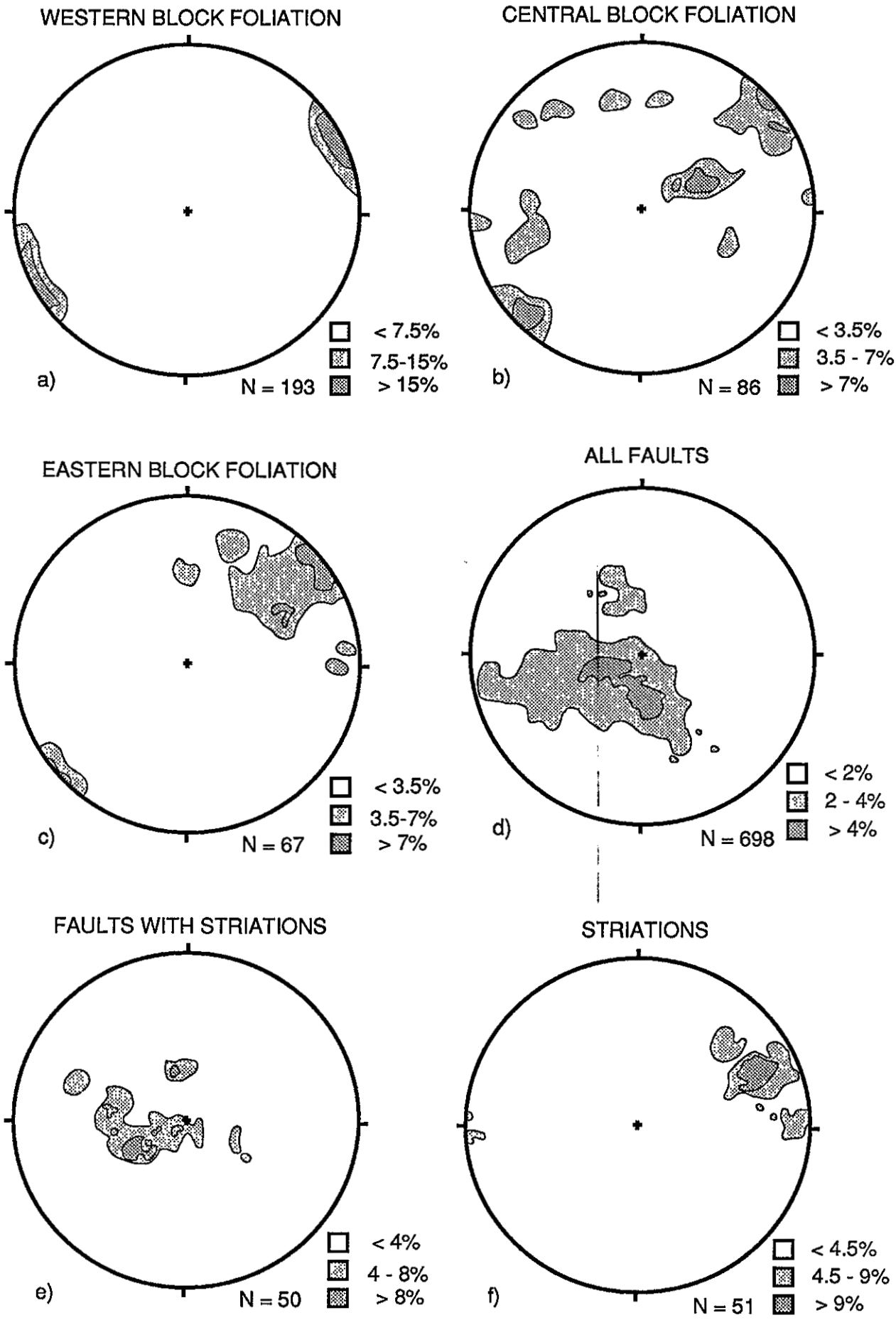
WESTERN BLOCK FOLIATION
a)
N = 193
< 7.5%
7.5-15%
> 15%
CENTRAL BLOCK FOLIATION
b)
N = 86
< 3.5%
3.5 - 7%
> 7%
EASTERN BLOCK FOLIATION
c)
N = 67
< 3.5%
3.5-7%
> 7%
ALL FAULTS
d)
N = 698
< 2%
2 - 4%
> 4%
FAULTS WITH STRIATIONS
e)
N = 50
< 4%
4 - 8%
> 8%
STRIATIONS
f)
N = 51
< 4.5%
4.5 - 9%
> 9%

Fig. 24

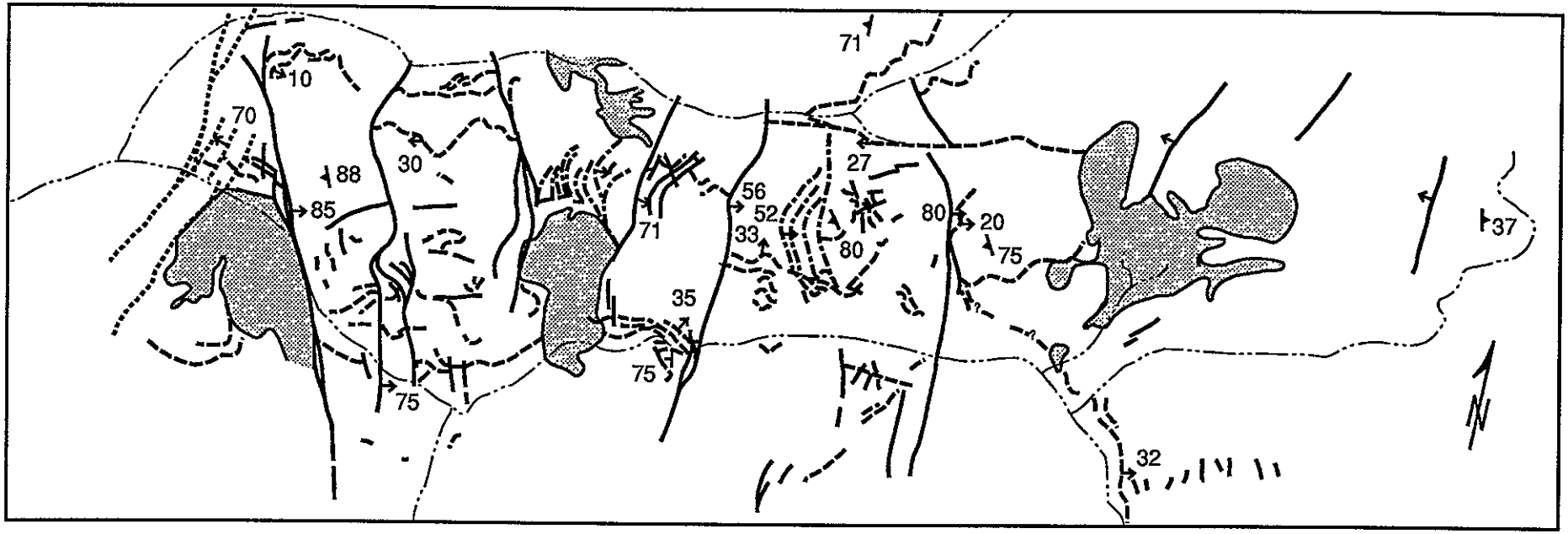
71
10
70
88
30
85
71
56
52
33
27
80
80
20
75
37
35
75
75
32
RIFT MARGIN NORMAL FAULTS
THOROUGH-GOING, HIGH-ANGLE FAULTS
DISCONTINUOUS MEDIUM TO HIGH-ANGLE FAULTS
LOW-ANGLE FAULTS
0
5 km
INTRUSIONS
STREAMS
STRIKE AND DIP OF EUTAXITIC FOLIATION
STRIKE AND DIP OF BEDDING

Fig. 25

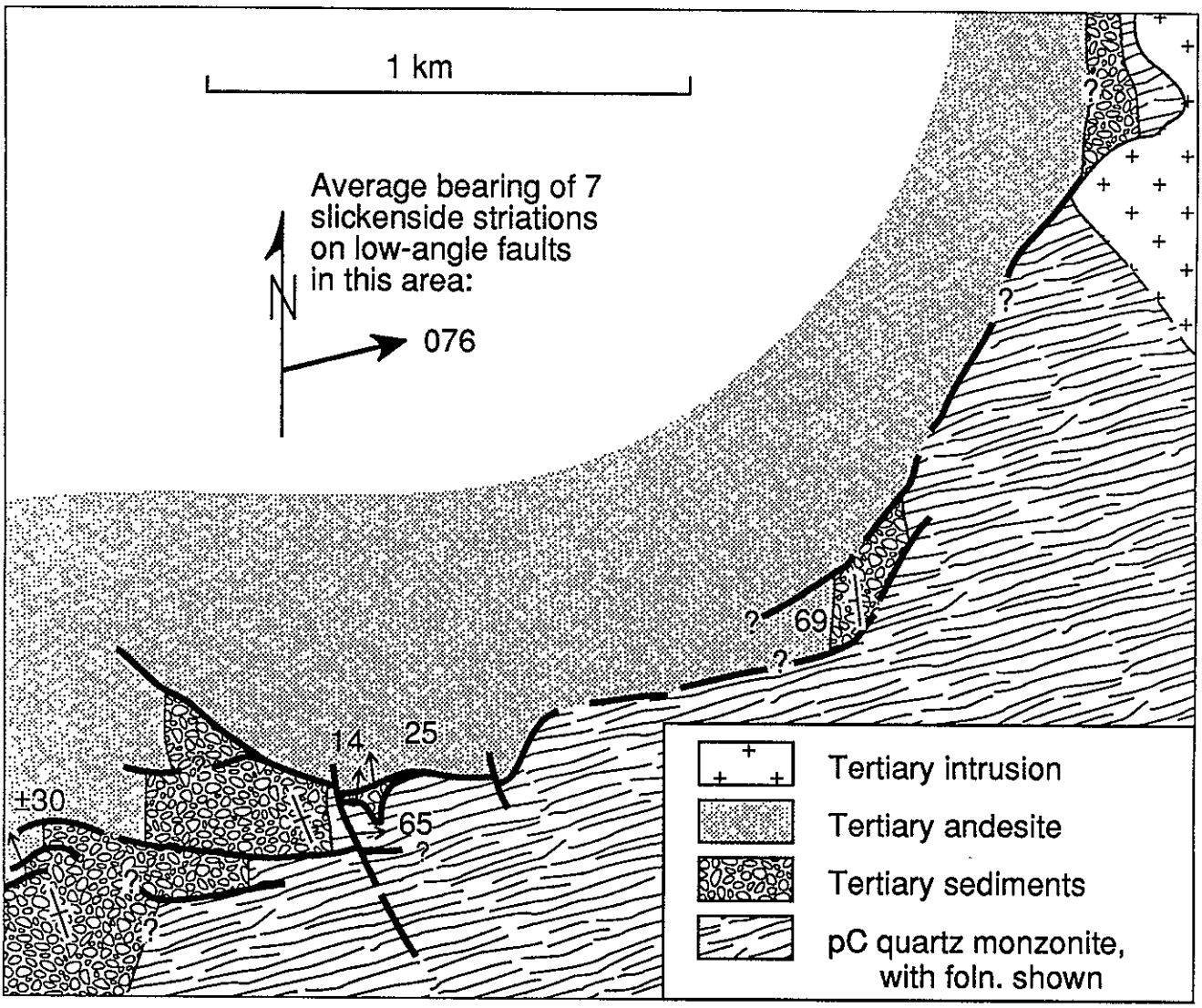
1 km
Average bearing of 7 slickenside striations on low-angle faults in this area:
N
076
69
14
25
65
±30
Tertiary intrusion
Tertiary andesite
Tertiary sediments
pC quartz monzonite, with foln. shown

Fig. 26

Fig-27

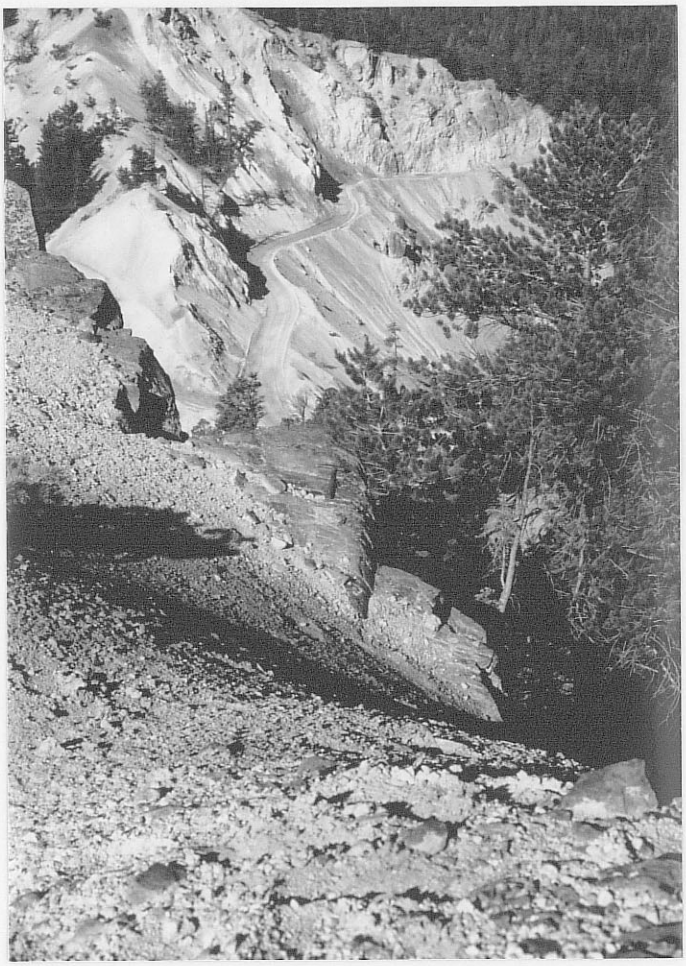

Fig. 28

Fig. 29

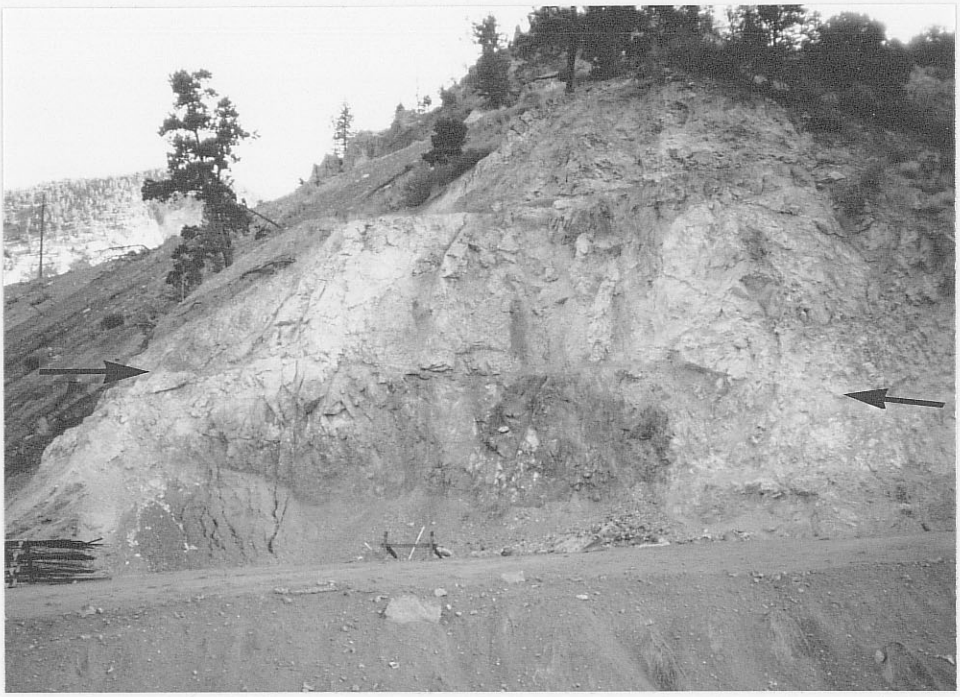

Fig 30

181

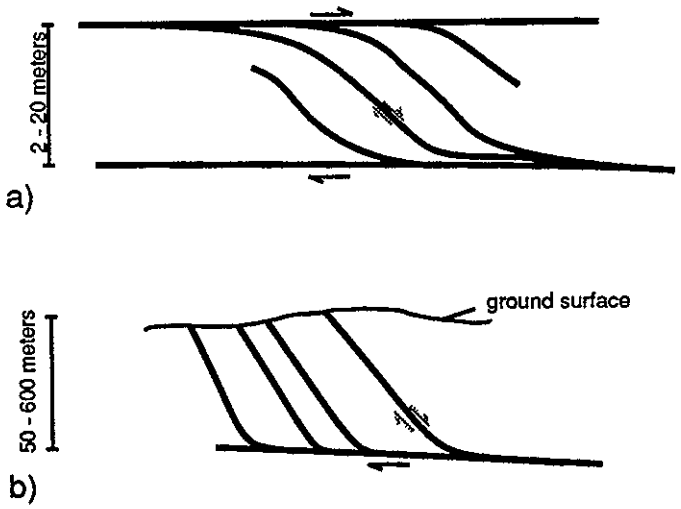

Fig. 31

a)

b)

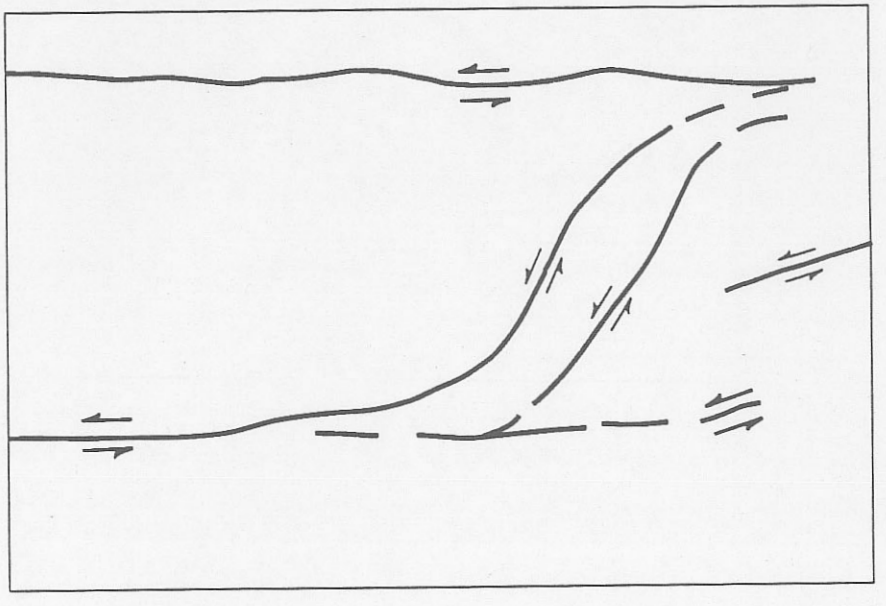

Fig. 32

a)

b)

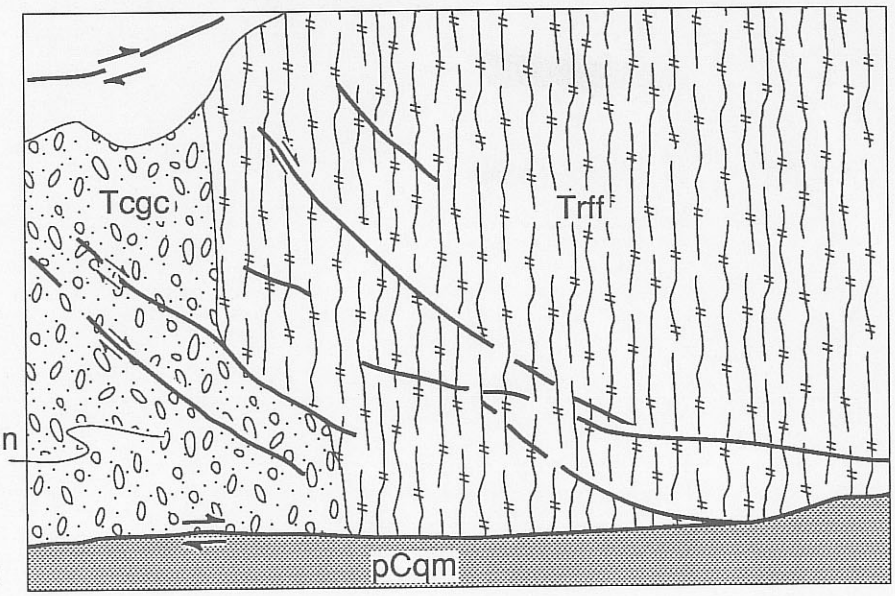

location of Fig. S-18

Fig. 33

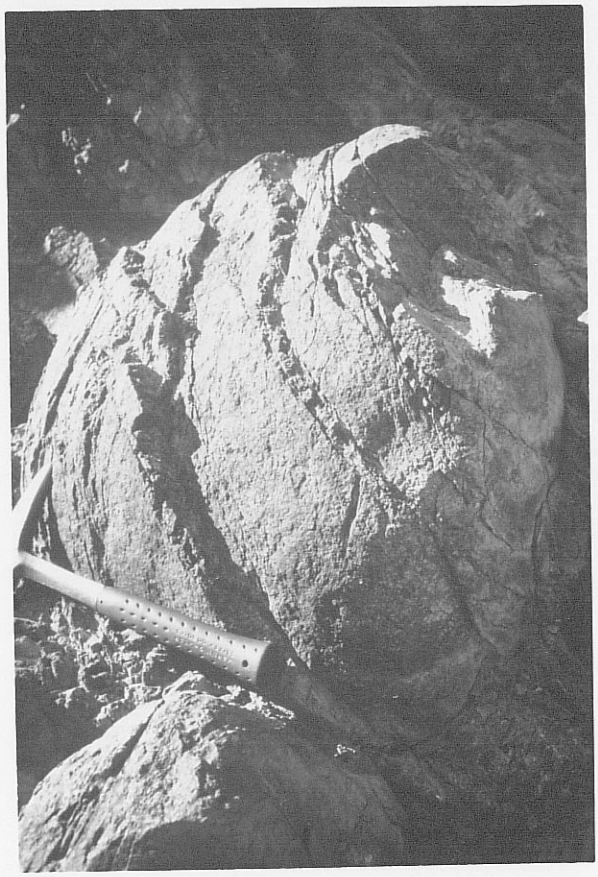

Fig. 34

Fig. 35

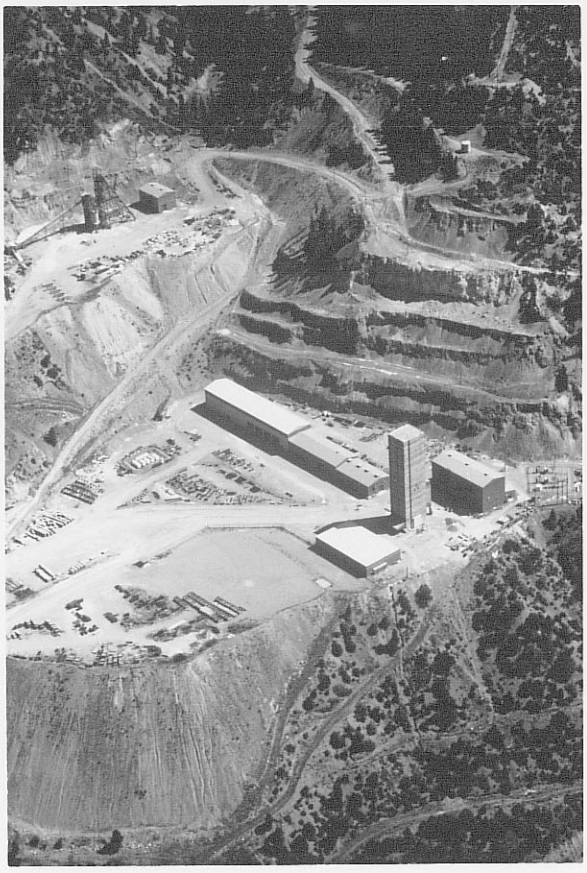

Fig. 36

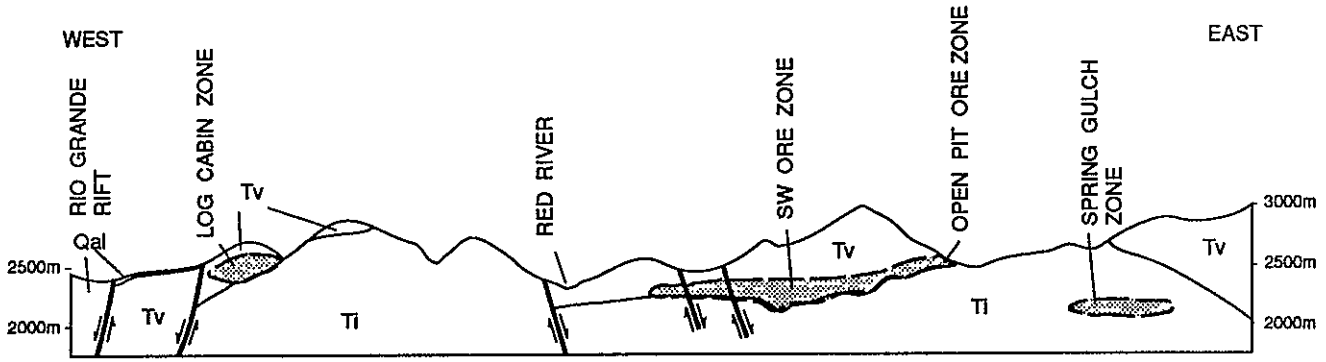
WEST
EAST
RIO GRANDE RIFT
LOG CABIN ZONE
RED RIVER
SW ORE ZONE
OPEN PIT ORE ZONE
SPRING GULCH ZONE
Qal
Tv
Ti
2500m
2000m
3000m

Fig 37

Fig. 38

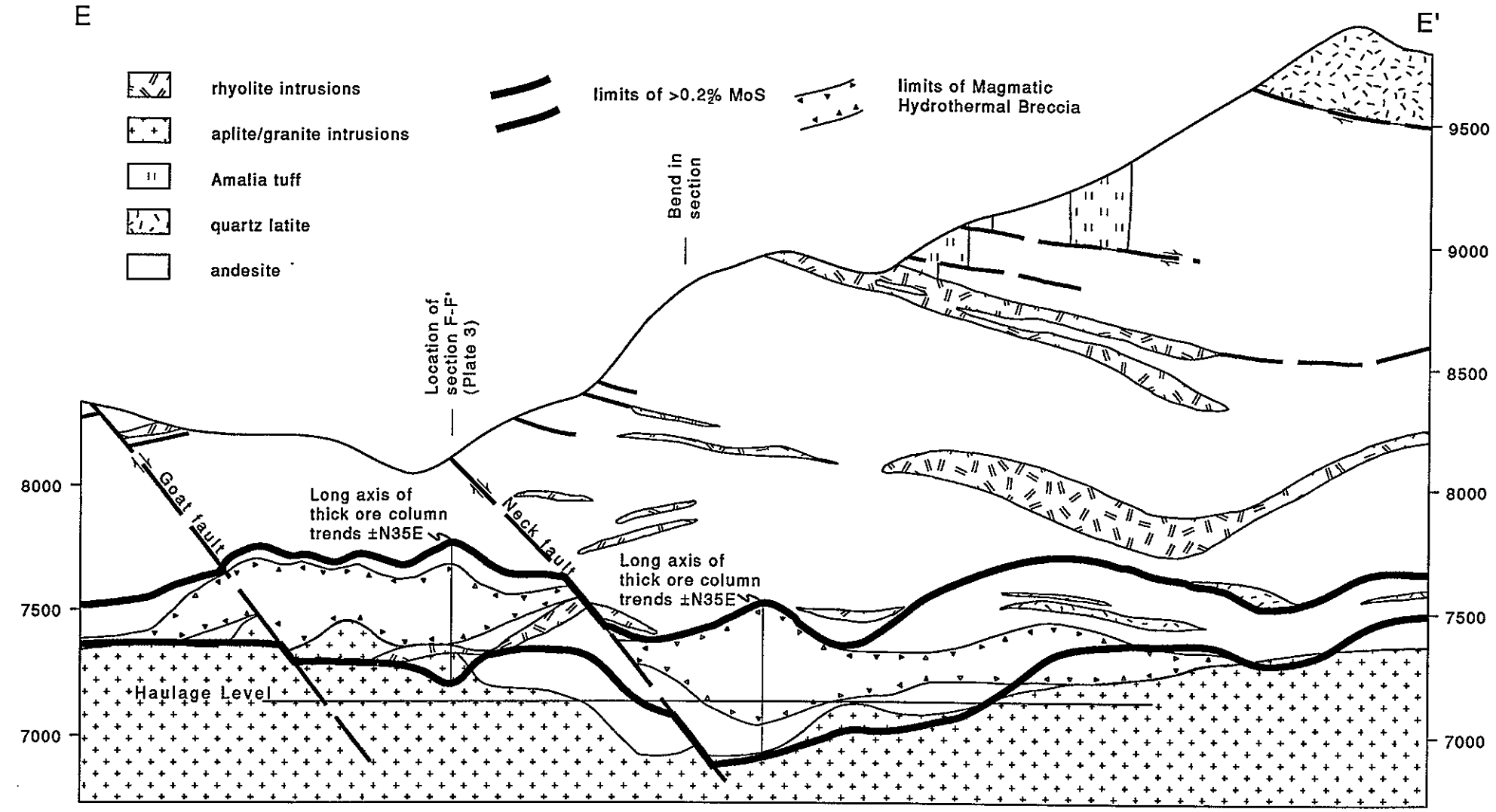
E
E'
rhyolite intrusions
aplite/granite intrusions
Amalia tuff
quartz latite
andesite
limits of >0.2% MoS
limits of Magmatic Hydrothermal Breccia
Bend in section
Location of section F-F' (Plate 3)
Goat fault
Neck fault
Long axis of thick ore column trends ±N35E
Long axis of thick ore column trends ±N35E
Haulage Level
9500
9000
8500
8000
7500
7000
8000
7500
7000

Fig. 39

Explanation

- Trff — rhyolite porphyry intrusion (dominantly post-ore)
- Tap — aplite porphyry intrusion (mineralization-related); locally xenolith-rich; locally abundant quartz veins
- Tapp — pre-ore aplite porphyry (contaminated phases)
- Trif — rhyolite porphyry intrusion (caldera-related)
- Tqil — quartz latite porphyry intrusion
- Tan — andesite porphyry flows

- outline of >0.2% MoS_2
- fault and fault zone
- quartz veins in aplite
- mining level
- xenoliths
- diamond drill hole

Magmatic-Hydrothermal Breccia:

- B — biotite, quartz, orthoclase matrix
- K — quartz, orthoclase matrix
- Q — quartz matrix

No vertical exaggeration

8000 ft.
2400m
2300m
7500 ft
2200m
Undercut Level
Grizzly Level
Haulage Level

Tan
Tqi
Trff
Tri
Tap
Tapp

Outline of >0.2% MoS_2

Tap with 25-95% quartz veins

Tap with 5-10% qtz veins

Tap with 6-10% qtz veins

Tan in fault zone

Fig. 40

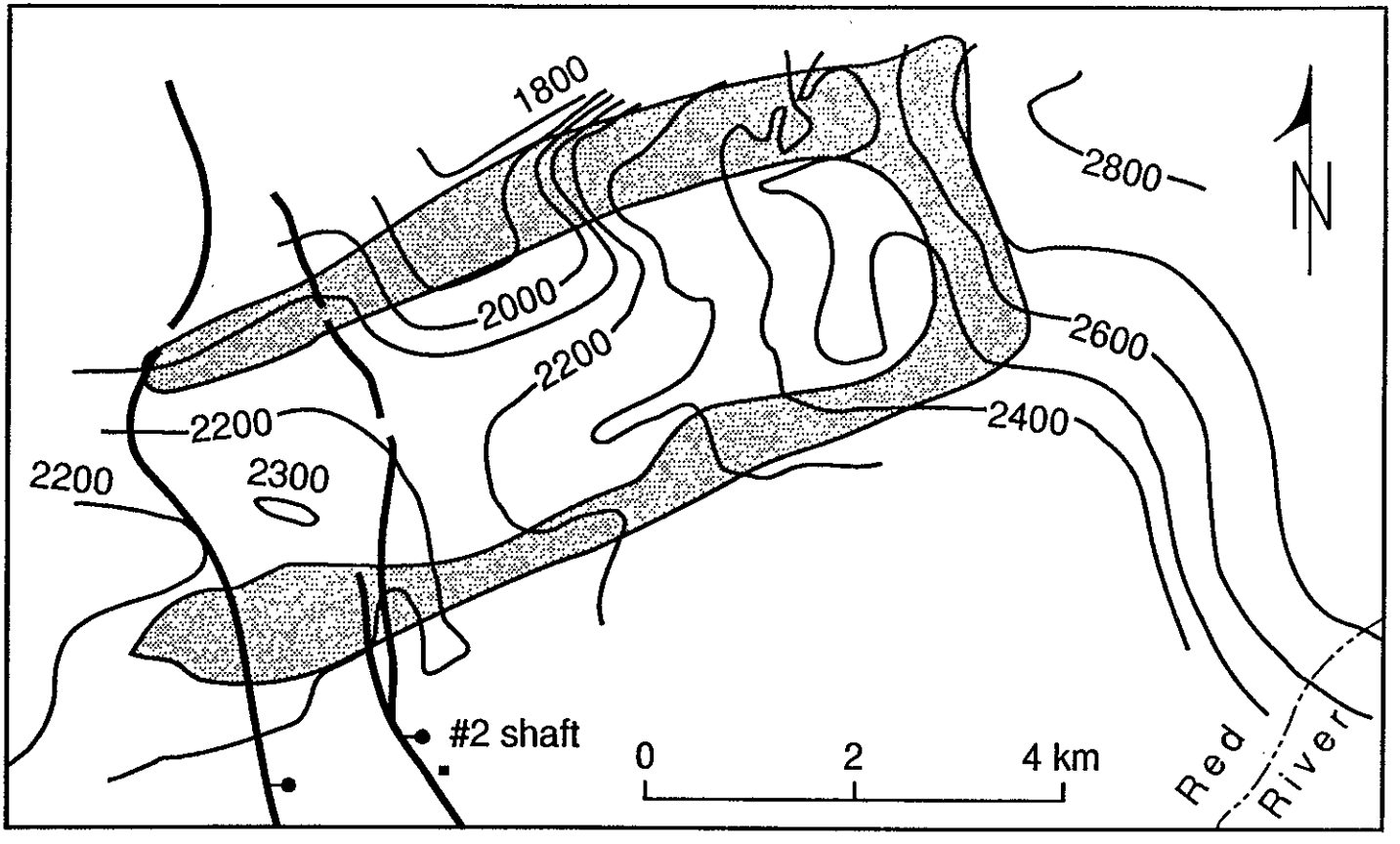
1800
2000
2200
2200
2200
2300
2400
2600
2800
N
#2 shaft
0
2
4 km
Red
River

Fig. 41

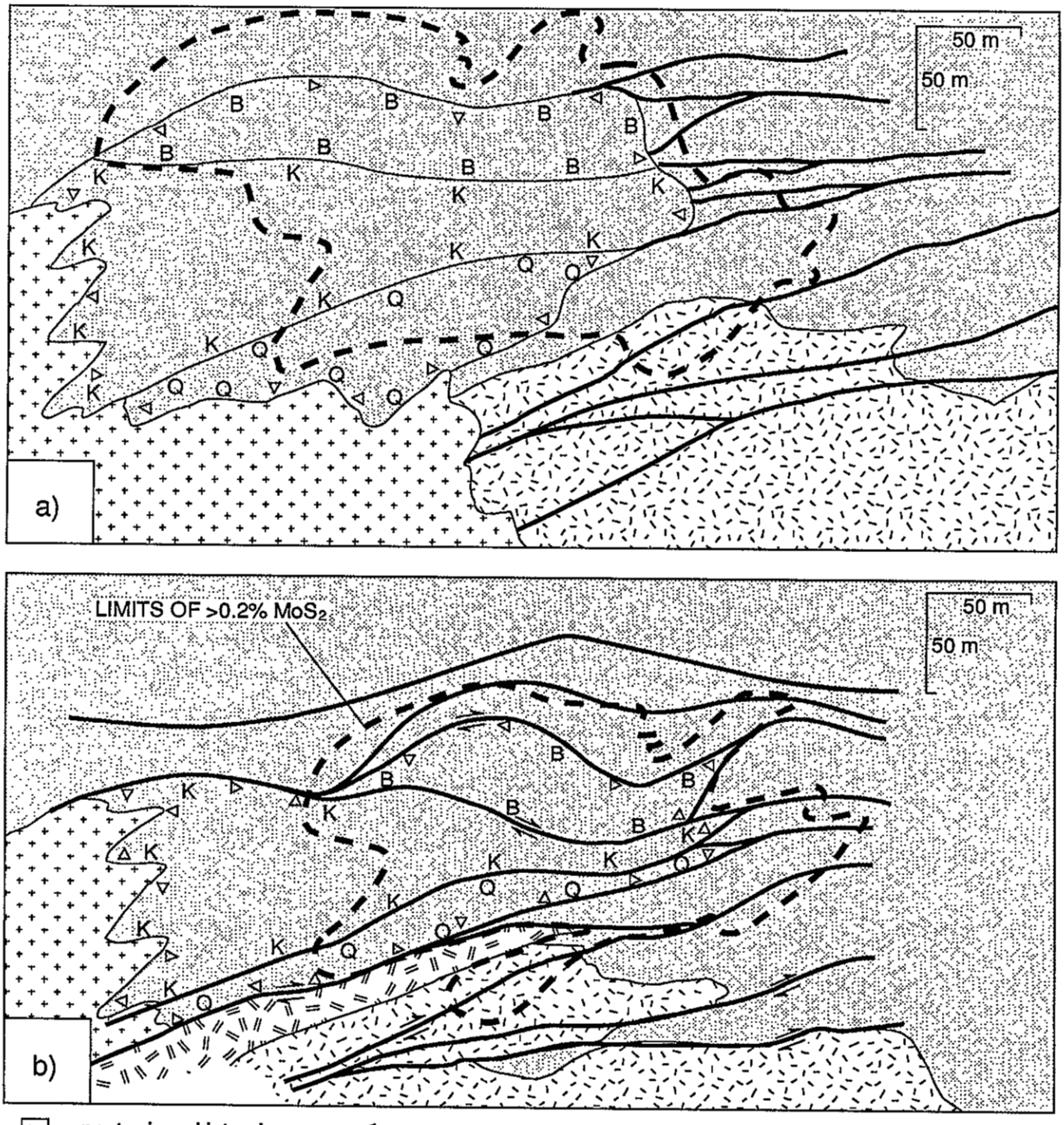
50 m
50 m
a)
LIMITS OF >0.2% MoS_2
50 m
50 m
b)
post-mineral intrusion
min-related intrusion
pre-mineral intrusion
host rock (dom. andesite)
>0.2% MoS_2 mineralization
outline of magmatic-hydrothermal breccia
B - quartz-biotite-orthoclase matrix
K - quartz-orthoclase matrix
Q - quartz matrix

Fig. 42

Fig. 43

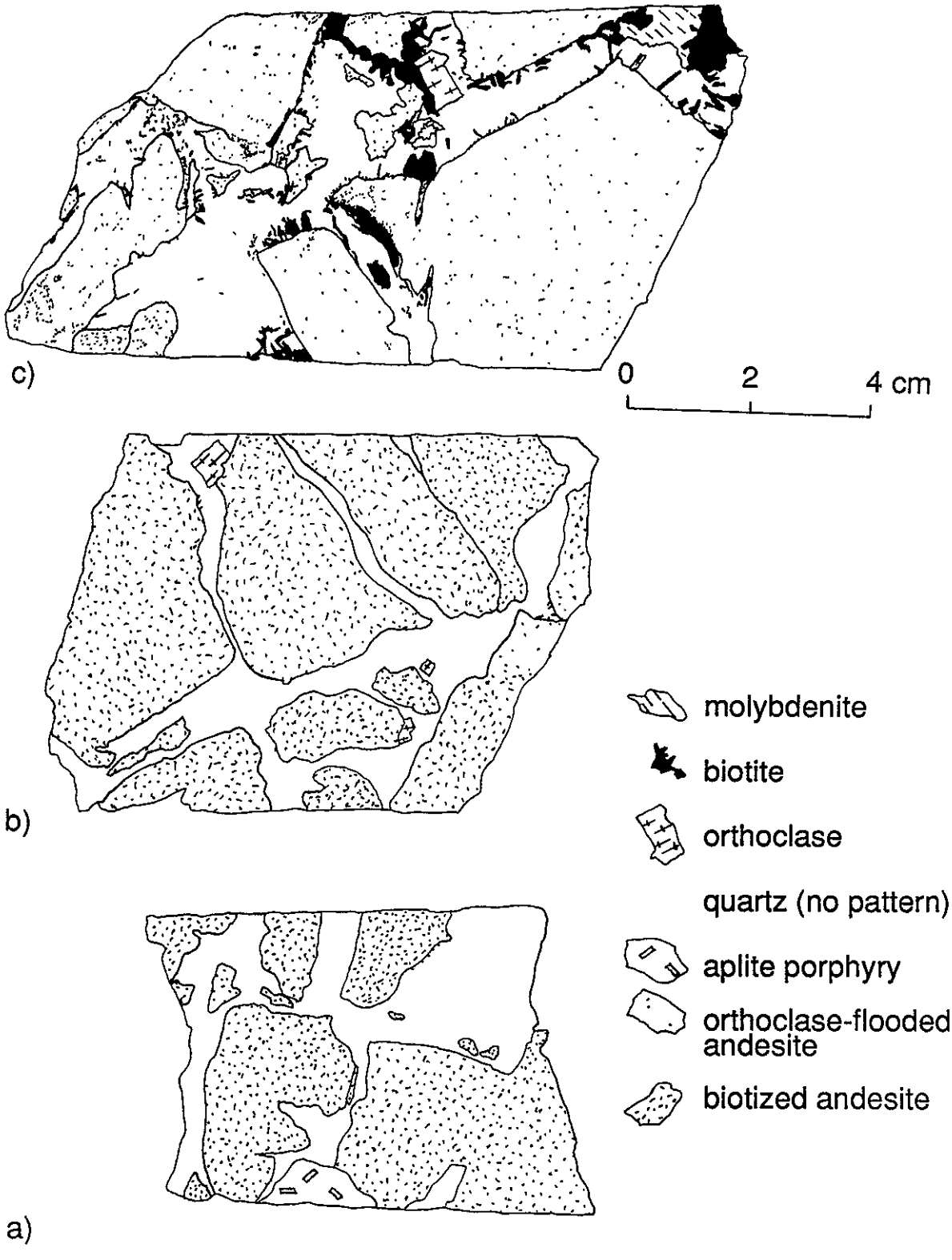
c)
0
2
4 cm
b)
molybdenite
biotite
orthoclase
quartz (no pattern)
aplite porphyry
orthoclase-flooded andesite
biotized andesite
a)

Fig 44

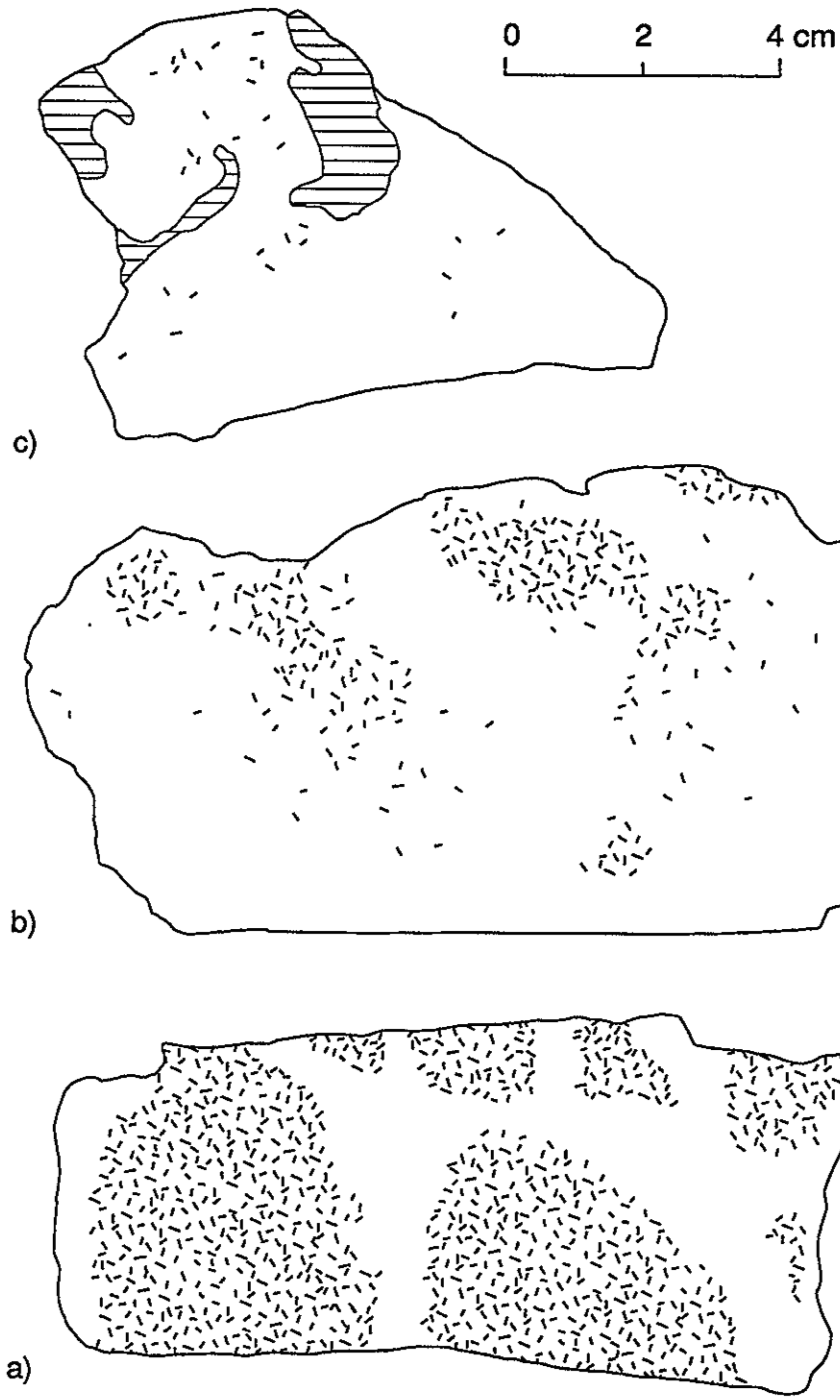
0
2
4 cm
c)
b)
a)
QUARTZ-SERICITE-GREEN SERICITE ALTERATION
QUARTZ-SERICITE ALTERATION
QUARTZ-SERICITE-SPECULAR HEMATITE ALTERATION

Fig. 45

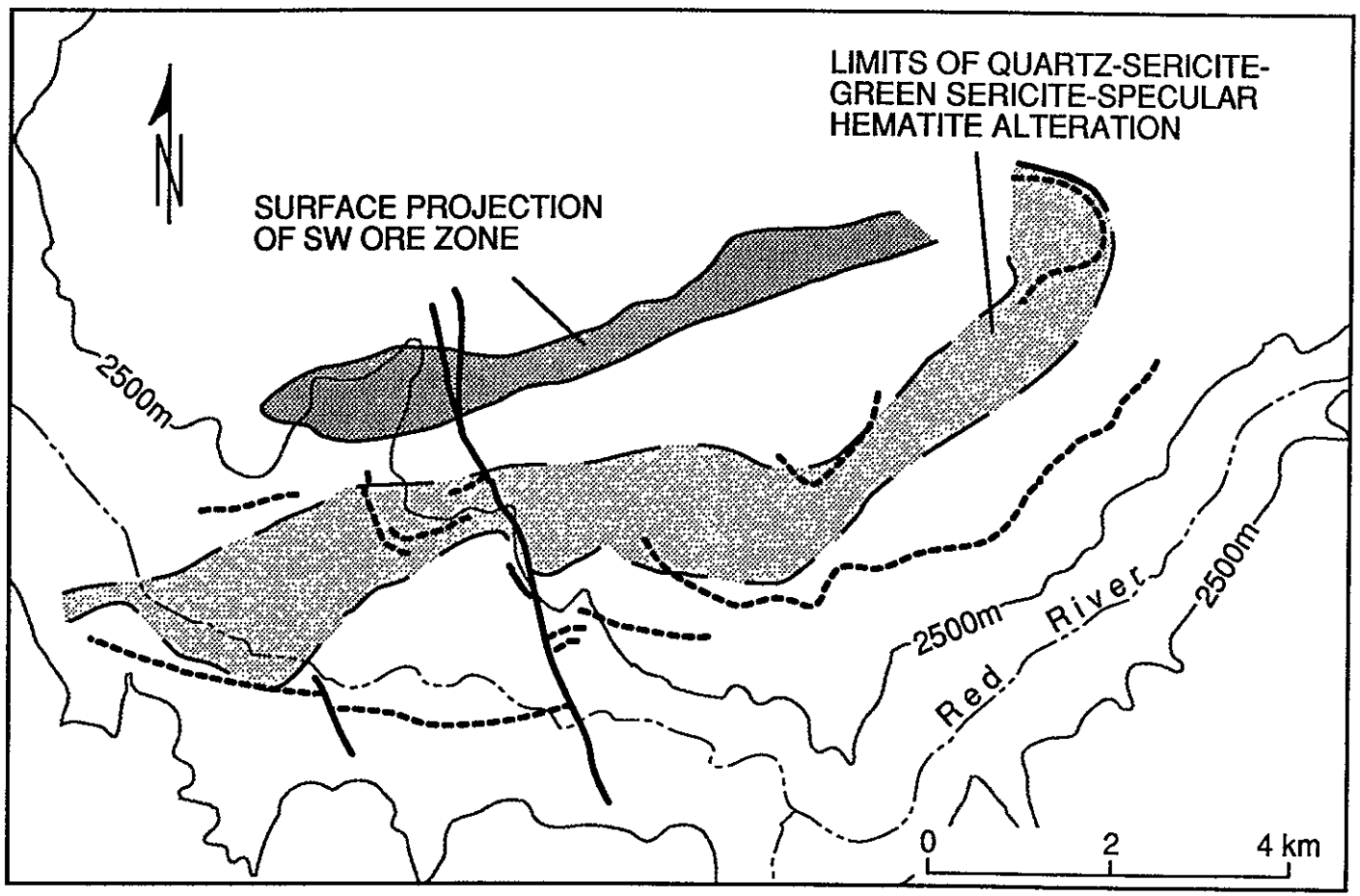
LIMITS OF QUARTZ-SERICITE-
GREEN SERICITE-SPECULAR
HEMATITE ALTERATION
SURFACE PROJECTION
OF SW ORE ZONE
2500m
2500m
Red River
2500m
0
2
4 km

Fig. 46

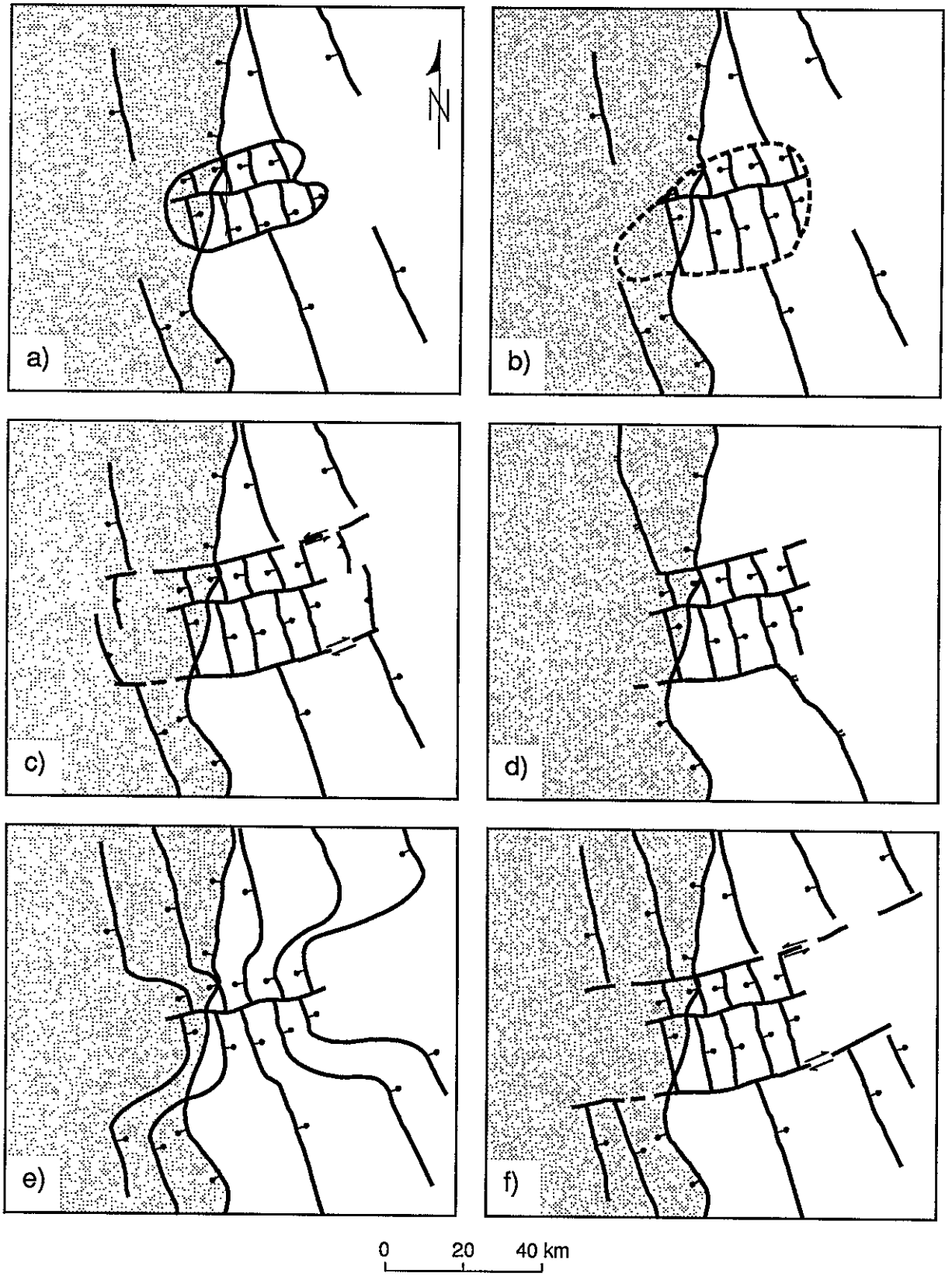

Fig. 47

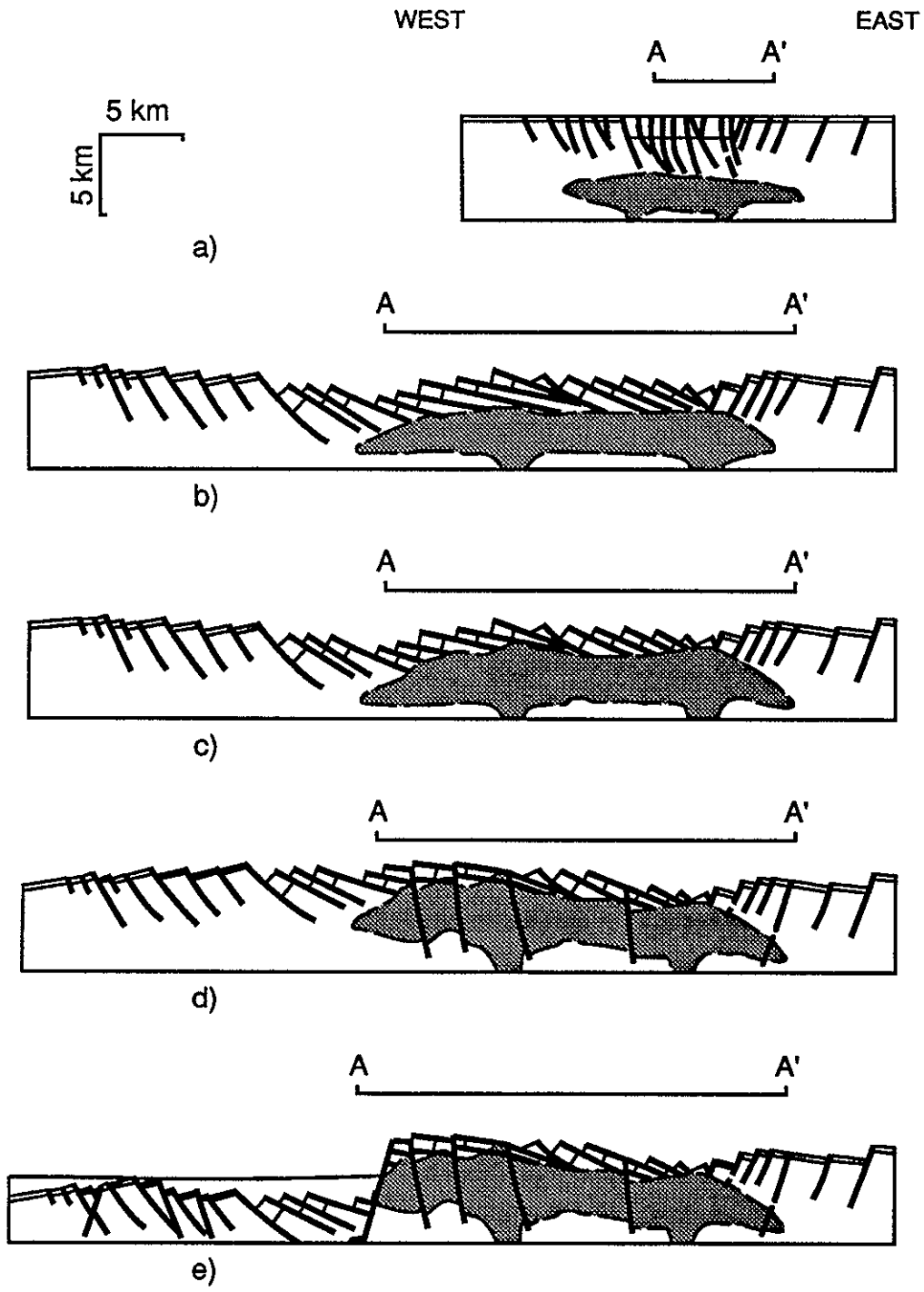

Fig. 48

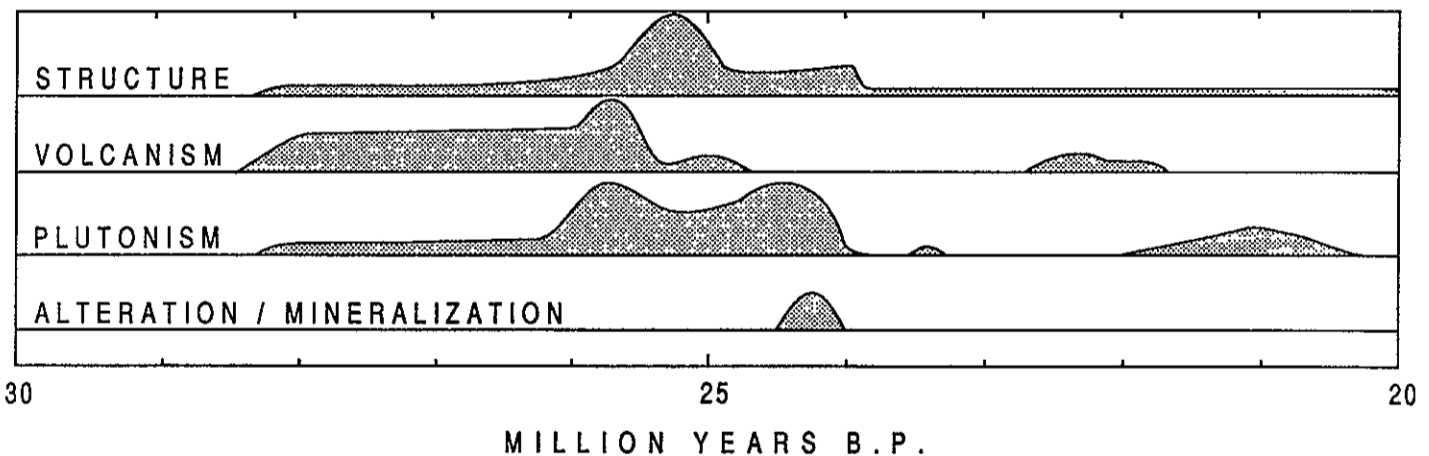
STRUCTURE
VOLCANISM
PLUTONISM
ALTERATION / MINERALIZATION
30
25
20
MILLION YEARS B.P.

Fig. 49

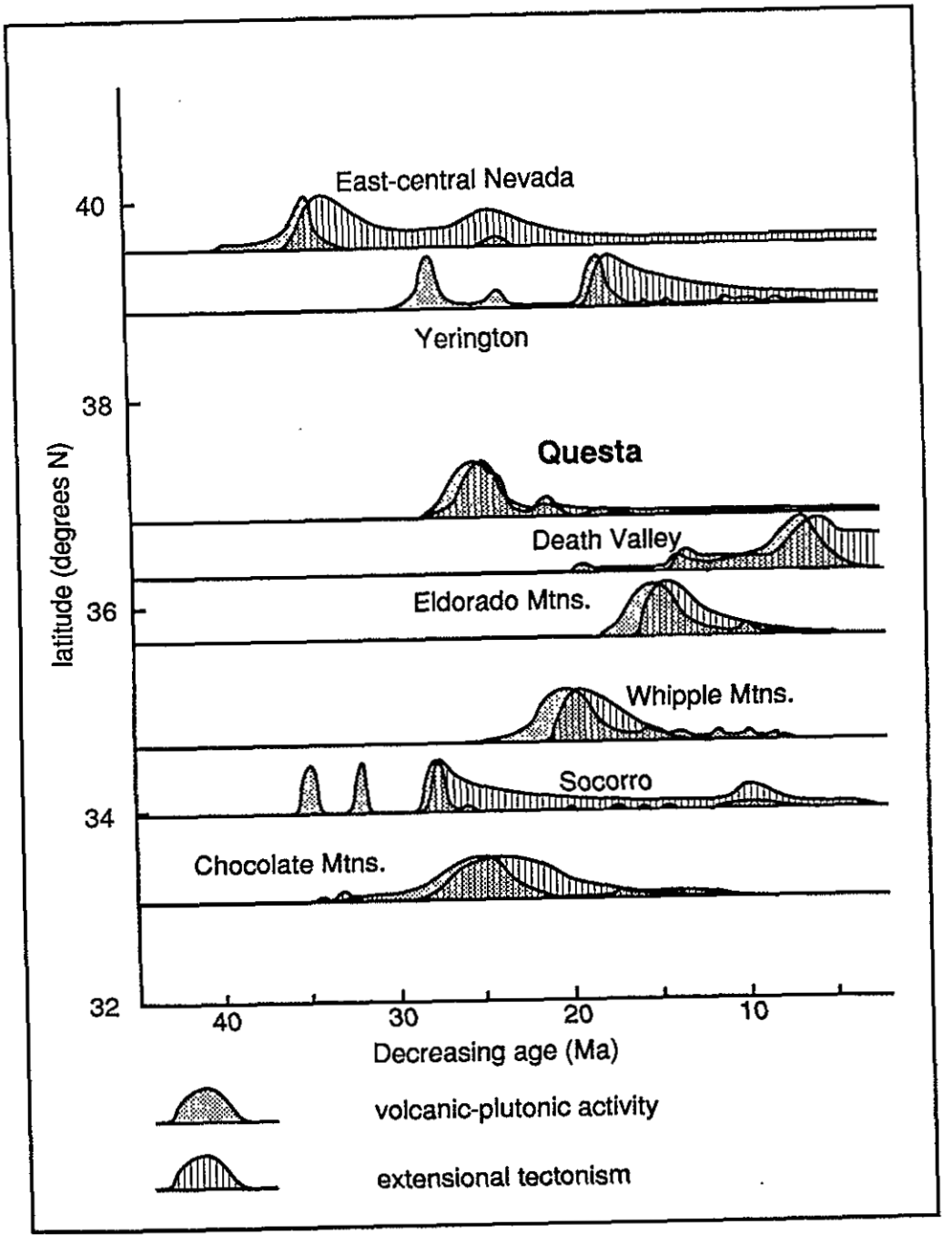
East-central Nevada
40
Yerington
38
Questa
Death Valley
Eldorado Mtns.
36
Whipple Mtns.
Socorro
34
Chocolate Mtns.
32
latitude (degrees N)
40
30
20
10
Decreasing age (Ma)
volcanic-plutonic activity
extensional tectonism

Fig. 5D

Alteration	Location	Sample No.	Rock type	SiO2	TiO2	Al2O3	FeO	Fe2O3	MnO	MgO	CaO	Na2O	K20	L.O.I.	P2O5
Lt. prop.	Shafts area	3296	Tqli	58.30	0.80	15.00	2.25	3.35	0.10	3.00	4.40	2.90	5.70	4.77	0.32
Lt. prop.	Decl. pilot hole - 57'	2358	Tqli	64.00	0.55	15.00	4.70		0.08	1.95	3.15	4.20	3.50	3.29	0.27
Mod. qtz-ser	Goat Hill gulch	2549	Trg	70.50	0.30										
High py./tr mag.	DDH 27.7-26.1 - 395'	3636	Trq	72.00	0.10										
Lt. clay alt./feox staining	Shafts area, surface	3684	Trh	73.50	0.15	12.60	0.60	1.60	0.04	0.35	0.15	4.60	4.60	0.76	0.05
Lt. clay alt./feox staining	South Haulage loop u.g.	3629	Trs	76.30	0.10	12.70	0.50	0.05	0.05	0.15	0.65	4.00	5.00	0.49	0.04
"Fresh"	Sulphur Gulch Stock	Avg. of 3	Tgp	76.57	0.18	12.53	0.30	0.73	0.02	0.13	0.45	3.43	4.67	0.41	0.10
"Fresh"	S. Haulage loop, u.g.	3638	Tap	75.00	0.25	12.50	0.40	0.30	0.08	0.15	0.65	3.70	4.90	0.77	0.06
Lt. prop.	S of river near office	3322	Tqlc	66.40	0.40	14.50	1.05	2.00	0.05	2.30	2.80	3.60	4.50	3.09	0.24
Lt. clay alt.	S of No. 1 shaft	2440	Tqlf	65.00	0.50										
Lt. clay alt.	E of No. 1 shaft	2464	Trdf	72.50	0.20	13.40	0.30	2.30	0.01	0.20	0.15	4.50	5.40	0.52	0.07
Lt. clay alt.	P-7 - 732'	3616	Tcrf	75.10	0.10	12.10	0.40	1.50	0.04	0.10	0.25	4.10	4.70	0.42	0.02
Lt. clay alt.	E of No. 1 shaft	3285	Trlf	76.00	0.10	12.40	0.20	1.50	0.01	0.05	0.20	4.20	5.30	0.31	0.03
"Fresh" to mod. clay alt.	Capulin Ridge	2403	Trt	76.50	0.25	12.00	0.40	0.70	0.01	0.05	0.30	3.70	4.80	0.43	0.07
Lt. prop.	Bonita canyon area	JM-86-103	Tqlk	57.42	1.14	14.29	3.10	1.70	0.09	2.57	4.20	3.22	4.63	6.20	0.46
lt. - mod. prop.	June Bug area	RC-4310	Tqlo	65.00	0.16	13.70		2.90	0.06	1.50	3.40	3.40	4.90	4.05	0.16
Lt. prop.	P-7 - 390'	3615	Tqli	63.90	0.60	15.40	2.00	2.80	0.09	2.20	3.90	3.80	3.60	2.04	0.29
Lt. prop.	Capulin ridge - near pit	800	Tql	63.50	0.60	13.90	0.65	4.70	0.08	2.25	4.30	3.70	3.90	1.62	0.44
Lt. prop.	N of #2 shaft	2504	Tanq	67.00	0.40										
Mod. biotization	N. of pit	988	Tan	54.00	1.00	14.80	3.90	4.00	0.14	6.30	6.90	3.10	3.20	2.85	0.54
"Fresh"	4th of July area	1834	Tan	60.50	0.60	16.50	0.70	6.50	0.12	1.75	5.80	3.10	2.10	1.39	0.37
Light prop alt.	E of Singing River Ranch	JM-87-38	Tlt	72.62	0.09										
"Fresh"	P5A - 990'	3633	pCqm	72.00	0.15	13.40	0.85	0.80	0.05	0.25	1.10	5.00	3.50	0.54	0.05
"Fresh"	P7 - 1152'	3625	pCs	57.00	0.64	16.00	3.85	6.90	0.20	3.70	5.00	3.70	1.70	1.06	0.68

Table 1

Rock type	totals	Sn	Ba	Rb	Sr	Rb/Sr	Zr	Nb	Y	Cu	Pb	Zn	Mo	Ni	Co	Bi	F	W	S	SO4	CO2	Comments
Tqll	100.89	<5	1,010	220	390	0.56	140	18	12	34	13	71	<1	48	15	<1	1,100	2	0.04	0.02	2.56	Megacrystic.
Tqll	100.69			89	390	0.23	130	17	<5				<1				320					Megacrystic.
Trg				260	61	4.26	185	35	8													
Trq				305	60	5.08	120	37	6													
Trh	99.00	<5	590	170	145	1.17	150	39	11	9	17	36	3	5	2	<1	650	2	0.02	<.02	<.04	
Trs	100.03	<5	90	195	47	4.15	105	42	7	7	8	9	<1	3	1	<1	880	2	0.14	0.06	0.22	
Tgp	99.52	<5	257	223	53	4.21	118	45	8	13	8	12	30	4	2	<1	647	7	0.19	0.25		
Tap	98.76	<5	50	180	57	3.16	105	42	<5	17	12	10	4	3	<1	<1	920	2	0.04	0.26	0.30	
Tqlc	100.93	<5	1,430	105	455	0.23	165	19	5	20	16	42	<1	19	6	<1	620	2	0.02	0.02	1.28	
Tqlf				96	405	0.24	320	32	34													
Trdf	99.55	<5	1,340	150	130	1.15	310	45	21	4	6	24	1	2	1	<1	280	2	0.02	<.02	<.04	
Tcrf	98.83	<5	<20	175	5	35.00	405	58	57	7	16	110	<1	4	1	<1	930	2	>19	<.02	<.03	
Trff	100.30	<5	<20	150	22	6.82	475	57	69	4	6	11	<1	4	1	<1	85	2	<.02	0.02	<.03	Interior of dike.
Trl	99.21	<5	30	155	15	10.33	305	30	180	5	15	130	7	3	<1	<1	920	2	<.02	<.02	0.03	
Tqlk	99.02	<5	1,500	73	570	0.13	145	26	<5	22	11	72	<1	32	12	<1	800	2	0.15	<.05	2.68	
Tqlo	99.23			110	600	0.18	13	16	<5	9	13	50	9	12	5		650					
Tqli	100.62	<5	1,380	83	780	0.11	105	17	<5	22	21	70	<1	27	9	<1	700	3				
Tql	99.64	<5	1,390	73	725	0.10	125	15	6	6	13	48	<1	36	10	<1	600	2	<.02	<.05	0.08	
Tanq				125	485	0.26	155	18	<5													
Tan	100.73	<5	1,570	42	1,345	0.03	105	14	13	51	4	63	<1	111	18	<1	2,000	2	0.05	0.03	0.77	
Tan	99.43	<5	1,360	43	695	0.06	135	18	<5	23	7	93	<1	15	10	<1	460	2				Flow foliated
Tlt				190	120	1.58	155	18	26													
pCqm	97.69	<5	1,570	85	130	0.65	185	28	6	2	5	36	2	4	2	<1	750	2	0.03	0.02	0.18	
pCs	100.43	<5	730	49	365	0.13	120	9	7	9	2	45	2	6	16	<1	1,000	3	0.08	0.02	0.25	Garnet porphyroblasts.

Table 1 (cont.)

rock type	rock symbol	texture	composition	grain size (mm)	color	distinguishing features/ occurrence/ association
volcanic sandstone	Tsv	sandstone	immature graywacke sands with volc. source	< 2mm	reddish - green hue	unit occurs locally, mostly outside of map area
early Tertiary sandstone	Ts	sandstone and minor shale and carbonates	immature sandstone; pC provinence	<5% cobbles	reddish brown	well indurated; can have up to 5% muscovite; channels are common; upper-part of graded sequence with conglom.
early Tert. conglom., fine	Tcgf	conglomeritic	immature sands and clasts of local pC derivation	clasts up to 10 cm	med- grey to brown	well indurated in the mine area; cobbles are often imbricated; sandstone matrix can contain up to 3% muscovite;
early Tert. conglom., coarse .	Tcgc	conglomeritic	immature sands and clasts of local pC derivation	clasts up to 2 meters	med- grey to brown	well indurated in the mine area; cobbles are often imbricated; sandstone matrix can contain up to 3% muscovite;
diabase	Od	diabasic, local ophitic textures	plag., hbl., mag., bio.,sphene, apatite	0.1-1	grey to black	pre-Mississipppian intrusions; correlates with 500 Ma Rb-Sr dated units to the north (Reed, 1984)
quartz monzonite of Old Mike Peak	pCom	non- to weakly foliated; dominately equigranular	qtz (25-30%) k-spar-(30-45%) plag. (35-40%) biotite (approx. 0-7%)	0.1-1.3mm	white to med. grey	quartz monzonite to granite; common pegmatite and aplite zones; large aplite body north of Red River town site
quartzite	pCq	massive to weak foln.	qtz. (99-100%) tr. feldsp., musc.	0.01-1.5	white	meta-arkose
mica gneiss	pCmg	equigranular to porphyritic; stg. foln.	qtz. (70-90%) feldsp. (0-2%) bio.-hbl. (3-28%) muscovite (0-5%) local sillimenite	equig. (< 1mm); porph. (< 1cm)	med. grey to tan	represents a meta-sediment; pelitic; gradational with pCq
quartz monzonite of Columbine Creek	pCqm	very weakly to moderately foliated; dominately equigranular	qtz (20-30%) k-spar-(30-45%) plag. (35-45%) biotite (approx. 0-7%)	0.1-1.5mm	white to med. grey	locally granitic or pegmatitic
schist	pCs	mod.-strg. foln.	qtz. (30-65%) feldspar (10-35%) bio.-hbl. (10-35%) local garnet	0.25-1.5	med. grey to black	foliated qtz.-feldspar±hbl.±bio.±garnet schist; occurs in sub-surface of mine area and locally at the surface at boundary between meta-igneous and meta-sedimentary rocks; on Plate 1 this unit also includes felsic schist SW of the mill
amphibolite (dom. meta-mafic ign. rx.)	pCa	equigranular; lt to mod. foln.	qtz (0-40%) feldspar (20-65%) hbl. (35%)	0.25-2	med. grey to black	amphibolite, amphibolite schist, mafic schist and gneiss; occurs locally in pC section

Table 2a

rock type	rock symbol	quartz phenocrysts			K-spar phenocrysts			plagioclase phenocrysts			biotite phenocrysts		
		%	size (mm)	shape/ comments	%	size (mm)	shape/ comments	%	size (mm)	shape/ comments	%	size (mm)	shape/ comments
qtz. latite-lamphyre	Tqll	0-3	0.5-3	strongly resorbed, often multi-xtal.	0-4	1-15	subhedral; min. incl. common	2-8	0.5-10	subhedral; some min. incl.	0.5-3	0.2-5	euhedral
rhyolite porph.	Tr	2-13	0.2-8	euh.-anh.; some rnd.; oft. agglom.,	5-15	0.2-15	subhedral	1-8	0.25-7	subhedral	tr.-1	<3	euhedral
tuffisite	Tt	4-12	0.2-4	euh.-anh; sub-rounded to broken	2-5	<3	broken	1?		hard to tell from K-spar due to alt.	?		
fragmental tuffisite	Ttf	4-12	0.2-4	euh.-anh; sub-rounded to broken	2-5	<3	broken	1?		hard to tell from K-spar due to alt.	?		
rhyolite of Goat Hill	Trg	2-7	0.2-6	mod.-stg. resorbed; orig. bipyramids	4-15	0.5-15	subhedral; some min. incl.	0-12	0.5-8	subhedral	0.25-2	<3	euhedral
rhyolite w. abund. qtz.	Trq	8-15	0.5-10	euh.-subh..; orig. bipyr; some agglom	8-15	0.2-15	subhedral	0-3	0.2-10	subhedral	0-0.5	<2	euh.
rhyolite w. hornblende	Trh	4-10	0.5-8	mod. resorbed; orig. bipramids	6-15	0.5-15	euh.-subh.; some w. min. incl.	1-10	< 15	subhedral; often as K-spar cores	0.5-1	<3	euh.
rhyolite to qtz. latite	Trl	3-6	0.5-5	strongly resorbed	2-10	0.5-8	subhedral; some min. incl.	0-8	0.5-5	subhedral	tr.-5	<3	euh.
scritate text. rhyolite	Trs	8-20	0.1-10	lt.-mod. rounded; orig. bipyramids	8-20	0.5-8	subhedral	0-10	<5	euhedral	tr.-3	0.2-2.5	euh.
granite porphyry	Tgp	17-25	0.5-8	anhedral	20-30	0.5-12	subhedral	13-20	0.5-9	subhedral; An 4-15	0-3	1-5	euh.
aplite porphyry	Tap	0-10	0.1-7	subhedral to anhedral	0-20	0.2-10	euhedral to subhedral	0-30	0.2-8	euhedral - subhedral	0-5	0.5-8	euh.
contam. rhy. to latite	Tqlc	0.5-2	1-10	stg. resorbed; qtz and maf min. incls.	0.5-8	1-10	euh.-subh.	8-15	1-6	subhedral	0-1	<8	euh.-subh.
comp. rhy. to latite dikes	Tqlcz												
tuff-related qtz. latite	Tqlf	0			0-4	<6	euh. -subh.	8-20	0.2-10	euh.-subh.; An 32-35	3-5?	<4	prob. orig. biotite alt. to chl., sec. bi
tuff-related rhyodatite	Trdf	1-6	0.2-2	subh.-anh.; orig. bipyramids	1-7	<5	euhedral; Na-sanadine	2-8	0.2-5	subhedral; An 7-8	0-0.5?	<1	prob. orig. biotite alt. to chl., sec. bi
tuff-related rhyolite	Tcrf	8-10	0.2-2.5	euh.-anh.; orig bipyramids	20-30	0.2-11	euhedral; Na-sanadine	0			0-tr.?		alt. to py.
tuff-related rhyolite	Trff	0-3	0.2-1.25	euh.-anh.; orig. bipyr.; tr. agglom..	0.25-5	0.2-4	euh.-subh.; Na-sanadine	0-tr.			0-tr.?		alt. to py.

Table 26 (page1)

rock type	rock symbol	quartz phenocrysts			K-spar phenocrysts			plagioclase phenocrysts			biotite phenocrysts		
		%	size (mm)	shape/ comments	%	size (mm)	shape/ comments	%	size (mm)	shape/ comments	%	size (mm)	shape/ comments
Amalia Tuff	Trt	4-5	0.2-1.75 dom. < 1	15%euh.-65%subr-20% rnd. or broken	4-7	0.2-2	subh.; Na-sanadine	0			0		
Amalia Tuff megabreccia	Trtbx	tr.-5	< 1.5	euh. to broken	0-7	<2	commonly broken	0			0		
A.T. basal broken zone	Trtb	2-7	0.1-1.25 dom <.75	mod. broken	0-3	0.1-1.5	subh.- broken	0			0		
xenocrystic basaltic and.	Txba	0-3 as xenos	< 15	strongly resorbed	0-8	4-20	subh.; metacrysts or xenocrysts	0-15	0.1-2	subh.; some pilotaxitic	1-7 bio. or opx?	0.2-3 dom < 2	
qtz. latite w. orthoclase	Tqlk	0-3	0.2-5	rounded-resorbed	3-7	2-40	subh.; larger x-tals have min. incl.	10-30	1-6	subh.; larger x-tals have min. incl.	2-4	0.25-3	euh.
qtz. latite w. orbic. qtz.	Tqlo	15-20	2-15	rnded; stg.resorb. w. radial pattern	5-8	5-30	subh.; commonly with min. incl.	15-20	0.5-7	subh.	0.5-3	0.25-4	euh.
qtz. latite intrusions	Tqli	0-2;rare 2-10	0.5-2	strongly rounded, resorbed	0-2	2-15	anh.-euh.; often with min. incl.	15-30	0.2-5	subh.; rarely with mafic min. incl.	2-4	0.2-5	euh.
lahar	Tlh	0			0								
qtz. latite flows	Tql	0-tr.			0-tr.			8-25	0.2-8	subhedral	3-5	0.1-3	euh
andesite to qtz. latite	Tanq	0-0.25	<1	strongly rounded, resorbed	0			10-25	0.2-2	subh.	1-5	<2	euh.-subh.
andesite flows	Tan	0			0			10-25	0.2-2	subh.	1-5	<2	euh.-subh.
lithic tuff (some flows)	Tlt	1-10	0.1-2	subh.-anh.; broken	10-25	0.5-2	subh.-anh.	5-10	0.5-2	subh.-anh.	0-2	< 1.5	euh.-subh.

Table 2b (page 2)

rock symbol	groundmass	accessary/ metallic minerals	pumice/ lithics/ other	distinguishing features/ occurrence/ association
Tqll	microxtal.; med-dk. grey-olive green; 0.2 mm pl. microlites	tr. sphene; tr. ap.; avg. 1% magnetite		cross-cuts all altertaion, but is deuter. altered (propylitic); qtz. lat. - lamp.
Tr	aphanitic, porcelaneous; wht.-lt. grey, local tan-olive green	0-5% pyrite; tr. sph.; tr. zr.		includes all rhyolite dikes outside of the mine area
Tt	v. fine grained, fragmental to aphanitic, silicic.; lt. grey	3-5 pyrite	0-10% xenoliths	associated with Trg intrusions; fragmental equivalent?
Ttf	v. fine grained, fragmental to aphanitic, silicic.; lt. grey	3-5 pyrite	0-40 Tql,0-80 Tbr 10-30Tan,0-35Trt	lithic rich, commonly border facies of Tt
Trg	aph., porc.; wht.	0-5 pyrite	0-40% xenos. (Tap, Tan, qtx. vnd. apl)	stock-like; low qtz. pheno content; wide contact zones
Trq	aph., porcelaneous; wht.- lt. grey	pyritized		abundant euhedral quartz phenos.; high pheno content; foliated margins
Trh	aph., porc.-silicic.; lt grey w tan or green hues	v.f.g. dissem mag. in matrix; 0-tr. py.	0-3% re-xtallized Tan xenoliths	large hornblende phenos.; mineral inclusions in K-spar; magnetite in mtx.
Trl	aph., porc.; wht.-lt. grey, local tan-green hues			variably textured; low percent and strongly resorbed quartz pheocrysts
Trs	aph., silicic. to v.f.g. aplitic; lt. grey w. tan-green hues	tr. py.; tr. apatite		seriate texture; E-W strike, near 90° dips
Tgp	0.05-5 mm; allotriomorphic to hypidiomor. k-spar-qtz.-plag.	tr. zr.; tr. apatite	0-10% xenoliths	variable textures and phenocryst abundances
Tap	0.03-0.5 mm; ≥ 50% of rock; k-spar-qtz.-pl. in decr. abund.	tr. zr.; tr. apatite	0-20% xenoliths	highly variable
Tqlc	aph., silicic.; lt. grey to cloudy wht.		0-2% Tan xenoliths	variable textures; composite dikes; common mineral inclusion
Tqlcz				comp. zones dikes from low pheno., latite exterior to high pheno., felsic interior
Tqlf	aph., silicic.; lt. grey to grey-brown-olive	tr. zircon; 0-0.12% apatite		high incompatible trace element chemistry; assoc. with other peralk. dikes
Trdf	aph. silicic; lt. grey	tr. zircon; tr. apatite		high incompatible trace element chemistry; some comingled dikes with Tcrf
Tcrf	aph. silicic; lt. grey	tr. zircon		high incompatible trace element chemistry; always in association with Trdf
Trff	aph. silicic; lt. grey	tr. zircon; tr.-0.5% dissem. magnetite	0-20% lithics; one dike has "fiamme"	high incompatible trace element chemistry; low % of phenos.; some sherulitic margins

Table 2 b (page 3)

rock symbol	groundmass	accessary/ metallic minerals	pumice/ lithics/ other	distinguishing features/ occurrence/ association
Trt	aphanitic. silicic; lt. grey	tr.-0.5% dissem mag.; tr. zircon	20-30% pumice; 0-5% lith. (dom. Tan)	distinguished by pumice, pheocrysts and high incompatible trace element chemistry
Trtbx	mix of aph.silic. (shards) to f.g. fragmental (rx. flour)		0-8 pum.;9-90 lith (Tan>Tql>Txb>Tqli)	distinguished by Trt matrix if evident; otherwise by being a heterolithic breccia
Trtb	aph. ,sil. ; lt. grey to f.g. fragmental		0-30 lith (Tan>Tql>Trt)	distinguished by broken crystals; often on top side of megabreccia blocks
Txba	aph., sil.; med.-dk. grey; commonly with autobx. text.	tr. mag.	0-15% vugs <2mm; 0-5% qtzt xenos	only found as megabx blocks; distinguished by mafic comp., vugs, and common xenos.
Tqlk	aph., silic. to porcelaneous; lt.-dk. grey with olive hue	tr. sphene,<0.7mm; tr. apatite	rare xenoliths	distinguished by large metacrystic? orthoclase
Tqlo	aph., porc. to silicic.; wht.-lt. grey w. local green casts	0-tr. sphene, < 1.5mm	rare xenoliths	distinguished by large orbicular quartz phenocrysts
Tqli	aph. silicic.; lt.-dk. grey w. green hues	tr. sphene; 0-0.5 apatite; tr. mag.	0-5% Tan xenoliths	generally coarser and more homogenous than Tql
Tlh	30-70% mtx.; v.f.g. <.01mm; red.; hem. rich	tr. mag.; tr. spec. hem.	30-70% lith., <1 M, dom Tql,Tan, subr.	distinguished by heterolithic breccia and muddy matrix; rare unit
Tql	aph., silicic. mtx; commonly auto- flow-brecciated	0-tr. sphene; tr. apatite		distinguished from Tqli by common autobreccia texture
Tanq	aph., silicic.; often homog.; significant qtz in mtx.	tr. apatite		texturally like Tan but contains up to 5 % quartz and is comp. a latite; homog. texture
Tan	aph., silicic.; often highly autobx.; local flow foln.	0-tr. apatite		massively bedded, fine grained
Tlt	aph. to v.f.g. silicic.; wht-lt. grey		0-10%pumice; 1-20% Tql,Trd liths.	text. variable; distinguished from Trt by low tr. elem chem, high phenos., & biotite

Table 2b (page 4)

Explanation

- Tri — rhyolite porphyry intrusion (dominantly post-ore)
- Tap — aplite porphyry intrusion (mineralization-related); locally xenolith-rich; locally abundant quartz veins
- Tapp — pre-ore aplite porphyry (contaminated phases)
- Trff — rhyolite porphyry intrusion (caldera-related)
- Tqli — quartz latite porphyry intrusion
- Tan — andesite porphyry flows

- outline of >0.2% MoS_2
- fault and fault zone
- quartz veins in aplite
- mining level
- xenoliths
- diamond drill hole

Magmatic-Hydrothermal Breccia:

- B — biotite, quartz, orthoclase matrix
- K — quartz, orthoclase matrix
- Q — quartz matrix

No vertical exaggeration

8000 ft — 2400 m — 2300 m — 7500 ft — 2200 m — Undercut Level — Grizzly Level — Haulage Level

Outline of >0.2% MoS_2

Tap with 25-95% quartz veins

Tap with 5-10% qtz vns

Tap with 5-10% qtz veins

Tan in fault zone

Fig. 40

44 x 17 IMAGE

EXPLANATION

rock units	description
Qd	- mine dumps
Qal	- alluvium (modern and ancient)
Tr	- dom. ryh. porph. dikes and stocks; local qtz. latite-rhy compositions; local tuffisite
Tgp	- granite porphyry intrusions
Tap	- aplite porphyry intrusions
Trf	- qtz. latite to rhyolite porph. dikes and local sills (dom. with a high incompatible trace element chemistry)
Trt	- Amalia Tuff, rhyolite tuff; includes local megabreccia zones
Tqlk	- qtz. latite porphyry intrusions with >1cm orthoclase phenocrysts
Tqlo	- qtz. latite porphyry intrusions with orbicular quartz phenocrysts
Tqli	- quartz latite porphyry intrusions
Tql	- quartz latite porphyry flows
Tan	- andesite porphyry flows
Tlt	- early lithic tuff and local rhyolite porphyry flows
Tsv	- volcanic-derived sandstone/siltstone
Ts	- fluvial sandstone; Precambrian provinance
zcg	- fluvial conglomerate; Precambrian provinance
pCqm	- quartz monzonite of Old Mike Peak
pCmg	- mica gneiss and quartzite (sedimentary protolith)
pCqm	- quartz monzonite of Columbine Creek
pCs	quartz-biotite-feldspar schist, amphibolite, amphibolite schist and gneiss; local felsic schist

EXPLANATION OF MAP SYMBOLS FOR PLATES 1&2

- contact; dashed where inferred, dotted where covered; strike and dip shown
- fault; dashed where inferred; dip shown; arrows show relative offset in cross-section
- landslide block
- foliation in metamorphic or igneous rock; metamorphic foliation in Tuff (indicates poles horizontal)
- strike and dip of bedding
- imbrication in conglomerate
- surface projection of molybdenite mineralization

LEGEND

- CONTROL POINT
- DRILL HOLES
- X 9815 SPOT ELEVATIONS
- 9800 INDEX CONTOURS
- INTERMEDIATE CONTOURS
- DEPRESSION CONTOURS
- CONTOURS THRU HEAVY VEGETATION
- STREAM / RIVER
- BUILDING
- POWER POLES
- FENCES
- PIPELINES
- TANKS
- DIRT ROAD
- HARD SURFACED ROAD
- TRAILS
- BRIDGES
- CULVERT
- TREES

SCALE IN FEET
2000 0 2000 4000 6000
CONTOUR INTERVAL 10'
1:24,000

Plate 1 Geologic map and cross-sections of the Questa mining district

Plate 2 Geologic map of the Questa mine area

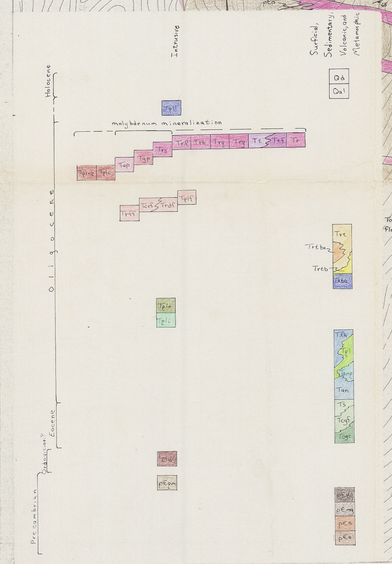

EXPLANATION AND CORRELATION TO UNITS IN PLATE 1

(equiv. units on Plate 1)	rock units	description
(Qd)	Qd	mine dumps
(Qal)	Qal	alluvial and mud flow deposits(modern and ancient)
(NA)	Tqll	quartz latite porphyry and lamprophyre dikes (too small to show on 1"-2000' map)
(Tr)	Tr	undifferentiated rhyolite porphyry dikes
(Tr)	Tt	tuffisite
(Tr)	Trf	fragmental tuffisite
(Tr)	Trg	rhyolite to rhyodacite dikes and stocks
(Tr)	Trq	quartz-rich rhyolite porphyry dikes
(Tr)	Trh	hornblende bearing rhyolite porphyry dikes
(Tr)	Trl	rhyolite to quartz latite porphyry dikes
(Tr)	Trs	sericite textured rhy. to v.f.g. aplite porphyry dikes
(Tgp)	Tgp	granite porphyry
(Tap)	Tap	aplite porphyry
(Tr)	Tqlc	rapakivi, zenolith-rich, hbl. bearing dikes and intrusions
(Tr)	Tqlcz	composite rhyolite to quartz latite porphyry dikes
(Trf)	Tqlf	quartz latite porphyry dikes (high incom. tr. elements.)
(Trf)	Trdf	rhyodacite porphyry dikes (high incom. tr. elements)
(Trf)	Trrf	high pheno. rhy. porph. dikes (high incom. tr. elements)
(Trf)	Trff	low pheno rhy. porph. dikes (high incom. tr. elements)
(Tr)	Trt	Amalia Tuff
(Tri)	Trtbx	Amalia Tuff breccia (>10% lithic fragments)
(Tri)	Trtb	Amalia Tuff, basal broken crysta zone
(NA)	Txba	commonly xenocrystic basaltic andesite (too small to show on 1"-2000' map)
(Tqlk)	NA	not exposed in 1"=500'scale map area

(equiv. units on Plate 1)	rock units	description
(Tqlo)	Tqlo	- quartz latite porphyry intrusions; orbicular qtz. phenos.
(Tqli)	Tqli	- quartz latite porphyry intrusions; dom. <2% qtz. phenos.
(NA)	Tlh	lahar (too small to show on 1"-2000' map)
(Tql)	Tql	- quartz latite porphyry flows
(Tan)	Tanq	- andesite to quartz latite porphyry flows
(Tan)	Tan	- andesite porphyry flows
(Tlh)	NA	- not exposed in 1"=500'scale map area
(Tsv)	NA	- not exposed in 1"=500'scale map area
(Ts)	Ts	- sandstone (includes minor siltstone)
(Tcg)	Tcgf	- fine-grained conglomerate (clasts <10 cm)
(Tcg)	Tcgc	- coarse-grained conglomerate (some clasts >10 cm)
(NA)	Qd	- pre-Mississippian diabase dikes (too small to show on 1" 2000' map)
(pCom)	NA	- not exposed in 1"=500'scale map area
(pCmg)	pCq	- quartzite
(pCmg)	pCmg	- mica gneiss (sedimentary protolith)
(pCqm)	pCqm	quartz monzonite of Columbine Creek; qtz. monzonite to local granite, v. weakly to mod. foliated
(pCs)	pCs	- quartz-biotite-feldspar schist
(pCs)	pCa	- amphibolite, amphibolite schist, mafic schist and gneiss

LEGEND

- CONTROL POINT
- DRILL HOLES
- SPOT ELEVATIONS (x 9815)
- INDEX CONTOURS (9500)
- INTERMEDIATE CONTOURS
- DEPRESSION CONTOURS
- CONTOURS THRU HEAVY VEGETATION
- STREAM / RIVER
- BUILDING
- POWER POLES
- FENCES
- PIPELINES
- TANKS
- DIRT ROAD
- HARD SURFACED ROAD
- TRAILS
- BRIDGES
- CULVERT
- TREES

SCALE IN FEET
500 0 500 1000 1500
CONTOUR INTERVAL 10'
1:6,000

KEY MAP
(1" = 500' MAPPING)
SHEET 5 OF 8

1	2	3	4	5	6	7	8

SCALE	1"=500' C.I. 10'
DATE	SEPT., 1982
DRAWN	
TRACED	
CHECKED	
APPROVED	

UNION MOLY CORP.
QUESTA DIVISION

FILE NO.

BOVAY 6026-028 DATE OF PHOTOGRAPHY 5-26-82

45 x 36